Toward a Mechanistic Understanding of Cofactor Biogenesis and Catalysis in Copper Amine Oxidases from *Hansenula polymorpha*

A DISSERTATION SUBMITTED TO THE FACULTY OF THE GRADUATE SCHOOL OF THE UNIVERSITY OF MINNESOTA

BY

VALERIE JANE KLEMA

IN PARTIAL FULFILLMENT OF THE REQUIREMENTS FOR THE DEGREE OF DOCTOR OF PHILOSOPHY

ADVISER: CARRIE M. WILMOT

June, 2012

Acknowledgements

Although only one name appears on the cover of this dissertation, a number of people contributed to its completion and provided me with support that I will always appreciate.

My sincerest gratitude goes to my adviser, Dr. Carrie Wilmot. Carrie has been a true mentor, and has shown me incredible patience. I cannot imagine having completed my graduate work with anyone else, and greatly appreciate the encouragement and education that I have been given.

I would also like to acknowledge members of the Wilmot lab for all of their assistance and ideas, as well as for creating a wonderful work environment. Many thanks go to Dr. Lyndal Jensen, Corinne Solheid, Peder Cedervall, Dr. Brandon Goblirsch, Dr. Erik Yukl, Dr. Teresa de la Mora, Dr. Bryan Johnson, and Dr. Chris Carrell.

My thanks go to members of the Lipscomb lab, particularly Dr. Melanie Rogers, as well as Leah Randles and Dr. Kelaine Haas for advice and assistance with experimental design. In addition, I am grateful to those who maintained the equipment and computers which were necessary to my work, including Ed Hoeffner, Dr. Can Ergenekan, and Nancy Rowe.

I have a wonderful group of friends who helped keep me sane through this process, and appreciate their emotional support and camaraderie. Particular thanks go to Molly Marshall, Kelaine Haas, and the members of HP.

Lastly, this dissertation would not have been possible without the support I received from my parents, Martin and Rebecca Klema. No one has felt more love or encouragement, of which I am more grateful than I can say.

Dedication

This dissertation is dedicated to my parents, who have always believed in me. Words cannot say how much I appreciate the unconditional love, support, and encouragement you have offered throughout this process.

Dissertation Abstract

Copper amine oxidases (CAOs) are a ubiquitous class of enzymes responsible for the oxidation of primary amines to their corresponding aldehydes with the concomitant reduction of O_2. Found in nearly every aerobic organism, CAOs take on a myriad of roles depending on source, cellular location, and physiological substrate. In addition to their catalytic activity, CAOs also produce their own redox-active cofactor, called 2,4,5-trihydroxyphenylalanine quinone (TPQ), from an endogenous tyrosine residue. This process occurs without additional enzymatic activity and requires only oxygen and copper.

Two CAO paralogs from the yeast *Hansenula polymorpha* have been used for structural studies aimed at deciphering mechanistic details of metal binding in TPQ biogenesis as well as amine substrate specificity during catalysis. The X-ray crystal structures of metal-free HPAO-1 (apoHPAO-1) as well as apoHPAO-1 in complex with Cu(I) and Co(II) have been solved and are described in Chapter 3 of this work. Analysis of these complexes has shed light into how different coordination geometry may influence whether a metal is capable of initiating biogenesis in apoCAO.

In order to investigate amine substrate specificity in CAOs, the structure of a second CAO from *H. polymorpha* (HPAO-2) has been solved and is presented in Chapter 2 of this work along with steady-state kinetic data for the reaction of HPAO-2 with methylamine and benzylamine. HPAO-2 preferentially oxidizes benzylamine over methylamine, while HPAO-1 prefers methylamine. Structural differences in the amine substrate channels of these two paralogs begin to account for their inverted substrate preferences. Amine substrate specificity is further investigated in crystal structures of HPAO-1 in complex with methylamine, ethylamine, and benzylamine. Substrate-protein interactions in these three complexes shed light into this CAO's preference for aliphatic amines over the aromatic amines preferred by some of its homologs.

Finally, Chapter 5 of this work outlines two projects currently underway. The first involves single site mutations in HPAO-1 and HPAO-2 at a position in the primary sequence thought to contribute to substrate selection. An additional ongoing project

involves solving the crystal structures of two aniline-substituted HPAO-1 proteins to examine the factors governing the formation of a proposed Cu(I)/tyrosyl radical complex during biogenesis.

Table of Contents

List of Tables

List of Figures

List of Schemes

List of Abbreviations

AGAO	copper amine oxidase from *Arthrobacter globiformis*
ANAO	copper amine oxidase from *Aspergillus nidulans*
apoCAO	precursor CAO that lacks copper and TPQ
BSAO	copper amine oxidase from *Bos taurus* (bovine) serum
CAO	copper/TPQ-containing amine oxidase
CTQ	cysteine tryptophylquinone
DAO	diamine oxidase
DPQ	dopaquinone
ECAO	copper amine oxidase from *Eschericia coli*
EDTA	ethylaminediaminetetraacetic acid
EPR	electron paramagnetic resonance
HPAO-1	copper (methylamine) amine oxidase from *Hansenula polymorpha*
HPAO-2	copper (benzylamine) amine oxidase from *Hansenula polymorpha*
ICP-MS	inductively coupled plasma-mass spectrometry
LMCT	ligand-to-metal charger transfer
LOX	lysyl oxidase
LOXL	lysyl oxidase-like protein
LSAO	copper amine oxidase from lentil seedling
LTQ	lysine tyrosylquinone
MAO	monoamine oxidase
pAF	*p*-amino phenylalanine
PAO	polyamine oxidase
PLP	pyridoxal phosphate
PMF	potential of mean force free energy map
PPLO	copper amine oxidase from *Pichia pastoris* (lysyl oxidase)
PQQ	pyrroloquinoline quinone
PSAO	copper amine oxidase from *Pisum sativum*
rmsd	root-mean-square deviation
SHE	standard hydrogen electrode

SSAO	semicarbazide-sensitive amine oxidase
TTQ	tryptophan tryptophylquinone
TPQ	2,4,5-trihydroxyphenylalanine quinone
TPQ_{red}	2-electron reduced TPQ
VAP-1	vascular adhesion protein-1

CHAPTER 1: INTRODUCTION

Klema, V.J., and Wilmot, C.M. (2012) The role of protein crystallography in defining the mechanisms of biogenesis and catalysis in copper amine oxidase, *Int. J. Mol. Sci. 13*(5), 5375-5405.

1.1 Background

Amine oxidases are responsible for the oxidative deamination of amines to their corresponding aldehydes coupled with the reduction of O_2 to H_2O_2. Members of this ubiquitous group of enzymes can be further classified based on the chemical identity of the organic cofactor used during catalysis into either the flavin adenine dinucleotide-containing amine oxidases (monoamine oxidase (MAO) (E.C. 1.4.3.4) and polyamine oxidase (E.C. 1.5.3.17)) or the copper/quinocofactor-containing amine oxidases. MAO is found exclusively in the outer mitochondrial membrane of mammalian cells, and catalyzes the deamination of primary, secondary, or tertiary amines. This flavoprotein has a firmly established role in the metabolism of aminergic neurotransmitters such as serotonin, norepinephrine, epinephrine, and dopamine (*1*). Polyamine oxidase preferentially deaminates polyamines such as spermine and spermidine and has a role in the regulation of cellular growth (*2*).

In contrast, the copper/quinocofactor-containing amine oxidases are active against only primary amines, and possess one of two quinone-containing cofactors: 2,4,5-trihydroxyphenylalanine quinone (topaquinone or TPQ) or lysyl tyrosylquinone (LTQ). Although the TPQ- and LTQ-containing amine oxidases both oxidatively deaminate primary amines through the use of an organic quinone-containing cofactor and a copper ion, these two enzyme families are non-homologous. LTQ is found in the lysyl oxidase (LOX)-like family of proteins (LOXL, E.C. 1.4.3.13), named for their ability to convert the ε-amino group of peptidyl lysine residues to an aldehyde. This peptidyl aldehyde product can condense with a neighboring lysine residue or react with a second lysine-derived aldehyde to form crosslinks important in the formation and stabilization of

collagen and elastin (*3*). Amine oxidases containing TPQ (CAOs, for copper-containing amine oxidases, E.C. 1.4.3.21) were the first to be characterized in a growing number of bifunctional enzymes which contain "home-made" cofactors produced *in situ* by the post-translational modification of endogenous amino acid side chains (*4*). This work refers to features related to cofactor biogenesis and catalysis in two CAOs from the yeast *Hansenula polymorpha*.

1.2 Physiological significance of CAOs

In the decades since the first discovery of amine oxidase activity in the blood plasma of sheep in 1929 (*5*), CAOs have been found to exist almost ubiquitously in aerobic organisms, taking on a myriad of functional roles depending on enzyme source, cellular location, and physiological substrate. In bacteria and yeast, CAOs are thought to play mainly a catabolic role, allowing for the use of primary amines as a sole carbon and/or nitrogen source for cellular growth (*6, 7*).

In eukaryotes these enzymes have more poorly defined roles but are known to contribute to a variety of complex cellular activities. CAO activity helps regulate several processes in plants due to the compartment-specific production of product H_2O_2, which affects plant germination, seedling establishment, and root growth (*8*). Hydrogen peroxide production is also associated with cell wall maturation and lignification during growth, as well as wound healing and the reinforcement of cell walls during cellular stress due to pathogenic attack (*9, 10*). Moreover, amine catabolism is known to influence the plant stress response upon exposure to cadmium or excess salt (*11*).

Several CAO homologs are expressed in mammalian tissues. In order to study their distribution amongst mammalian species, four complete genes (*AOC1-4*, for "amine oxidase, copper-containing") were cloned and characterized from porcine genomic DNA. All of these encode a bona fide CAO which displays catalytic activity toward primary amines (*12*). These were used to identify orthologs in other mammalian genomes; all four *AOC* genes have been identified in cows, horses, dogs, mice, rats, chimpanzees, macaques, and humans (*12*). *AOC1* encodes a soluble secretory enzyme called diamine oxidase (DAO) (*13*), *AOC2* encodes a retina-specific amine oxidase (*14*), and *AOC3* encodes an endothelial vascular adhesion protein (known as VAP-1 in humans) (*15*). *AOC4* was found to encode an additional serum/plasma CAO homologous to VAP-1 which lacks the N-terminal transmembrane domain found in VAP-1. However, the *AOC4* gene in humans is truncated and nonfunctional due to an internal stop codon, and AOC4 protein encoded by rodent genomes is present only in small fragments (*12*). In humans, a proteolytic cleavage product of AOC3 may function instead of the nonfunctional *AOC4* gene product (*12*).

In mammals, nearly all biogenic primary amines can act as CAO substrates, including the neurotransmitters serotonin, norepinephrine, epinephrine, and dopamine. A large number of additional amines have been identified as CAO substrates, including methylamine, ethylamine, aminoacetone, benzylamine, phenylethylamine, agmatine, spermine, spermidine, histamine, tyramine, mescaline, putrescine, and cadaverine (*14*, *16*, *17*).

Members of the CAO protein family contribute to the regulation of a myriad of

complex processes in mammals due to the diversity in their substrates, their wide distribution throughout mammalian tissues (including the brain, blood plasma, kidneys, placenta, adipocytes, endothelial tissues, and throughout the cardiovascular and gastrointestinal systems), and changes in expression and activity during disease and throughout pregnancy (*18*). For example, histamine, a pro-inflammatory amine produced by mast cells upon allergic reaction or cellular damage, is cleared in human tissues by DAO (*19*). Tumor cells are known to contain higher concentrations of amines than cells from normally proliferating tissues, and the oxidation of spermine or spermidine by CAOs produces acrolein, a known cytotoxin which can induce cellular death in cancerous tissues (*20*). Agmatine (produced from the decarboxylation of arginine) binds to α2 adrenergic receptor and imidazoline binding sites; its regulation through CAO activity has been shown to modulate withdrawal anxiety in rats (*21*).

Changes in CAO activity are correlated with a variety of human diseases, including diabetes mellitus, Alzheimer's disease, and additional inflammatory disorders (*22*). A truncated soluble form of membrane-bound VAP-1 known as semicarbazide-sensitive amine oxidase (SSAO) is known to mediate glucose uptake in adipocytes via the recruitment of the glucose transporter GLUT4 from vesicles within the cellular interior to the cell surface (*23*). VAP-1 also controls leukocyte extravasation to sites of inflammation through its activity against amine groups from solvent-exposed lysine residues of membrane-associated counter-receptors, including sialic acid binding Ig-like lectins (siglecs) (*22*, *24*). Mice deficient in AOC3 expression exhibit impaired immune responses, but notably present no other detectable phenotypic changes (*25*). The highly

reactive aldehydes produced from the oxidation of methylamine and aminoacetone in human tissues contribute to protein cross-linking, β-amyloid aggregation, and advanced glycation end-product formation in patients with Alzheimer's disease or diabetes mellitus (*26*, *27*). With CAO activity playing a critical role in such numerous and diverse physiological processes, ranging from basic metabolism in bacteria and yeast to roles in multifaceted disease states in humans, an understanding of TPQ production and catalysis in these enzymes is critical to the development of any potential pharmaceutical therapies that may regulate their activity (*22*).

1.3 Post-translationally modified amino acid cofactors

A large number of enzymes require low-molecular weight cofactors for catalytic activity, some of which are covalently attached to the protein component. Most cofactors are non-proteinaceous and independently synthesized before their association with the protein component of the relevant enzyme; however, it is now well-established that some enzymes utilize the post-translational modification of endogenous amino acid side chains to form cofactors *in situ* (*4*). This approach allows an enzyme to avoid the energetic costs of cofactor import both to and within the protein, and furthermore could help sequester potentially deleterious intermediates produced during cofactor formation. For example, TPQ as a free molecule is a known neurotoxin; however its production from an endogenous tyrosine residue in the deeply buried CAO active site circumvents this problem (*28*). Most importantly, this strategy increases the diversity of chemical properties available within an enzyme active site beyond that afforded by the twenty

canonical amino acids.

Variations in both the physical properties of these modified amino acid cofactors as well as the mechanisms employed for their formation are widespread. Many modifications involve the crosslinking of two amino acid side chains, for example cytochrome *c* oxidase and catalase (Tyr-His); tyrosinase, hemocyanin, and catechol oxidase (His-Cys); and galactose oxidase (Tyr-Cys) (*29-35*). Cofactor biogenesis can also entail the modification of a single side chain (sulfatases (cysteine converted to formylglycine); rubisco, urease, and phosphotriesterase (carbamylation of a lysine residue); and NADH peroxidase, NADH oxidase, and nitrile hydratase (cysteine converted to cysteinesulfenic acid)) (*36-42*).

Figure 1.1 Quinone-containing cofactors formed by the post-translational modification of tyrosine or tryptophan side chains.

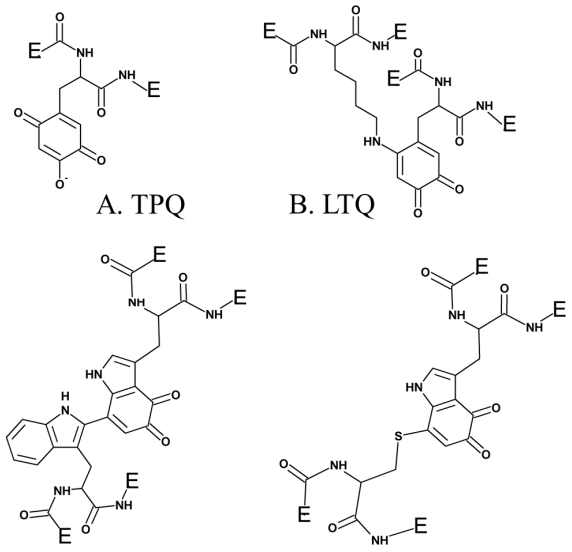

Several additional enzymes undergo post-translational modification of an endogenous tyrosine or tryptophan residue to form cofactors that contain a quinone

moiety. To date, these include 2,4,5-trihydroxyphenylalanine quinone (topaquinone or TPQ) in CAO (Figure 1.1A) (*28*), lysine tyrosylquinone (LTQ) in LOXL (Figure 1.1B) (*43*), tryptophan tryptophylquinone (TTQ) in bacterial amine dehydrogenases (Figure 1.1C) (*44*), and cysteine tryptophylquinone (CTQ) in bacterial quinohemoprotein amine dehydrogenase (Figure 1.1D) (*45*).

The first of these four quinocofactors to be identified was TPQ, which is located in the deeply buried CAO active site. The formation of a chromophoric complex between CAO protein and hydrazine derivatives had originally suggested pyridoxal phosphate (PLP) as a likely candidate for the CAO cofactor (Figure 1.2A) (*46*). Two independent studies later reported the cofactor in *Bos taurus* serum amine oxidase (BSAO) to be covalently bound pyrroloquinoline quinone (PQQ) (*47, 48*) (Figure 1.2B), which was strengthened by resonance Raman experiments conclusively eliminating PLP as a possible CAO cofactor (*49-51*). The true identity of the CAO cofactor was unequivocally confirmed to be TPQ (Figure 1.1A) by Janes et al. through the use of mass spectrometry, UV/visible spectroscopy, and proton NMR studies of a pentapeptide isolated from BSAO digests in comparison to a peptide analog of 6-hydroxydopa (*28*).

Figure 1.2 Structures of initially proposed CAO cofactors (A) PLP and (B) PQQ.

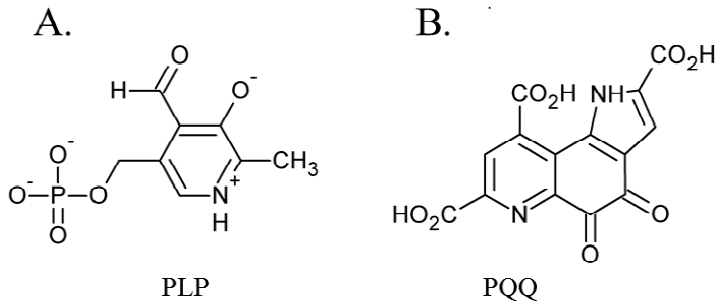

1.4 Overall CAO fold

The structures of CAOs isolated from a variety of organisms have been solved by X-ray crystallography (Table 1.1). Despite sharing only 20-40% sequence homology, they all adopt an archetypal fold that brings together a number of conserved residues to form the CAO active site where both cofactor biogenesis and catalysis take place. There is currently no crystal structure of the LTQ-containing LOXL proteins, which are non-homologous to the TPQ-containing CAOs.

Table 1.1 TPQ-containing CAOs with available X-ray crystal structures.

Source	**Organism**	**Reference**
Mammalian	*Homo sapiens*	VAP-1/SSAO: (*52, 53*), DAO: (*19*)
	Bos taurus	BSAO: (*54*)
Yeast	*Hansenula polymorpha*	HPAO-1: (*55*), HPAO-2: (*56*)
	Pichia pastoris	PPLO: (*57*)
Bacterial	*Arthrobacter globiformis*	AGAO: (*6*)
	Escherichia coli	ECAO: (*58*)
Plant	*Pisum savitum*	PSAO: (*59*)
Fungal	*Aspergillus nidulans*	ANAO: (*60*)

All CAOs structurally characterized thus far are homodimeric, with individual protein subunit masses ranging from ~70-80 kDa with eukaryotic CAOs having additional mass through glycosylation (*61*). The CAO monomer can be divided into four domains (D1-D4) organized along its primary sequence. The shape of the CAO dimer is similar to that of a mushroom cap, with the amino-terminal domain D1 (present only in the ECAO crystal structure) acting as a "stalk" (D1 not present in HPAO-1, Figure 1.3) (*58*). D2 and D3 are small α/β-roll domains composed of ~100 residues each, and are thought to have arisen from a gene duplication event given their sequence homology and

near identical topology (in HPAO-1, alignment of equivalent D2 and D3 main chain atoms gives a root-mean-square deviation (rmsd) of ~1.1 Å) (purple (D2) and green (D3) in Figure 1.3) (*55*).

Figure 1.3 Overall fold of HPAO-1 viewed along the molecular dyad axis. One monomer is shown as a cartoon, and colored by domain (D2, purple; D3, green; D4, blue; connecting loop, yellow; β-hairpin arms, red). The second monomer is shown as a semi-transparent grey molecular surface. TPQ side chains from both monomers are shown as space-filling spheres and colored by atom type (carbon, grey).

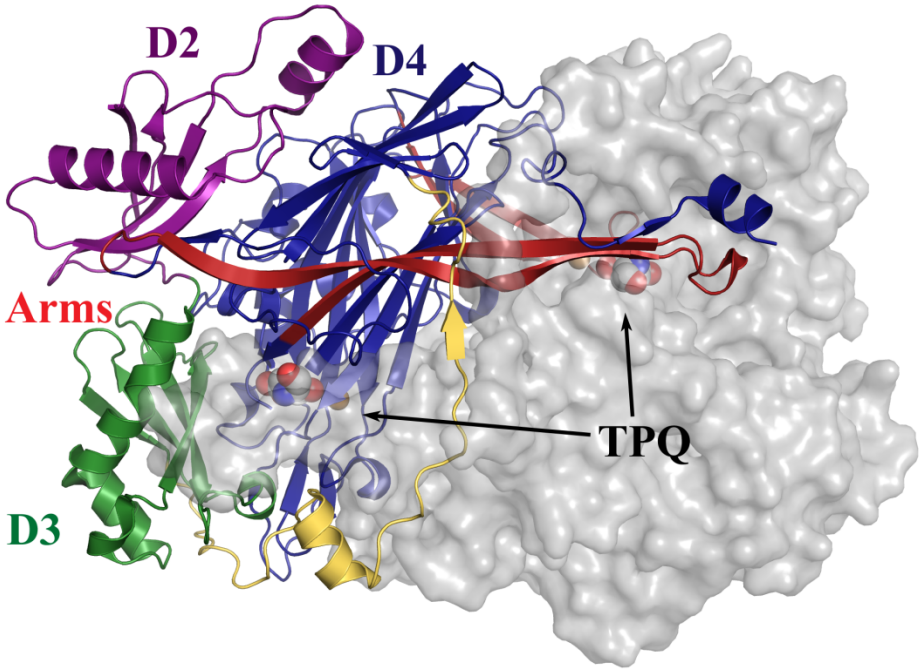

The large carboxy-terminal domain D4 is composed of ~500 residues and contributes the majority of the conserved amino acids that form the enzyme active site (blue in Figure 1.3). The topology of D4 is that of a complex antiparallel β-sheet sandwich structure. Two β-hairpin arms protrude from the D4 domains of each monomer and interlock the protein dimer. These arms also form a portion of the back wall of the

second monomer's active site (red in Figure 1.3), and are thought to be important for the maintenance of dimer stability and the regulation of substrate specificity in CAOs. The region between monomers encloses a solvent-filled cavity known as the "inland lake," and the dimer interface is extensive with a buried surface area comprising ~50% of the total surface area (*55*) (Figure 1.3).

All structurally characterized CAOs besides HPAO-1 and -2 contain two metal binding sites distinct from the active site copper, one of which is solvent exposed and one of which is less accessible (~36 Å and ~30 Å from the active site in ECAO, respectively) (*62*). These metal sites primarily bind Ca(II), with the plant CAOs binding Ca(II) or Mn(II) at the less accessible site depending on the availability of divalent metal ions (*59, 63*). The X-ray crystal structures of HPAO-1 and HPAO-2 indicate a salt bridge at the corresponding position (HPAO-1: Glu69 and Arg467, HPAO-2: Lys42 and Asp445) (*55, 56*). A study conducted using EDTA-treated ECAO found that calcium binding at these two sites is not essential for activity, but its removal decreases catalytic efficiency by ~60-90%, which can be partially recovered by the addition of an exogenous divalent cation (*62*). This effect has been attributed to long-range structural changes which either alter the conformation of TPQ, or affect the dynamics of a hydrophobic channel important for oxygen transport to the active site (*62*).

1.5 Structure of the CAO active site

The deeply buried CAO active site contains a mononuclear type 2 Cu(II) ion bound in a distorted square pyramidal geometry by the imidazole groups of three

conserved histidine residues at a distance of ~2.0 Å, a well-ordered axial water ligand at a distance of ~2.4 Å (W_a), and a more labile equatorial water ligand visualized in some CAO structures at a distance of ~2.0 Å (W_e) (Figure 1.4A). TPQ can adopt two possible conformations that are named based on the relationship between TPQ and the bound copper ion. The "off-copper" TPQ conformer does not act as a copper ligand; instead, its O2 atom interacts with the metal center via the conserved axial water molecule (Figure 1.4A). The oxygen atom at position 4 of the TPQ ring is involved in a short hydrogen bond (~2.3 Å) with the phenolic hydroxyl of a conserved active site tyrosine residue (Tyr305 in HPAO-1). As this distance is less than 2.5 Å, it indicates a shared proton between Tyr305 and TPQ. The side chain of Tyr305 also interacts with the axial water ligand (W_a) via an intervening water molecule (W in Figure 1.4A). The carbonyl group at position 5 of the TPQ ring points away from the copper center and toward the amine substrate channel. This "off-copper" species represents a catalytically productive CAO active site, as its C5 atom is the site of nucleophilic attack by amine substrates. A conserved aspartate residue, which acts as a general base during catalysis, sits near the substrate binding pocket (Asp319 in HPAO-1) and interacts with the cofactor through an intervening water molecule (W2 in Figure 1.4A). TPQ can also adopt an "on-copper" conformation, in which the ring has rotated about its Cα-Cβ and Cβ-Cγ bonds. This represents an unproductive state because the C5 atom of TPQ is inaccessible for nucleophilic attack by substrate moieties (Figure 1.4B). In this conformation, TPQ displaces the axial water molecule which is coincident with the "off-copper" TPQ conformer (W_a) and instead interacts directly with copper via its O4 atom.

Figure 1.4 Diagram of the HPAO-1 active site with TPQ in its (A) "off-copper" or (B) "on-copper" conformation. Residues are shown in stick and colored by atom type (carbon, grey). Copper ions are shown as gold spheres, and water molecules are shown as small red spheres. Hydrogen bonds are indicated by dashed lines, and metal-ligand interactions are indicated by solid lines. In (B), the "off-copper" TPQ conformer from panel (A) is shown in semi-transparent stick.

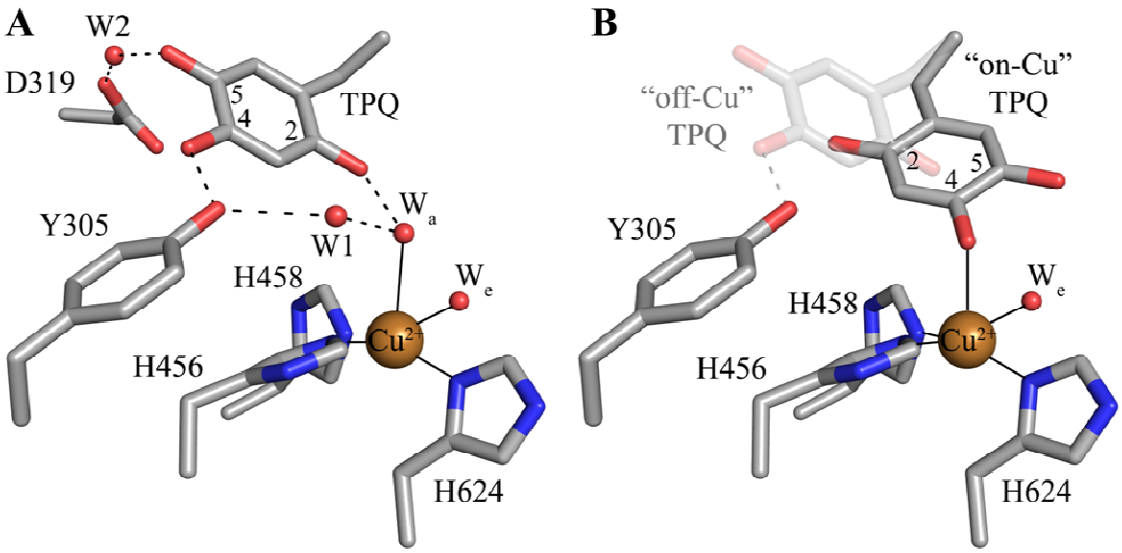

1.6 Biogenesis of TPQ

The mechanism by which fully-folded CAO synthesizes its own quinone-containing cofactor *in situ* has been an intriguing question in the field. A number of biochemical studies first established the process to be autocatalytic, requiring oxygen and copper but no auxiliary enzymatic activity or reducing equivalents (*64*, *65*). Two moles of O_2 are consumed for every mole of TPQ and H_2O_2 produced (Scheme 1.1) (*66*).

Scheme 1.1 An endogenous tyrosine residue is converted to TPQ in an autocatalytic oxygen- and copper-dependent process. E represents the enzyme polypeptide.

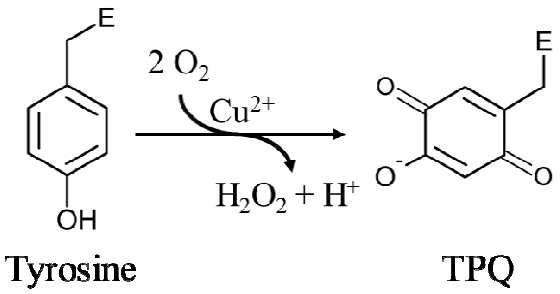

Kinetic and structural investigations using metal-free precursor (apo) protein from *Hansenula polymorpha* (apoHPAO-1) and *Arthrobacter globiformis* (apoAGAO), the only metal-free precursor CAO proteins currently available, have led to a proposed mechanism for TPQ biogenesis. This process in HPAO-1 is outlined in Scheme 1.2. ApoCAO is defined as amine oxidase protein that lacks both active site cofactors: a mononuclear copper ion and TPQ. The tyrosine residue that undergoes modification is contained within the conserved active site consensus sequence Thr-X-X-Asn-Tyr-Asp/Glu (precursor tyrosine residue underlined) (*67*). TPQ biogenesis begins with apoCAO, in which the precursor tyrosine side chain is unmodified (A in Scheme 1.2) (*6, 68*). Copper binds at the active site and is ligated by three strictly conserved histidine residues (A→B in Scheme 1.2). A kinetic study conducted using apoHPAO-1 with and without prebound copper reported a rate of TPQ formation which was unchanged with the prebinding of Cu(II), indicating that copper binding is a fast process relative to biogenesis overall (*69*).

In HPAO-1, molecular oxygen then binds in a nearby off-copper hydrophobic pocket, which induces a conformational change in the precursor tyrosine side chain such

that its hydroxyl group becomes oriented toward the copper (B→C in Scheme 1.2). Structural work suggests that at this point, the tyrosine residue is present in its protonated form, as indicated by the long distance between the phenolic oxygen and bound copper (~2.5 Å) in a crystal structure of an anaerobic Cu(II)-apoAGAO complex (*68*).

Scheme 1.2 Proposed TPQ biogenesis mechanism in HPAO-1. Figure adapted from (*6*).

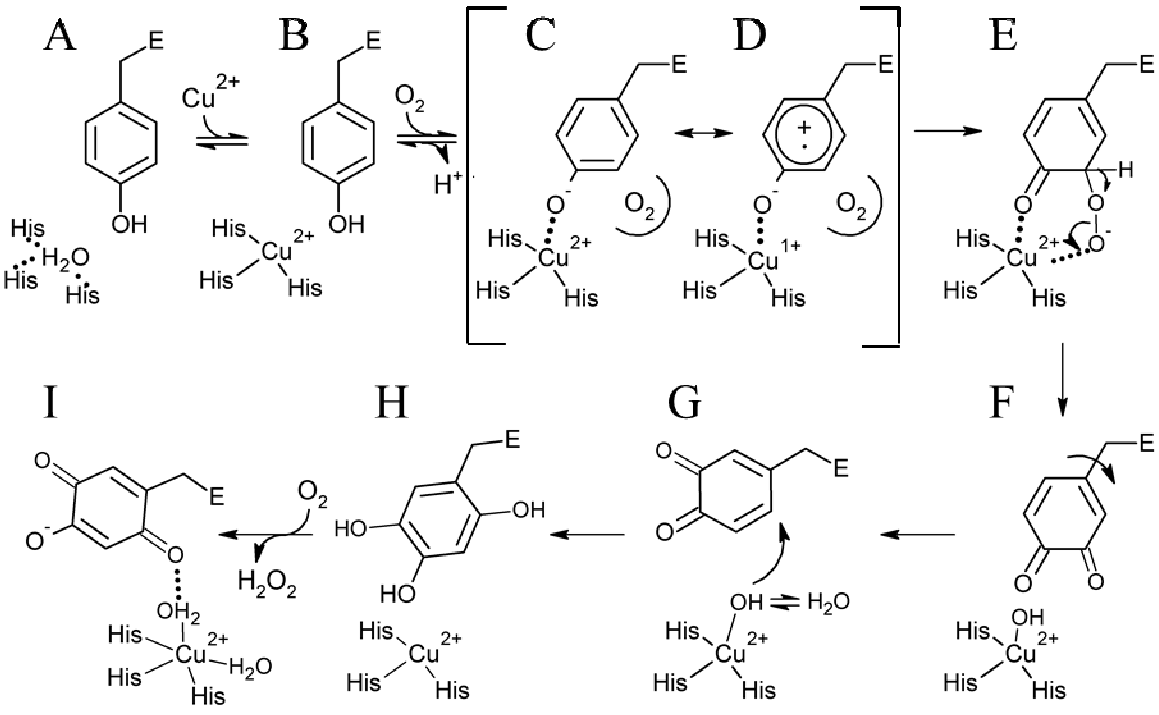

Support for the oxygen-dependent formation of a tyrosine/copper complex comes from spectroscopic studies carried out using apoHPAO-1 (*70*). The pre-incubation of apoHPAO-1 with copper followed by exposure to molecular oxygen resulted in a feature that absorbs at λ_{max} = 350 nm (*70*). This species decays isosbestically with the formation of TPQ, as indicated by a broad feature absorbing at 480 nm. Importantly, oxygen was

found to be required but not consumed during this process, suggesting that oxygen binding results in a conformational change in the side chain of the precursor tyrosine residue. This movement, followed by deprotonation of the tyrosine, results in the formation of a ligand-to-metal charge transfer (LMCT) species that gives rise to the feature at 350 nm (C in Scheme 1.2) (*70*). A putative oxygen binding pocket composed of residues Met634, Tyr407, and Leu425 has been identified in HPAO-1, and the rate of TPQ biogenesis is linked to the volume of the hydrophobic residue at position 634 (*71, 72*).

The Cu(II)-tyrosine complex, along with its Cu(I)-tyrosyl radical resonance form (D in Scheme 1.2), is activated for monooxygenation at position 3 of the tyrosine ring by the prebound O_2, which forms a bridged peroxo adduct (C/D→E in Scheme 1.2). This species rapidly collapses to produce dopaquinone (DPQ) (E→F in Scheme 1.2). The DPQ ring flips ~180° about its Cα-Cβ bond by an unknown mechanism (F→G in Scheme 1.2), which leaves it positioned for the incorporation of a second oxygen atom from a copper-activated water/hydroxyl at position 6 of the ring (G→H in Scheme 1.2). This produces TPQ_{red} (2,4,5-trihydroxyphenylalanine = 2-electron reduced TPQ) (H in Scheme 1.2), which is then oxidized to mature TPQ with the concomitant reduction of molecular oxygen to hydrogen peroxide (H→I in Scheme 1.2). Lastly, TPQ moves to the catalytically productive "off-copper" position seen in structures of native CAO (I in Scheme 1.2).

The preceding mechanism is strongly supported by a crystallographic investigation of TPQ biogenesis in apoAGAO (*68*). The crystal structure of apoAGAO

has been solved to a resolution of 2.2 Å, and unambiguously shows the precursor tyrosine residue (Y382 in AGAO) in its unmodified form with its hydroxyl group pointed toward the vacant metal binding site (*6*) (Figure 1.5A). This residue and the three conserved active site histidine residues which ligate copper in the native enzyme (His431, His433, and His592 in AGAO) are arranged around the empty metal binding site in a tetrahedral geometry. His431 and His433 adopt the conformers seen in the native enzyme, but His592 is present as two conformers, indicating some positional flexibility at this site. The two water molecules normally observed in the native CAO active site which ligate the copper (W_a and W_e in Figure 1.4A) are absent in the apoAGAO structure.

A series of crystal structures containing AGAO biogenesis intermediates were solved by exposing anaerobic apoAGAO crystals, which had been prebound with Cu(II), to O_2 followed by freezing after different lenghts of time (*68*). This study produced structures of an anaerobic complex between apoAGAO and Cu(II) (flash-frozen after 0 min of O_2 exposure), an early intermediate (flash-frozen after 10 min of O_2 exposure), and a late intermediate (flash-frozen after 100 min of O_2 exposure) of biogenesis (B, C, and D in Figure 1.5, respectively), which are consistent with the mechanism presented in Scheme 1.2. Finally, exposure of apoAGAO crystals prebound with Cu(II) to O_2 for a week before flash-freezing resulted in the structure of a species identical to holoAGAO, confirming that biogenesis can occur to completion in the crystal (E in Figure 1.5).

Figure 1.5 Structurally characterized TPQ biogenesis intermediates in AGAO: (A) apoAGAO (PDB code 1avk) (B) apoAGAO/Cu(II) complex (PDB code 1ivu) (C) dopaquinone (DPQ)-containing early intermediate (PDB code 1ivv) (D) 2-electron reduced TPQ (TPQ_{red})-containing late intermediate (PDB code 1ivw) and (E) holoAGAO generated in the crystal (PDB code 1ivx). Residues are shown in stick and colored by atom type (carbon, grey). Copper ions are shown as gold spheres, and water molecules are shown as small red spheres. Solid lines indicate metal-ligand interactions, and a dashed line indicates a hydrogen bond.

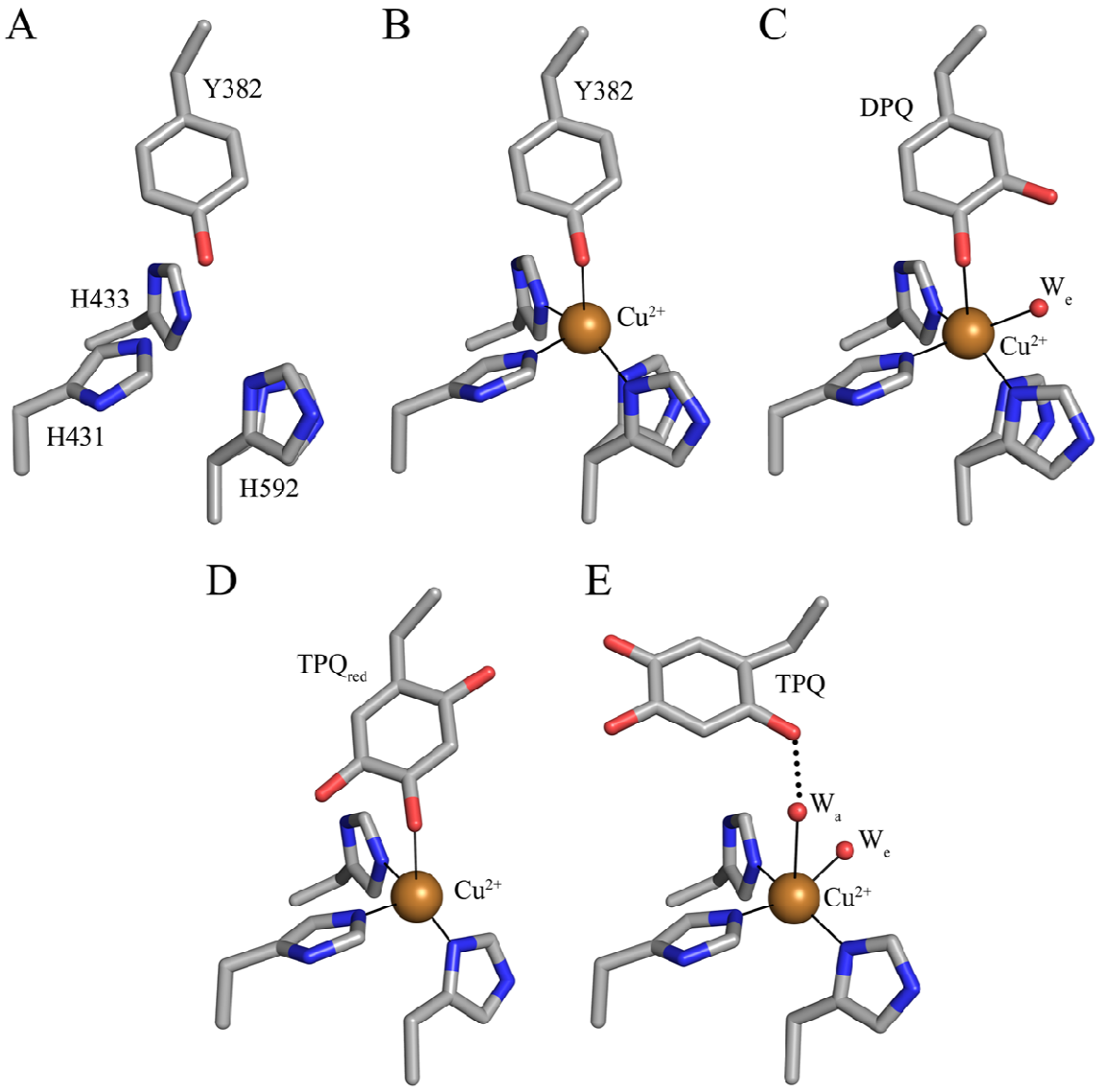

The structure of the anaerobic complex between apoAGAO and Cu(II) was solved to a resolution of 1.9 Å (Figure 1.5B). The electron density clearly shows the unmodified side chain of Tyr382, consistent with the requirement of molecular oxygen for TPQ biogenesis. The phenolic group of Tyr382 is thought to be protonated based on the distance between its hydroxyl group and the bound copper (~2.5 Å). Aside from the bound copper ion, this structure is identical to that of apoAGAO (Figure 1.5A), and represents the first step prior to the formation of TPQ, activating the precursor tyrosine side chain for monooxygenation at position 3 of the phenyl ring.

The structure of apoHPAO-1 in complex with Zn(II) (PDB code 1ekm) solved to 2.5 Å resolution reinforces the importance of the tyrosyl/copper complex in activating the precursor tyrosine ring for the initial oxygenation reaction (*73*). Zinc is known to bind tightly at the CAO active site and resist displacement by copper (*74*). Because zinc cannot support TPQ production, the structure of the Zn(II)-apoHPAO-1 complex mimics the copper binding step (A→B in Scheme 1.2) prior to biogenesis. Similar to the anaerobic Cu(II)-apoAGAO complex, zinc was found to bind at the copper binding site, ligated by the three conserved histidine residues and the unmodified precursor tyrosine residue in a tetrahedral geometry (*73*).

A crystal structure containing the dopaquinone intermediate formed during TPQ biogenesis was solved to a resolution of 2.1 Å (C in Figure 1.5) (*68*). The electron density confirmed that in this intermediate one oxygen atom had been inserted into the ring of Tyr382, and the residue had been modified to dopaquinone. An additional feature of this structure is the presence of an equatorial water ligand at a distance ~2.1 Å from

the copper center (W_e in Figure 1.5C) that is absent in the anaerobic complex between apoAGAO and Cu(II) (Figure 1.5B).

Exposure of apoAGAO crystals to O_2 for 100 min trapped the TPQ_{red} intermediate formed during biogenesis, which was solved to a resolution of 1.9 Å (Figure 1.5D) (*68*). As indicated by the electron density, two oxygen atoms had been inserted into the Tyr382 ring, forming either TPQ_{red} or TPQ. This intermediate is formed only after the rotation of the dopaquinone ring by ~180°, resulting in a species in which the O4 atom acts as a direct ligand to the bound copper. Single crystal microspectrophotometry experiments as well as the presence of a hydrogen bond between the O2 atom of the ring with the backbone carbonyl of Thr403 (indicating that the O2 atom is protonated), confirmed that this species is TPQ_{red} and not TPQ (*68*).

Biogenesis requires precise control in terms of positioning the precursor tyrosine residue and the intermediates formed during biogenesis within the active site. These species undergo rotations about their Cα-Cβ and Cβ-Cγ bonds to occupy both on- and off-copper positions. A number of active site residues, including some within the consensus sequence which contains the precursor tyrosine residue, contribute to this high level of conformational regulation by stabilizing the emerging cofactor in conformations accessed during biogenesis (Figure 1.6).

A strictly conserved active site tyrosine residue (Tyr305 in HPAO-1) is involved in a short hydrogen bond with the O4 atom of TPQ, helping to stabilize it in the appropriate position for catalysis of amine oxidation. The mutation of Tyr305 to a phenylalanine residue interferes with normal O—O bond cleavage during biogenesis and

results in indiscriminant oxidative damage, indicating that this strictly-conserved residue plays a role in conformational stabilization of the precursor tyrosine residue during biogenesis as well (*75*). In HPAO-1, the mutation of the strictly conserved residue N-terminal to the precursor tyrosine (Asn404) to an alanine results in only 5-10% TPQ formation relative to the native enzyme, while the mutation of Asn404 to an aspartate results in a 2-fold decrease in k_{TPQ} (*70, 76*). The rate of TPQ biogenesis is also decreased by an order of magnitude when the residue C-terminal to the precursor tyrosine in HPAO-1 (Glu406) is mutated to a glutamine (*70*). These effects illuminate the importance in balancing the chemical properties of active site residues during biogenesis such that they allow for flexibility of the precursor tyrosine side chain at appropriate times but stabilize it at others.

Figure 1.6 Amino acid residues in HPAO-1 that are involved in stabilizing biogenesis intermediates. Residues are shown in stick and colored by atom type (carbon, grey). The active site copper ion is shown as a gold sphere, and a water molecule is shown as a small red sphere. Dashed lines indicate hydrogen bonds.

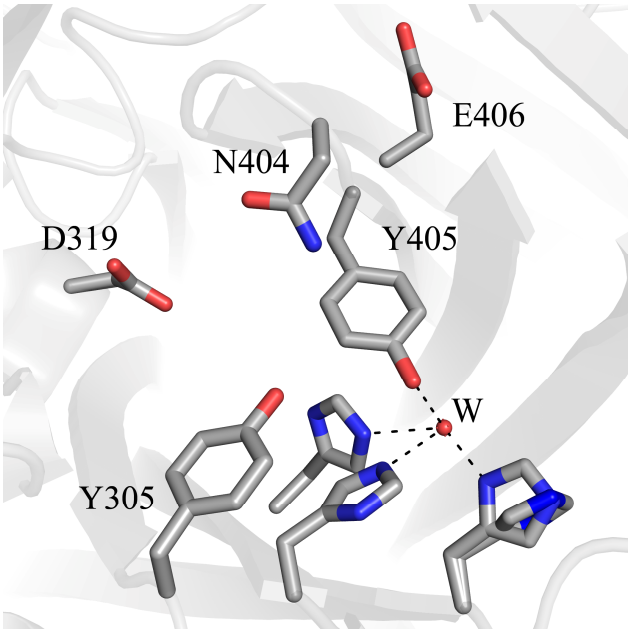

After the 6-electron oxidation of tyrosine, the resultant TPQ cofactor serves as a chromophoric handle that allows for both biogenesis and changes in the electronic properties of TPQ during catalysis (discussed next) to be monitored. ApoCAO protein is colorless with no UV/visible absorption peak, whereas the mature protein is yellow-pink in color (λ_{max} = 480 nm) due to electronic transitions within the cofactor (*77*). When apoHPAO-1 is aerobically reconstituted with Cu(II), an intermediate absorbing at 380 nm forms and decays before the formation of the species at 480 nm which indicates mature TPQ (Figure 1.7). The rates of formation and decay of the 380 nm species are unaffected by pre-incubation with zinc or the addition of Cu(II) to the mature TPQ-containing HPAO-1. Thus, this species is thought to arise from an off-pathway LMCT interaction (*70*).

Figure 1.7 Solution UV/visible spectra showing the time course of the aerobic reconstitution of apoHPAO-1 with Cu(II) at pH 7.0. The directions of change for UV/visible absorbance features over time are indicated by arrows.

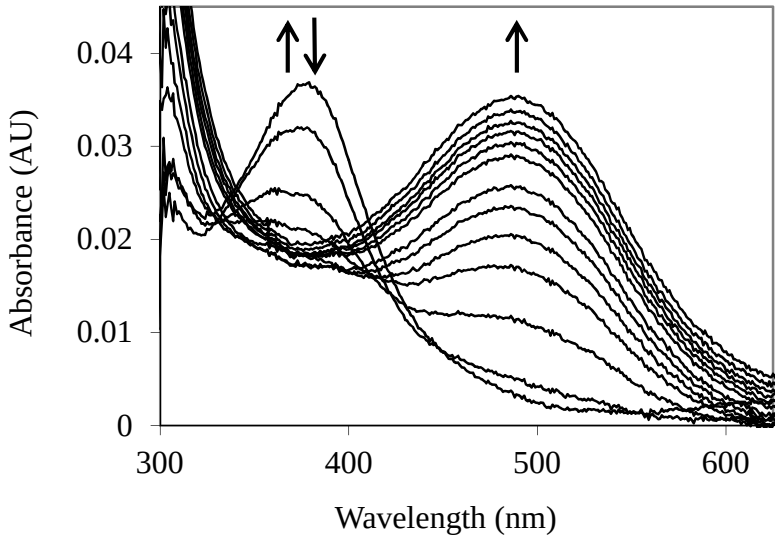

The copper bound at the CAO active site is ligated by three N and one/two O ligands and thus is type 2 or "non-blue" copper. Consequently, the intense spectral feature absorbing at ~600 nm associated with type 1 "blue" copper sites (ε = ~5000 $M^{-1}cm^{-1}$) due to the presence of a cysteinic sulfur ligand is absent in CAO (*78*). The coupling of X-ray crystallography with single crystal spectroscopy is a powerful tool, allowing chromophoric species formed during enzymatic reactions to be identified before, during, and after X-ray data collection.

1.7 Catalysis in CAOs

Catalysis in CAOs utilizes a ping-pong mechanism and therefore can be thought of as two distinct half-reactions: (1) the oxidation of primary amine substrates, generating product aldehyde and the 2-electron reduced aminoquinol form of the cofactor, in which the O5 atom is displaced by a substrate-derived amine group (known as the reductive half-reaction) and (2) the re-oxidation of TPQ with concomitant reduction of O_2 to H_2O_2 and the release of NH_4^+ (known as the oxidative half-reaction) (Scheme 1.3).

Scheme 1.3 The two half-reactions of CAO catalysis. $RCH_2NH_3^+$ is representative of all primary amines; TPQ_{amq}, aminoquinol.

reductive half-reaction: $\text{E-TPQ} + RCH_2NH_3^+ \rightarrow \text{E-TPQ}_{amq} + RCHO$

oxidative half-reaction: $\text{E-TPQ}_{amq} + O_2 + H_2O \rightarrow \text{E-TPQ} + H_2O_2 + NH_4^+$

The active site of resting native CAO contains oxidized TPQ and Cu(II) (A in Scheme 1.4). Catalysis is initiated with a nucleophilic attack by a primary amine at the

C5 atom of TPQ, forming a covalent substrate Schiff base complex between the two (A→B in Scheme 1.4). Proton abstraction by a conserved aspartate residue from the C1 atom of the substrate, which is expected to have a decreased pK_a, forms the corresponding product Schiff base species (D in Scheme 1.4) via the rapid rearrangement of a carbanionic intermediate (C→D in Scheme 1.4) (*79*, *80*). Hydrolysis of the product Schiff base releases the corresponding aldehyde product and leaves the cofactor as a 2-electron reduced aminoquinol (D→E in Scheme 1.4) (*80*).

Scheme 1.4 Proposed CAO catalytic mechanism. $RCH_2NH_3^+$ is representative of all primary amine substrates.

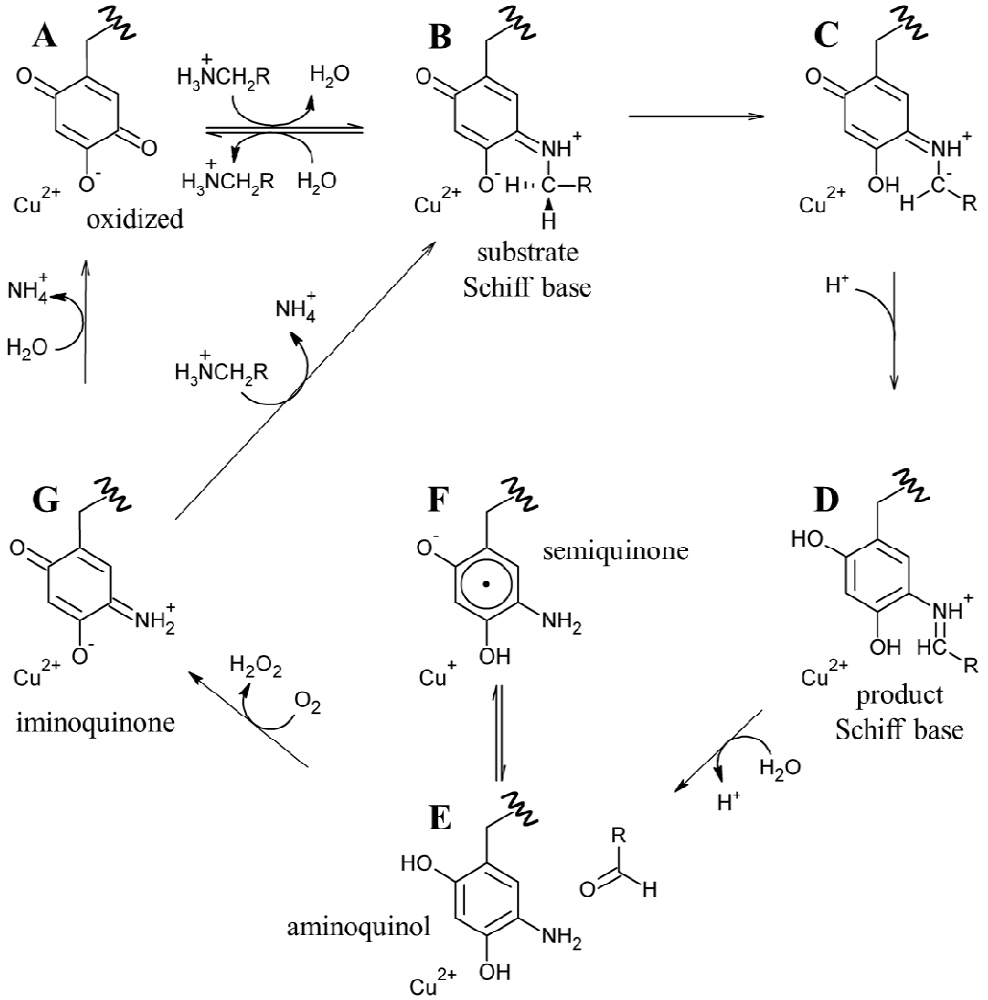

The aminoquinol marks the conclusion of the reductive half-reaction, and acts as the initial intermediate during the oxidative half-reaction. While the study of CAOs from several sources has led to a general consensus regarding the reductive half-reaction, details concerning the oxidative half-reaction have remained unclear, particularly concerning the nature of the first electron transfer from reduced cofactor to O_2 (*81*). Reduced TPQ exists in an equilibrium between the aminoquinol/Cu(II) couple and a semiquinone radical/Cu(I) form (E and F, respectively, in Scheme 1.4) (*82*). The distribution of the aminoquinol/semiquinone equilibrium is source-, pH-, and temperature-dependent (*83-85*). At pH 7, CAOs derived from plant sources form as much as 40% semiquinone when anaerobically reduced with substrate, while other non-plant eukaryotic CAOs contain very low levels of semiquinone near or below the limit of detection (*83*). Bacterial CAOs contain semiquinone at levels somewhere in between those of the two eukaryotic groups.

Two proposals to describe the first electron transfer to O_2 have been put forth. The first utilizes an inner sphere electron transfer mechanism, in which O_2 binds to the reduced copper in the semiquinone/Cu(I) couple. This is followed by electron transfer from Cu(I) to O_2 to form copper(II)/superoxide. The transfer of another electron and two protons from the semiquinone to the superoxide yields the iminoquinone form of cofactor (G in Scheme 1.4) and hydrogen peroxide (*82, 86*). Support for an inner sphere electron transfer mechanism derives from the detection of the semiquinone radical form of TPQ (*82*) and the demonstration of a catalytically competent electron transfer rate from the aminoquinol to Cu(II), which is greater than the rate-limiting step for catalysis with any

amine oxidase (*85, 87*). Additionally, azide, which is expected to ligate copper, was found to exhibit competitive inhibition with respect to O_2 in PSAO and a CAO isolated from pig plasma, as well as partially competitive inhibition in DAO (*88, 89*).

An outer sphere electron transfer mechanism has also been proposed, in which an electron from aminoquinol is transferred directly to O_2 bound in a nearby hydrophobic pocket, forming superoxide and the semiquinone (*71, 90*). This mechanism does not involve an obligate change in the oxidation state of the copper, with its primary role being to stabilize the resultant superoxide. A kinetic study using BSAO demonstrated that the single electron reduction of O_2 is rate-limiting during the oxidative half-reaction (*71*). Chemical intuition suggests that this should be a fast process if the electron is derived from reduced Cu(I); thus an outer sphere electron transfer mechanism consistent with the kinetic data was proposed. Major support for an outer sphere electron transfer mechanism derives from work done with HPAO-1 (*90, 91*). The removal of copper from the HPAO-1 active site followed by reconstitution with Co(II) resulted in fully-functional protein with kinetic parameters indistinguishable from those of the native enzyme (*91*). In addition, copper-depleted lentil seedling amine oxidase (LSAO) that was fully reconstituted with Co(II) regained partial catalytic competency (*92*). The reduction potential of the Co(II)/Co(I) couple is very low (for example -400 to -500 mV vs. standard hydrogen electrode (SHE) in methionine synthase) (*93*). Co(II) is thus unlikely to be reduced during Co(II)-mediated catalysis, suggesting that a redox role for copper is unnecessary in the native enzyme. The use of a hydrophobic oxygen binding site near the copper is supported by kinetic data indicating that oxygen binding in HPAO-1 is

noncompetitive with azide, which is predicted to bind at the active site copper (*94*). In addition, the oxidation of a model compound for the reduced cofactor has been shown to occur in the absence of metal (*90*). Finally, the semiquinone in some anaerobically reduced CAOs is virtually undetectable, which lends additional support to an outer sphere electron transfer mechanism.

The issue of the first electron transfer from cofactor to O_2 is being actively pursued, and it has been suggested that CAOs may be capable of using more than one mechanism to reduce O_2, but that each different CAO has a clear preference for either inner or outer sphere electron transfer (*95, 96*). Regardless, O_2 ultimately accepts two electrons and two protons from the cofactor, yielding H_2O_2 and the oxidized iminoquinone (G in Scheme 1.4). Hydrolysis of the iminoquinone releases product ammonium and regenerates oxidized TPQ (G→A in Scheme 1.4). Alternatively, when substrate levels are high the iminoquinone can react with a second amine, releasing product ammonium and generating the substrate Schiff base (G→B in Scheme 1.4).

Similar to biogenesis, catalysis in CAO can be monitored spectroscopically owing to changes in the electronic form of TPQ, both in solution and in crystallo (Table 1.2).

Table 1.2 λ_{max} of spectroscopic intermediates formed during CAO catalysis.

Catalytic Intermediate	λ_{max}
TPQ (quinone)[a]	480
substrate Schiff base[b]	340
product Schiff base[c,d,e]	380
aminoquinol[b]	310
semiquinone[f]	360, 435, 465
iminoquinone[g,h]	450 or 350 (if charge is delocalized, as in HPAO-1)
Cu(II)-peroxy[g]	410

From refs. [a](*97*), [b](*98*), [c](*76*), [d](*99*), [e](*100*), [f](*82*), [g](*101*), [h](*102*)

A number of catalytic intermediates formed during both half-reactions have been structurally characterized. The active sites from structures of native TPQ-containing CAOs from a variety of organisms (Table 1.1) are nearly identical and contain oxidized TPQ, copper ligated by the imidazole groups of three strictly conserved histidine residues, an aspartate residue that acts as the catalytic base during catalysis, and several conserved water molecules. The active site structure of HPAO-1 is shown in Figure 1.8A (*103*). As described previously, catalytically productive TPQ in the native enzyme is in an "off-Cu" conformation with its C5 carbonyl pointed toward the substrate amine channel, ideally positioned for attack by a primary amine substrate. This conformation is stabilized by hydrogen bonding between the O2 atom of TPQ and an axial water molecule (W_a in Figure 1.8A), and between the O4 atom of TPQ and the hydroxyl of a conserved tyrosine residue. Results from resonance Raman spectroscopy using AGAO indicate that underivatized TPQ exhibits significant electron delocalization between the C2 and C4 oxygen atoms, with only the C5 atom possessing significant C=O character

(*104*). This is consistent with the formation of a covalent cofactor-substrate Schiff base complex following nucleophilic attack at the C5 position during catalysis as opposed to the C2 or C4 positions.

Figure 1.8 Structurally characterized intermediates formed during the CAO reductive half-reaction: (A) native HPAO-1 active site (PDB code 2oov) (*103*) (B) ECAO containing a substrate Schiff base analog formed with the inhibitor 2-hydrazinopyridine (PDB code 1spu) (*80*) (C) D298A AGAO containing the product Schiff base (PDB code 2cwv) (*105*) (D) substrate-reduced ECAO containing the aminoquinol (PDB code 1d6u) (*106*). Residues are shown in stick and colored by atom type (carbon, grey). Copper ions are shown as gold spheres, and water molecules are shown as small red spheres. Dashed lines indicate hydrogen bonding, and solid lines indicate metal-ligand interactions.

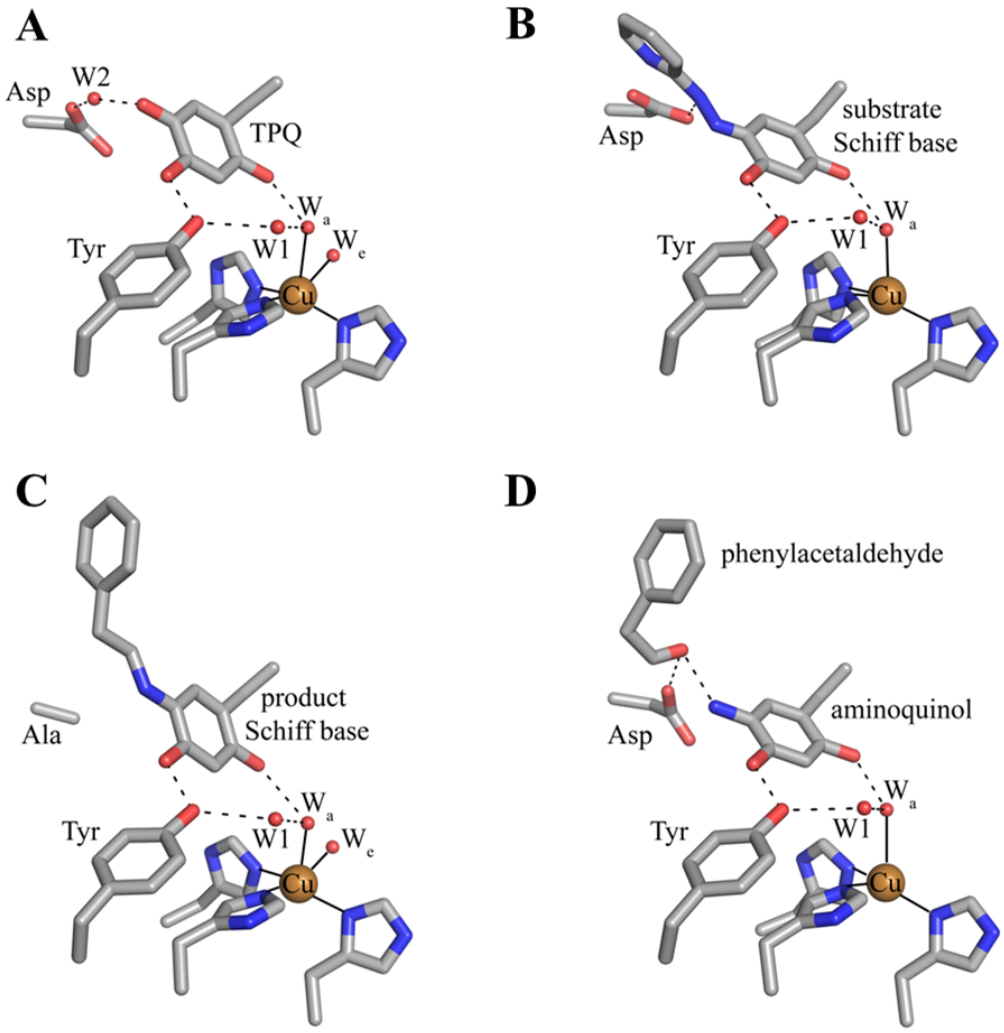

The structure of ECAO in a covalent complex with the inhibitor 2-hydrazinopyridine has been solved to a resolution of 2.0 Å (*80*) (Figure 1.8B). The inhibitor was found to bind to atom C5 of the cofactor, displacing the O5 atom and generating a Schiff base analog (B in Scheme 1.4). Because 2-hydrazinopyridine contains a nitrogen atom instead of a carbon at the Cα position, the Schiff base analog formed with the inhibitor cannot be deprotonated and thus accumulates in the crystal. The pyridine and quinone rings are not coplanar, suggesting that the complex is an analog of the substrate Schiff base and not the product Schiff base. A notable feature of this structure is the hydrogen bond between a nitrogen atom (corresponding to Cα in a physiological Schiff base) of the inhibitor/cofactor complex and a strictly conserved active site aspartate residue, which suggested this residue as the general catalytic base in the reductive half-reaction that abstracts a proton from the substrate Schiff base (*106*). This was unequivocally confirmed through the study of twelve amino acid variants at this site in ECAO, which established that only glutamate had catalytic activity, although its k_{cat} was reduced by a factor of 6.4×10^4 compared to the native aspartate (*79, 80*).

The mutation of the active site aspartate residue (D298 in AGAO) to an alanine in AGAO results in a decrease in catalytic efficiency by ~10^6 orders of magnitude, with a low level of activity possibly due to water acting as a base (*105*). The incubation of D298A AGAO crystals with the physiological substrate 2-phenylethylamine for one week before freeze-trapping and structure solution resulted in a 1.85 Å resolution crystal structure containing a product Schiff base intermediate (Figure 1.8C). This assignment was confirmed by single crystal microspectrophotometry (*105*). The product Schiff base

has not been observed in solution, presumably due to the fast rate of hydrolysis which produces aldehyde and the aminoquinol (D→E in Scheme 1.4). In the crystal, however, the reaction is considerably slower and the product Schiff base is able to accumulate. The Cβ atom of the product is coplanar with the TPQ ring and the imine double bond in this structure, which is anticipated for the product Schiff base formed with 2-phenylethylamine (Figure 1.8C).

The 2-electron reduced aminoquinol is the final cofactor intermediate formed during the reductive half-reaction, and marks the initiation of the oxidative half-reaction. Crystals containing the aminoquinol at the active site were prepared by freeze-trapping crystals of ECAO after their anaerobic reduction with 2-phenylethylamine, and the structure of this species was solved to a resolution of 2.4 Å (Figure 1.8D) (*106*). Single crystal microspectrophotometry indicated that the species was bleached, which is consistent with the aminoquinol (Table 1.2) (*98*). Present in the "off-Cu" conformation, the aminoquinol interacts with the copper ion through the axial water molecule seen in native CAO structures. A surprising feature in this structure was the presence of phenylacetaldehyde product bound at the back of the active site. Crystal contacts appeared to inhibit interdomain movement such that the ping-pong kinetics seen in solution were disrupted and aldehyde remained trapped in the enzyme at the back of the active site (*106*).

Intermediates formed during the oxidative half-reaction that have been structurally characterized are shown in Figure 1.9. The oxidative half-reaction involves the re-oxidation of TPQ, and begins with TPQ in an equilibrium between the

aminoquinol/Cu(II) couple and a semiquinone radical/Cu(I) species. A structure containing the aminoquinol has been solved, and is described in the preceding paragraph. Currently there is no published crystal structure of a reduced CAO containing semiquinone and Cu(I).

Figure 1.9 Structurally characterized intermediates formed during the CAO oxidative half-reaction: (A) substrate reduced ECAO containing the aminoquinol (PDB code 1d6u) (*106*), (B) ECAO containing the iminoquinone (PDB code 1d6z) (*106*). Residues are shown in stick and colored by atom type (carbon, grey). Copper ions are shown as gold spheres, and water molecules are shown as small red spheres. Hydrogen bonding interactions are indicated by dashed lines, and metal-ligand interactions are indicated by solid lines.

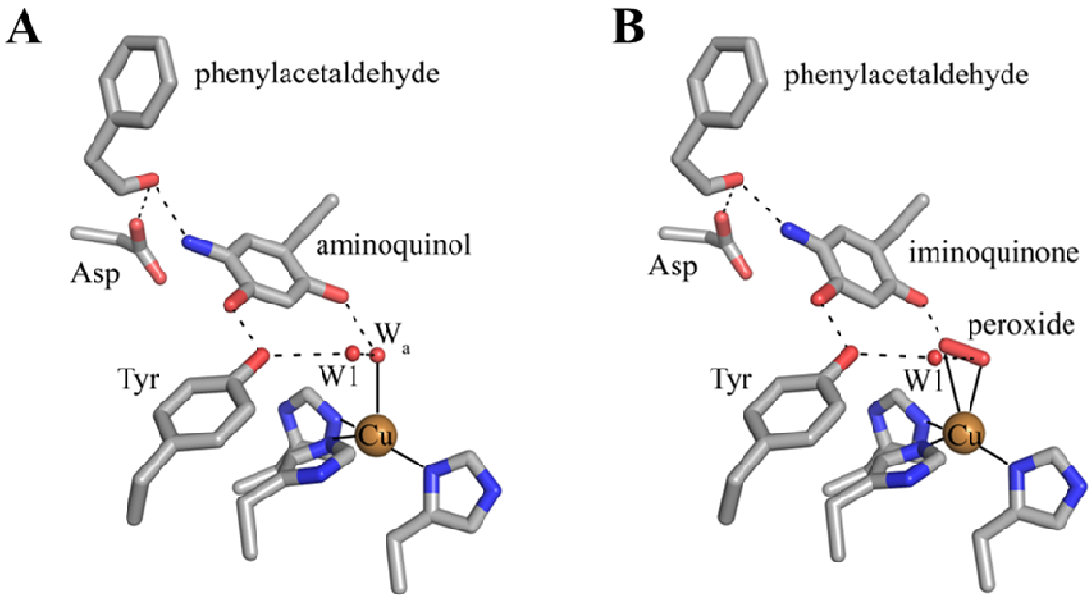

A structure containing the iminoquinone intermediate formed during catalysis was solved after the prolonged aerobic exposure of an ECAO crystal to 2-phenylethylamine (Figure 1.9B) (*106*). This steady-state structure contains not only the iminoquinone, but an oxygen species that has displaced the axial water molecule in the structure containing aminoquinol (Figure 1.9A). Phenylacetaldehyde product remains bound in the back of

the active site in the same position it occupies in the aminoquinol-containing structure (Figure 1.9A). The side-on geometry of the oxygen species and the presence of iminoquinone and product aldehyde suggested that this was most likely the product hydrogen peroxide. The presence of an oxygen species bound at the copper coincident with product aldehyde again demonstrates that in the crystal, the ping-pong kinetics seen in solution have been disrupted (*106*).

Finally it is well documented that CAOs function as obligate dimers, and evidence suggests that some, but not all, CAOs exhibit cooperativity through long-range conformational changes propagated through the CAO dimer from one active site to the other (*80, 107-110*). BSAO and ANAO exhibit half-site reactivity with regard to hydrazine inhibitors (*107, 108, 111*). In additional kinetic work using HPAO-1, heterodimers that contain zinc bound in one active site of the HPAO-1 dimer and copper in the second could not efficiently carry out the oxidative half-reaction at either active site, suggesting that communication between the two metal binding sites influences oxidative chemistry (*112*). It has been suggested that metal binding in one CAO active site induces conformational changes through a network of interactions that cross the dimer interface (*112*).

1.8 CAO channels and access to the active site

The substrates consumed during CAO catalysis (a primary amine and O_2) take different paths to the same deeply buried active site. A distinct substrate amine channel leads from the enzyme surface to the C5 atom of TPQ, the site of nucleophilic attack

during catalysis (a distance of ~18 Å in HPAO-1) (Figure 1.10B). Despite the well-conserved structural homology of the overall CAO fold, the dimensions and shape of the amine substrate channel vary radically depending on enzyme source. Amongst CAO homologs, only four amino acids within this channel display any sequence homology (besides the invariant aspartate residue which acts as the catalytic base and the consensus sequence containing the precursor tyrosine residue that is converted to TPQ). Position 323 (HPAO-1 numbering) corresponds to an aromatic residue, position 155 corresponds to either a proline or serine residue, position 305 corresponds to a tyrosine residue important in stabilizing TPQ, and position 156 corresponds to a bulky hydrophobic residue. This channel not only allows substrate amine access to the site of catalytic turnover, but also functions as an egress for product aldehyde exiting the active site.

Substrate preference in different CAOs is determined by the chemical properties of the residues lining the amine substrate/aldehyde product channel, as well as the general shape and size of this space. These vary significantly depending on enzyme source, with channels ranging from nearly obstructed (ECAO, Figure 1.10A) to channels so broad that entire peptides can be accommodated and serve as a substrate ((I) ANAO and (J) PPLO, Figure 1.10).

Figure 1.10 Diagram of the amine substrate channel in different CAOs. Each enzyme is shown as a grey molecular surface. TPQ is shown in stick and colored by atom type (carbon, white). Copper ions are shown as gold spheres. (A) ECAO (B) HPAO-1 (C) HPAO-2 (D) VAP-1 (E) DAO (F) PSAO (G) AGAO (H) BSAO (I) ANAO (J) PPLO.

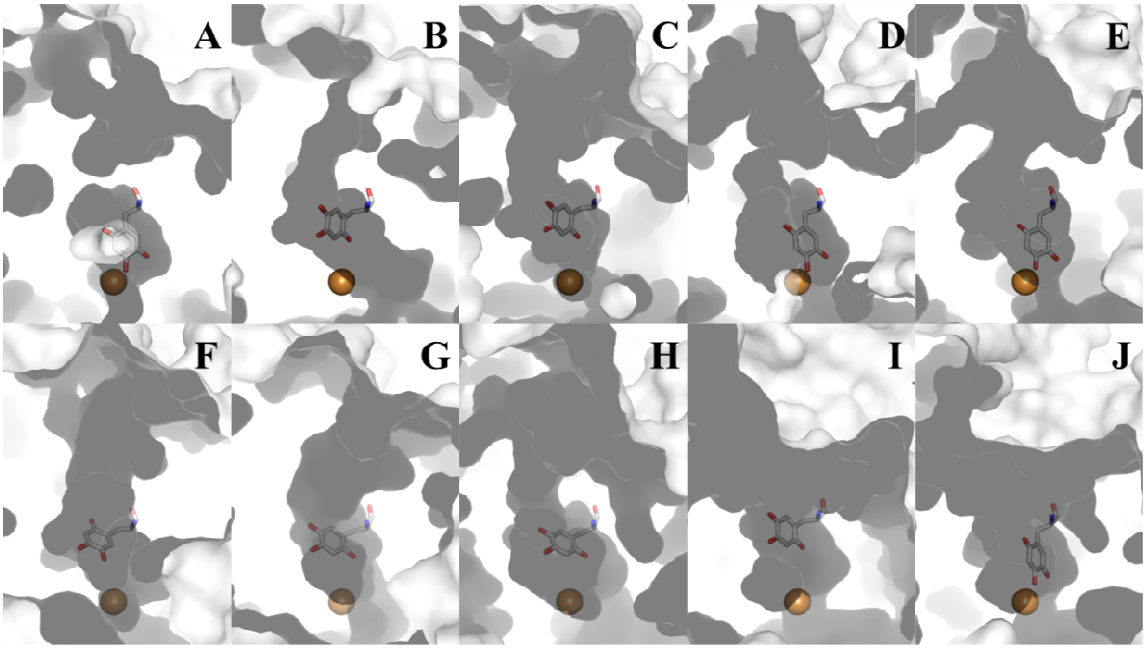

An additional proposed role for the residues lining the amine substrate channel involves the stereospecificity of the proton abstraction step during the CAO reductive half-reaction. Stereospecificity for this step varies depending on enzyme source and the identity of the amine substrate consumed (*113*, *114*). For example, PSAO selectively abstracts the *pro-S* proton from dopamine, tyramine, and benzylamine during the reductive half-reaction, while BSAO is non-stereoselective when dopamine or tyramine are used as a substrate, but abstracts the *pro-S* proton from Schiff base complexes formed with benzylamine, *p*-hydroxybenzylamine, and 3-methylbutylamine (*113*). In contrast, AGAO is known to selectively abstract the *pro-S* proton from Schiff base complexes formed with all substrates tested thus far (*115*). In all CAO homologs, the *pro-S* proton

from the Schiff base species formed with benzylamine is abstracted in favor of the *pro-R* proton. Given the strong structural homology between CAO active site residues, it has been suggested that the conformation of the substrate Schiff base complex itself is more important than the positions of active site residues relative to the amine substrate in determining the stereospecificity of the proton abstraction step (*116*). The residues lining the amine substrate channel are important for the accommodation of Schiff base intermediates and display relatively low sequence homology amongst CAOs compared to other regions of the protein. The interactions between these residues and the Schiff base complexes consequently influence the stereospecificity of the proton abstraction step during catalysis in a species- and/or substrate-dependent manner (*116*).

The second substrate consumed during catalysis, molecular oxygen, had previously been thought to travel to the CAO active site via the "inland lake" where the two monomers in the CAO dimer meet. While it is possible that the inland lake may act as a reservoir for molecular oxygen (based on potential of mean force (PMF) maps which illustrate regions of low free energy for the placement of O_2 inside the protein matrix) it has been proposed that the narrow polar channel connecting this region to the active site is more appropriate for exiting H_2O_2 (*103*). This is consistent with both the short length and polar nature of H_2O_2.

In order to visualize molecular oxygen movement through the protein matrix, crystal structures of the complex between CAO and xenon have been solved from several sources, including PSAO (*117*) , PPLO (*117*), ECAO (*118*), AGAO (*117*), and HPAO-1 (*103*). Xenon has the same volume as molecular oxygen and mimics oxygen binding in

hydrophobic pockets. Several recurrent O_2 binding sites have been identified from these xenon complexes, including in the β-sheet sandwich fold of the catalytic D4 domain, the amine substrate channel, and a channel from the inland lake.

Figure 1.11 Overlay of xenon binding sites in xenon/CAO complexes. Domain D4 from one HPAO-1 monomer is shown as a green cartoon, and active site residues are depicted in stick and colored by atom type (carbon, grey). Xenon atoms are shown as spheres and colored by enzyme source (PSAO, red; PPLO, yellow; AGAO, blue; HPAO-1, magenta). Arrows indicate the direction of O_2 movement toward the active site. Figure from (*103*).

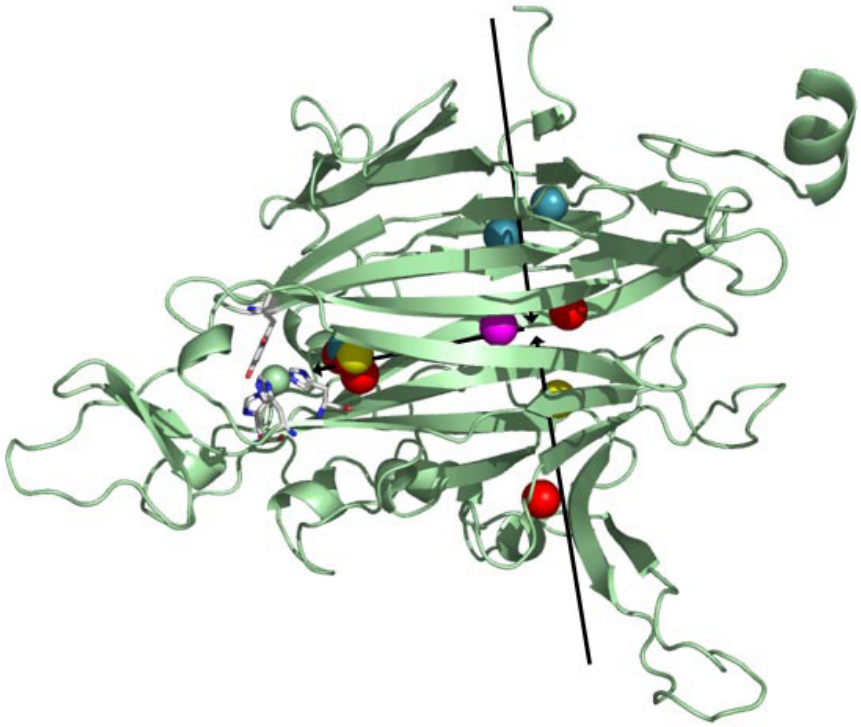

Taken together, crystallographic and PMF data from these studies suggest several species-dependent O_2 points of entry into the protein interior (two are shown as black arrows in Figure 1.11). After its initial entry into the protein matrix, O_2 is transiently held within the hydrophobic interior of domain D4, followed by migration closer to the active site where it is activated (Figure 1.11). Though the interior of domain D4 is largely composed of hydrophobic residues in all CAO homologs, source-specific

differences in the primary amino acid sequence of D4 could account for the different points of entry utilized by O_2 in different CAO homologs.

1.9 Research Goals

CAO is a bifunctional enzyme that catalyzes both the single-turnover production of its own "home-made" cofactor *in situ* as well as the multiple-turnover oxidative deamination of primary amines. The CAO active site displays remarkable plasticity, with the same set of active site residues supporting monooxygenase, hydrolase, and oxidase activities. In order to investigate mechanistic features related to both biogenesis and catalysis in CAO, X-ray crystallographic experiments were carried out using two CAOs from the yeast *Hansenula polymorpha* (HPAO-1 and HPAO-2). Only two metal-free CAO systems exist in which biogenesis can be readily studied: HPAO-1 and AGAO. The bacterial and yeast systems differ in several respects in terms of both biogenesis and catalysis, and as a eukaryotic CAO, HPAO-1 represents a well-suited model to study issues related to chemistry carried out by human CAO homologs. In addition, extensive biochemical and kinetic characterizations of both biogenesis and catalysis in HPAO-1 have been conducted, placing crystal structures of HPAO-1 within a rich biochemical context.

The crystal structure of a second CAO from the yeast *Hansenula polymorpha* (HPAO-2) that was identified from benzylamine-enriched media is reported in Chapter 2. A structural comparison of two CAO paralogs from *Hansenula polymorpha* (HPAO-1 and HPAO-2) in conjunction with steady state kinetic data available for each enzyme

when reacted with methylamine and benzylamine provide insight into substrate specificity, and help explain their different and opposing preferences for small aliphatic vs. aromatic amines.

Copper plays a critical role in the autocatalytic production of TPQ. The metal specificity for the step preceding biogenesis (metal binding) has been investigated and is presented in Chapter 3. The crystal structures of metal-free precursor HPAO-1 (apoHPAO-1) as well apoHPAO-1 in complex with Cu(I) or Co(II) have been solved, and add insight into the physiological use of copper during biogenesis. In addition, the features which determine whether alternate metals can initiate and support biogenesis are discussed.

The X-ray crystal structures of HPAO-1 in complex with three different primary amine substrates (methylamine, ethylamine, and benzylamine) are presented in Chapter 4. A comparison of substrate binding in these three complexes provides insight into substrate specificity and the changes incurred in the amine substrate channel. These structures represent the first structural study of substrate specificity using multiple physiological amines (all of which have been kinetically characterized) and their interactions in a single CAO.

Lastly, Chapter 5 presents the progress and future directions for two projects currently underway. The first involves attempting to reverse the small aliphatic vs. aromatic substrate preference of HPAO-1 and HPAO-2 proteins with mutations at a position in the primary sequence proposed to be a major contributor to substrate specificity (HPAO-1: Y323C; HPAO-2: C306Y). The crystal structures of these two

mutants are currently being pursued. An additional ongoing project utilizes the unnatural amino acid *p*-amino phenylalanine (pAF, aniline amino acid) incorporated at two positions in the HPAO-1 active site. An aniline amino acid has replaced either the precursor tyrosine residue which is transformed into TPQ (Y405pAF) or a conserved tyrosine residue which stabilizes the cofactor during biogenesis and catalysis (Y305pAF). Crystal structures of these aniline mutants would investigate the impact of redox potential vs. pK_a in the initial steps of biogenesis and are currently being pursued.

CHAPTER 2: THE PRECURSOR FORM OF *Hansenula polymorpha* COPPER AMINE OXIDASE-1 IN COMPLEX WITH CU(I) AND CO(II)

Klema, V.J., Johnson, B.J., Klinman, J.P., and Wilmot, C.M. (2012) The precursor form of *Hansenula polymorpha* copper amine oxidase 1 in complex with Cu(I) and Co(II), *Acta Crystallogr., Sect. F: Struct. Biol. Cryst. Commun. 68*, 501-510.

Copper amine oxidases (CAOs) catalyze the oxidative deamination of primary amines to their corresponding aldehydes, with the concomitant reduction of O_2 to H_2O_2. Catalysis requires two cofactors: a mononuclear copper center, and the cofactor 2,4,5-trihydroxyphenylalanine quinone (TPQ). TPQ is synthesized through the post-translational modification of an endogenous tyrosine residue, and requires only oxygen and copper to proceed. TPQ biogenesis in CAOs can be supported with alternate metals, albeit at decreased rates. A variety of factors are thought to contribute to the degree to which a metal can support TPQ biogenesis, including Lewis acidity, redox potential, and electrostatic stabilization capability. The crystal structure of one of two characterized CAOs from the yeast *Hansenula polymorpha* (HPAO-1) has been solved in its metal-free (apo) form, which contains an unmodified precursor tyrosine residue instead of fully-processed TPQ (HPAO-1 was denoted as HPAO in literature prior to 2010). The structures of apoHPAO-1 in complex with Cu(I) and Co(II) have also been solved, providing structural insight into metal binding prior to biogenesis.

2.1 Background

Copper amine oxidases (CAOs) are ubiquitous homodimeric enzymes responsible for the two-electron oxidative deamination of primary amines to their corresponding aldehydes. Found in aerobic organisms ranging from bacteria to higher eukaryotes, the physiological roles of CAOs and their sources are diverse. In bacteria and yeast, CAOs play a mainly metabolic role, enabling the use of primary amines as a sole source of carbon and/or nitrogen for growth (*6, 7*). The functions of these enzymes in higher eukaryotes are not as well understood, with CAOs thought to contribute to a number of complex processes including wound healing and cell wall maturation in plants; and inflammatory leukocyte extravasation, glucose regulation, and cell signalling in mammals (*10, 119, 120*). Aberrant human CAO activity has been linked to a number of disease states marked by protein crosslinking, including Alzheimer's disease, diabetic complications, and congestive heart disease (*22, 27, 121*).

Despite their wide variety of sources and biological functions, all CAOs catalyze the same chemistry: the oxidative deamination of primary amine substrates coupled to the reduction of O_2 to H_2O_2 in the following overall reaction (*28, 119, 122*):

$$RCH_2NH_3^+ + O_2 + H_2O \rightarrow RCHO + NH_4^+ + H_2O_2$$

CAOs are a member of a growing number of bifunctional enzymes which synthesize their own organic cofactors de novo. This increases the diversity of chemical properties available to an enzyme active site beyond that afforded by the twenty canonical amino acid side chains. In the case of CAOs, the redox-active cofactor 2,4,5-

trihydroxyphenylalanine quinone (TPQ) is produced autocatalytically by the oxidation of an endogenous tyrosine residue (Scheme 1.1) (*28, 64, 65*). This process occurs without auxiliary proteins and requires only the presence of oxygen and copper.

Understanding the role of copper is necessary for a complete picture of TPQ biogenesis in CAOs. Previous spectroscopic, kinetic, and structural studies suggest a critical role for copper via its direct ligation with the precursor tyrosine residue. In HPAO-1, this is thought to activate the phenolic ring for monooxygenation by prebound molecular oxygen in a nearby site (*69, 70, 73*). It had previously been believed that only copper, the physiologically relevant metal in CAOs, could support the biogenesis of TPQ. Works done with metal-free precursor CAOs from the yeast *Hansenula polymorpha* (HPAO-1) and the bacterium *Arthrobacter globiformis* (AGAO) have challenged this, revealing that alternate metals can support TPQ formation in vitro, albeit at decreased rates (Table 2.1) (*70, 123-125*).

Table 2.1 k_{TPQ} for biogenesis in HPAO-1 and AGAO supported by various metals.

	HPAO-1 (h^{-1})	AGAO (h^{-1})
Cu(II)	4.8 ± 0.2^{a}	$90 \pm 12^{b,e}$
Cu(I)	0.28 ± 0.06^{c}	Unmeasured
Ni(II)	0.028 ± 0.006^{d}	$(7.5 \pm 0.12) \times 10^{-2\ b,e}$
Co(II)	not supported	$(7.92 \pm 0.24) \times 10^{-2\ b,e}$
Zn(II)	not supported	not supported

Data from refs. [a] (*70*), [b] (*125*), [c] (*124*), [d] (*123*). [e] Data originally reported in min^{-1}

In HPAO-1, the biogenesis of TPQ can proceed with a Cu(II), Cu(I), or Ni(II) ion bound at the metal binding site, but is not supported by Co(II) (*70, 123, 124*). In contrast, TPQ biogenesis in AGAO is supported by bound active site Co(II) as well as Cu(II) and Ni(II) (*125*). Zn(II) is unable to promote TPQ biogenesis in CAOs, and furthermore resists displacement by copper when bound to the CAO active site (*74, 126*).

The initial assumption that it was necessary to fully reduce Cu(II) to form a Cu(I)-tyrosinate species for tyrosine ring activation has been challenged by studies using metal-free precursor (apo) AGAO (apoAGAO) and HPAO-1 (apoHPAO-1) (*124*). Although TPQ biogenesis is supported by Ni(II) and Co(II) in AGAO, the very low reduction potentials for both the Ni(II)/Ni(I) (-1.16V vs. standard hydrogen electrode (SHE) in complexes with N/O ligands) and Co(II)/Co(I) (for example, -0.4 to -0.5V vs. SHE in methionine synthase) couples would disfavor a mechanism that requires the reduction of metal by the TPQ precursor tyrosine (*93, 127*). Kinetic measurements of TPQ biogenesis in apoHPAO-1 indicate that TPQ is produced in Cu(I)-supplemented apoHPAO-1 protein at a rate 17-fold slower than in Cu(II)-supplemented apoHPAO-1, which is ascribed to a prior requisite oxidation of Cu(I) to Cu(II) (*124*). Additionally, in a study of Ni(II)-initiated cofactor production in apoHPAO-1, electron paramagnetic resonance (EPR) spectroscopy revealed that the bulk of the bound nickel is EPR silent, consistent with a +2 oxidation state being maintained throughout biogenesis (*123*). These studies disfavor a mechanism in which Cu(II) must first be fully reduced to Cu(I) for the initiation of cofactor biogenesis (*123*). The fact that HPAO-1 is localized to the *H. polymorpha* peroxisome, together with the lack of free copper or copper transporters associated with

this organelle, suggests that copper is initially inserted into apoHPAO-1 in the reducing cytosol as Cu(I) before subsequent oxidation to Cu(II) and TPQ biogenesis (*128-130*).

In light of these data, Lewis acidity has been proposed to contribute to the ability of a metal to support cofactor biogenesis as Cu(II) is a better Lewis acid than Co(II) and Ni(II) (*123, 125*). This does not explain, however, the complete inactivity with the effective Lewis acid Zn(II) bound at the active site (*73*). Thus, the inherent reduction potential of a metal appears to play at least some part in metal specificity during biogenesis. Differences in the versatility of a metal's coordination sphere may act as additional factors which influence a metal's ability to support TPQ formation (*73, 125, 131*). The current data regarding the role of metal in TPQ biogenesis suggest that a combination of several factors, including redox properties, Lewis acidity, and electrostatic stabilization capabilities contribute to the degree to which a metal can initiate and support TPQ biogenesis in CAOs.

To visualize the initial step of biogenesis, the X-ray crystal structure of precursor HPAO-1 in the absence of metal (apoHPAO-1) has been solved to a resolution of 1.7 Å. In addition, X-ray crystal structures of apoHPAO-1 in complex with Cu(I) and Co(II) have been solved to resolutions of 1.9 and 1.27 Å, respectively, which provide insight into the structural role of metal during biogenesis.

2.2 Methods

Protein expression, purification, and characterization

Metal-free apoHPAO-1 protein was expressed and purified in *E. coli* as previously described (*70, 74, 123*). Zinc is known to bind tightly to the HPAO-1 active site and inhibit copper-mediated TPQ biogenesis (*74*). Therefore, to prepare functional precursor HPAO-1 which forms TPQ upon its aerobic incubation with copper, the growth medium and buffers used for apoHPAO-1 expression and purification were kept free of all divalent transition metals. All buffers and solutions were prepared using water with a resistance greater than 18 MΩ (Millipore Super-Q water purification system). Plastic flasks and beakers used during *E. coli* growth and protein purification were soaked in an ethylenediaminetetraacetic acid (EDTA) bath (0.5 M) before thorough rinsing with metal-free water. The precursor protein (at 40 μM) was assayed for TPQ formation activity in 50 mM HEPES, pH 7.0, by the addition of a $CuSO_4$ solution to a final concentration of 0.04 mM. Absorbance changes were monitored over the course of 1 hour to visualize the appearance of a 480 nm absorbance feature indicating the formation of TPQ using a Cary 50-Bio (Varian). ApoHPAO-1 protein at a concentration of 1.2 mg/mL in 50 mM HEPES was subjected to inductively coupled plasma-mass spectrometry (ICP-MS) at the University of Minnesota Aqueous Geochemistry Lab.

ApoHPAO-1 crystallization and preparation of apoHPAO-1/metal complexes

ApoHPAO-1 protein was buffer exchanged into 50 mM HEPES (pH 7.0) and concentrated to 13 mg/mL for crystallization. Crystals of apoHPAO-1 were grown by hanging drop vapor diffusion using a 1:1 volume ratio (6 μL total) of purified protein and crystallization solution (8-9.5% w/v polyethylene glycol 8000, 0.28-0.30 M potassium phosphate, pH 6.0) which had been mixed and incubated with a small amount of Chelex (Biorad) for at least 1 hour to remove any divalent metal present in the crystallization solution. After equilibrating for ~24 hours, drops were seeded using a streak seeding technique, with a mature native HPAO-1 crystal as seed donor (*132*). Colorless crystals grew to full size within 7-9 days. To eliminate the possibility of contamination from the native HPAO-1 protein seeds, a subsequent round of streak seeding was performed using apoHPAO-1 crystals as seed donors. Cryoprotection for all crystals was performed by soaking in 25% high purity glycerol mixed with well solution for ~10 seconds before flash freezing in N_2(l).

The apoHPAO-1 crystal complex with Co(II) was prepared by soaking an apoHPAO-1 crystal in a crystallization solution containing 10 mM $CoCl_2$ for 1 hour before cryoprotection and flash freezing in N_2(l). This soak was performed in ambient air as Co(II) does not support TPQ formation and it was not necessary to work anaerobically to prevent the initiation of biogenesis.

To prepare crystals of an anaerobic complex of apoHPAO-1 with Cu(I), a solution of tetrakis(acetonitrile)copper(I) hexafluorophosphate was made anaerobic by passing high purity N_2(g) over the solution headspace while stirring for >10 minutes in a septum-

covered vessel. This was immediately brought into an anaerobic glove box (Belle Technology). Trays containing apoHPAO-1 crystals were brought into the anaerobic glove box and allowed to equilibrate for at least 1 week. ApoHPAO-1 crystals were soaked in a crystallization solution containing 5 mM tetrakis(acetonitrile)copper(I) hexafluorophosphate for 1 hour before cryoprotection and flash freezing in N_2(l).

Data collection, structure solution, and refinement

X-ray diffraction data from single apoHPAO-1, Cu(I)-apoHPAO-1 and Co(II)-apoHPAO-1 crystals were collected at 100 K at the Advanced Photon Source, Argonne National Laboratory (beamline 19-ID, SBC-CAT) and processed using HKL2000 and SCALEPACK (*133*). Two different apoHPAO-1 crystal polymorphs belonging to space groups $P2_1$ and $C222_1$ were found to grow from identical conditions (*134*). Difference Fourier techniques were used to produce initial electron density maps for the Co(II)-apoHPAO-1 structure in space group $P2_1$ using a previously deposited isomorphous HPAO-1 structure (PDB code 2oov with solvent molecules, metal, and the side chain of TPQ removed) and programs within the CCP4 suite (*103, 135*). Structures in space group $C222_1$ (apoHPAO-1 and Cu(I)-apoHPAO-1) were solved by molecular replacement using the program PHASER in the CCP4 suites with an HPAO-1 monomer from the structure of native HPAO-1 as a search model (PDB code 2oov with solvent molecules, metal, and the side chain of TPQ removed) (*103, 135*). Manual model building was performed using COOT (*136*), and refinement was carried out using the program REFMAC in the CCP4 suite (*137*). Test refinements and B-factor matching

were used to determine partial occupancies of alternate side chain conformations and bound metal ions. This approach involves the systematic variation of the occupancy of the components by increments of 0.10 (keeping a combined occupancy of 1.0) and subsequent refinement. The resulting B-factors for each set of contributing components were compared to those of surrounding well-ordered side chains. The occupancies that best matched the B-factors were assigned to the alternate conformers or metal ions. Refinement continued until peaks in the F_o-F_c electron density map were at the level of noise. The three apoHPAO-1 structures were validated with the programs PROCHECK, NUCHECK, SFCHECK, and MOLPROBITY (*138*-*141*). The final model coordinates and structure factors have been deposited in the PDB (www.rcsb.org) as entries 3sx1 (apoHPAO-1), 3t0u (Cu(I)-apoHPAO-1), and 3sxx (Co(II)-apoHPAO-1). Hydrogen bonds were defined by the program CCP4MG (*142*), and structural figures were produced using the visualization program PyMOL (available at www.pymol.org).

2.3 Results

ApoHPAO-1 protein analysis

Purified apoHPAO-1 protein was assayed for TPQ biosynthetic activity by the aerobic addition of Cu(II)SO_4. UV/visible spectroscopic analysis showed an absorbance feature at 380 nm which formed initially and then disappeared with the subsequent formation of a broad absorbance feature at 480 nm, corresponding to TPQ formation (Figure 2.1). Metal quantification by ICP-MS indicated that apoHPAO-1 protein contained 0.001 Cu^{2+}, 0.005 Zn^{2+}, 0.0001 Co^{2+}, and 0.0003 Ni^{2+} ions per monomer of apoHPAO-1.

Figure 2.1 UV/visible spectra showing the time course of the aerobic reconstitution of apoHPAO-1 with Cu(II) at pH 7.0. The directions of change for UV/visible absorbance features over time are indicated by arrows.

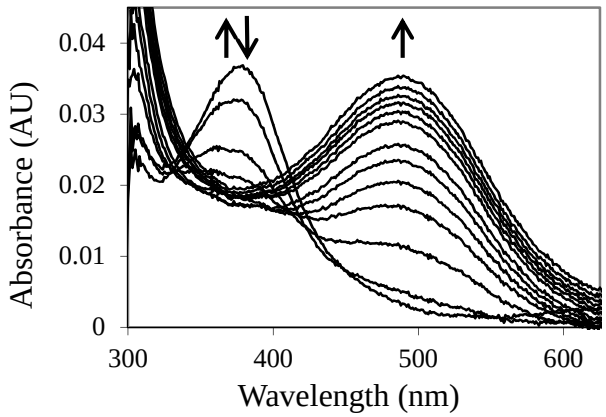

X-ray crystal structure analysis: overall fold

Table 2.2 contains X-ray crystallographic data collection, processing, and refinement statistics for apoHPAO-1 and apoHPAO-1 in complex with Cu(I) and Co(II).

Table 2.2 X-ray data collection, processing, and refinement statistics for apoHPAO-1, Cu(I)-apoHPAO-1, and Co(II)-apoHPAO-1

	apoHPAO-1	Cu(I)-apoHPAO-1	Co(II)-apoHPAO-1
PDB ID	3sx1	3t0u	3sxx
detector type	ADSC Quantum 315r	ADSC Quantum 315r	ADSC Quantum 315r
beamline and source	19-IDD SBC-CAT, Advanced Photon Source	19-IDD SBC-CAT, Advanced Photon Source	19-IDD SBC-CAT, Advanced Photon Source
temperature (K)	100	100	100
space group	$C222_1$	$C222_1$	$P2_1$
unit cell dimensions ($a \times b \times c$ (Å) ;β (°))	139.6 × 153.6 × 223.6; 90	139.4 × 153.7 × 223.5; 90	103.9 × 223.4 × 104.0; 95.6
no. of molecules in the unit cell, Z	1.5	1.5	3
wavelength (Å)	0.979	0.979	0.979
resolution (Å)[a]	50.00-1.73 (1.76-1.73)	50.00-1.90 (1.97-1.90)	50.00-1.27 (1.32-1.27)
no. of unique reflections	240,796	187,095	1,169,541
completeness (%)[a]	97.3 (88.1)	100.0 (99.8)	94.9 (85.3)
R_{merge} (%)[a,b]	0.074 (0.447)	0.110 (0.448)	0.073 (0.357)
$I/\sigma(I)$[a]	32.3 (3.9)	17.9 (4.1)	23.5 (3.4)
redundancy[a]	10.0 (8.7)	7.1 (6.8)	3.7 (3.4)
resolution range (Å)[a]	31.61-1.73 (1.77-1.73)	49.14-1.90 (1.95-1.90)	31.70-1.27 (1.30-1.27)
no. of reflections in the working set[a]	228,647 (15,773)	177,631 (12,933)	1,110,572 (72,499)
no. of reflections in the test set[a]	12,085 (869)	9388 (664)	58,671 (3,854)
R_{work} (%)[a,c]	13.4 (20.2)	12.5 (16.8)	10.8 (17.4)
R_{free} (%)[a,d]	16.3 (25.1)	17.5 (23.1)	13.8 (21.3)
no. of non-hydrogen atoms	18,574	18,804	39,005
no. of amino acid residues	1,970	1,990	3,974
no. of protein atoms	15,895	15,949	32,469
no. of solvent molecules	2,584	2,734	6,250
no. of metal ions	0	3	6
no. of other atoms	95	119	280

Table 2.2, continued. X-ray data collection, processing, and refinement statistics for apoHPAO-1, Cu(I)-apoHPAO-1, and Co(II)-apoHPAO-1.

	apoHPAO-1	Cu(I)-apoHPAO-1	Co(II)-apoHPAO-1
residues modeled	A16-V672	A16-H673, A682-G691	A15-V672, L683-G691
rmsd from ideal geometry			
Bond lengths (Å)	0.016	0.022	0.022
Bond angles (°)	1.53	1.96	1.96
Ramachadran plot			
energetically favored regions (%)	97.5	97.0	97.4
allowed regions (%)	2.4	2.8	2.5
outliers (%)	0.1	0.2	0.1
average *B* factor (Å^2)	16.7	15.1	13.1
main chain	13.2	11.4	8.7
side chain	16.3	14.1	11.6
ligands	40.8	36.6	26.9
solvent atoms	28.1	30.5	27.3
Cruickshank's DPI (Å)	0.09	0.10	0.03

[a]Numbers in parentheses refer to the highest resolution shell. [b]$R_{merge} = \sum_{hkl} \sum_I |I_{hkl,i} - I_{hkl}| / \sum_{hkl} \sum_I I_{hkl,i}$, where I is the observed intensity and $\langle I \rangle$ is the average intensity for multiple measurements. [c]$R_{work} = \sum ||F_o| - |F_c|| / \sum |F_o|$, where $|F_o|$ is the observed structure factor amplitude and $|F_c|$ is the calculated structure factor amplitude for 95% of the data used in refinement. [d]R_{free} based on 5% of the data excluded from refinement.

The structure of Co(II)-apoHPAO-1 contains six polypeptide chains, or three physiological HPAO-1 dimers, in the crystallographic asymmetric unit (ASU) in space group $P2_1$, while those in space group $C222_1$ (apoHPAO-1 and Cu(I)-apoHPAO-1) contain three chains or 1.5 physiological dimers in the ASU. The overall fold of all three structures is nearly identical to that of native HPAO-1 (PDB code 2oov), with superimposition of corresponding main chain atoms yielding root-mean-square deviations

(rmsd) of 0.29, 0.27, and 0.14 Å for apoHPAO-1, Cu(I)-apoHPAO-1, and Co(II)-apoHPAO-1, respectively. The structures of apoHPAO-1 and metal-bound apoHPAO-1 adopt the canonical CAO overall fold, containing three domains (D2-D4) arranged along the primary sequence (Figure 2.2). All significant structural differences between the metal complexes or apoHPAO-1 and the native HPAO-1 structure are localized to either the enzyme active site or the C-terminus.

Figure 2.2 Arrangement of the domains and β-hairpin arms in apoHPAO-1. The structure of apoHPAO-1 is shown in cartoon, with one chain colored by domain (D2, purple; D3, green; D4, blue; β-hairpin arms, red) and the other colored grey. The precursor tyrosine residues (Y405) from both monomers are shown as space-filling spheres and colored by atom type (carbon, white).

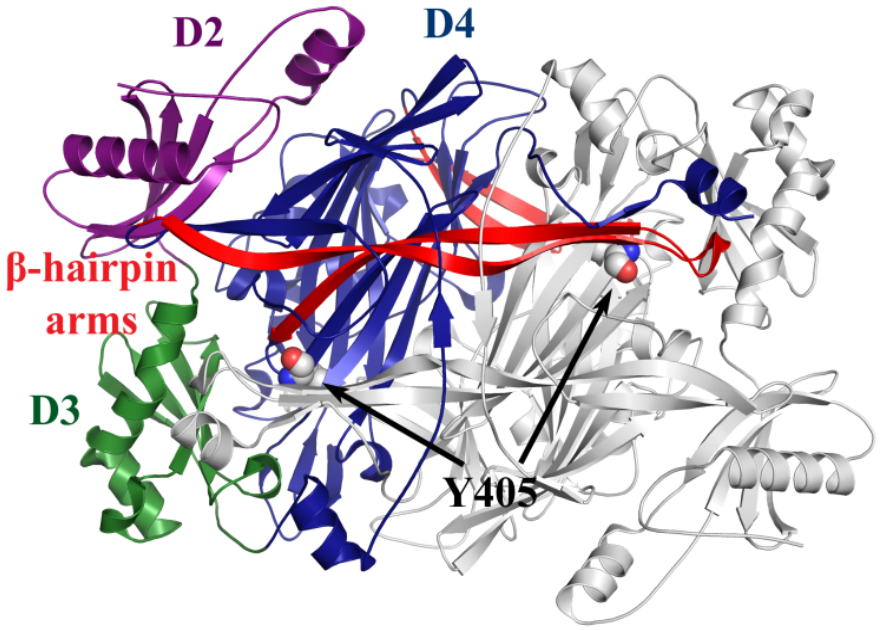

X-ray crystal structure analysis: apoHPAO-1 active site

X-ray diffraction data were collected for crystals of apoHPAO-1 to a resolution of 1.7 Å (Table 2.2). Distances are reported as the range observed across the three

polypeptides of the ASU following refinement. The HPAO-1 active site lies deeply buried within the protein interior. The absence of copper leaves room for an ordered water molecule at the metal binding site (W in Figure 2.3A). This water molecule is bound by His456 and His458 at distances of 2.8-2.9 Å as well as by the precursor tyrosine residue at a distance of 2.6-2.8 Å in a distorted tetrahedral geometry (Figure 2.3A). The side chains of histidine residues 456 and 458 adopt the orientations seen in the structure of native HPAO-1. The third histidine residue (His624) is observed in two conformations. One is equivalent to that of native HPAO-1, but is only 2.1-2.3 Å from the water, suggesting that water can only occupy the site when His624 adopts the second conformation. The second conformer is oriented away from the empty metal site by a rotation of ~90° around its Cβ-Cγ bond, and is hydrogen bonded to the carboxylate of Asp630. This alternate His624 conformer is present at varying occupancies within the three protein monomers located within the ASU (Chain A, occupancy = 1.0; Chain B, occupancy = 0.7; Chain C, occupancy = 0.5).

Figure 2.3 Stereoview of the active sites of (A) apoHPAO-1 (chain B) (B) Cu(I)-apoHPAO-1 (chain A) and (C) Co(II)-apoHPAO-1 (chain A). Residues are shown in stick and colored by atom type (carbon, grey). Metal ions are shown as spheres and colored by atom type (Cu(I), gold; Co(II), pink). Water molecules are shown as small red spheres. Hydrogen bonds are indicated by dashed lines, and ligand-metal interactions are indicated by solid lines.

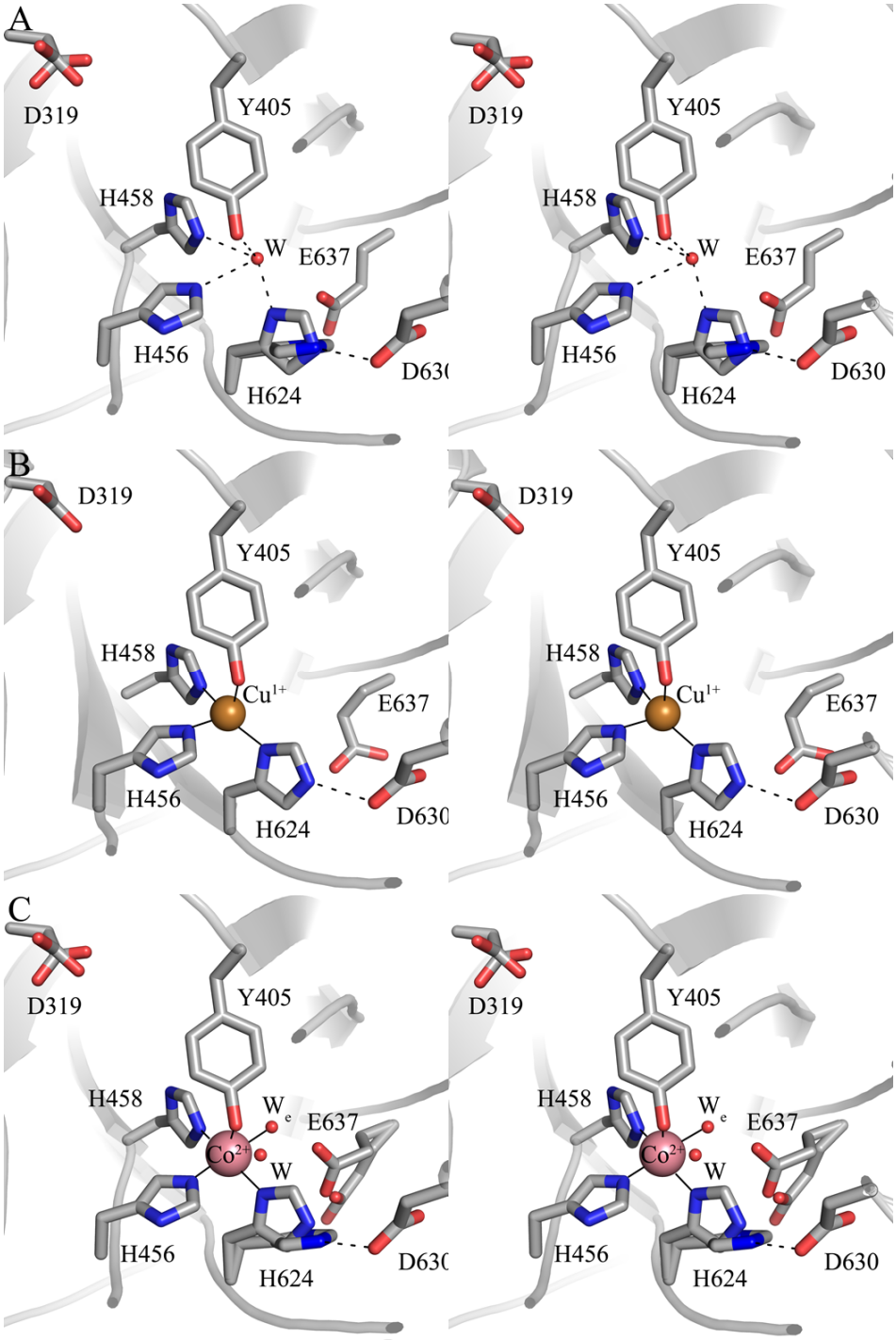

The side chain of Tyr405, the precursor amino acid residue that is converted to TPQ during biogenesis, adopts an orientation similar to that of TPQ in its "on-copper" conformation in the native enzyme (Figure 2.3A). During CAO catalysis, this conformation represents an unproductive form of TPQ, as the C5 carbonyl, which is the site of nucleophilic attack by substrate amine, is not pointed toward the amine channel of the mature enzyme. A second conformer of the catalytic base (residue Asp319), resulting from a ~70° rotation about its Cβ-Cγ bond, can also be seen at an occupancy of 0.5. Additional active site residues are virtually identical in position to those observed in the native HPAO-1 structure, which was also solved to a resolution of 1.7 Å but in space group $P2_1$.

X-ray crystal structure analysis: Cu(I)-apoHPAO-1 active site

X-ray diffraction data for apoHPAO-1 in an anaerobic complex with Cu(I) were collected to a resolution of 1.9 Å (Table 2.2). Like the structure of apoHPAO-1, the active site of Cu(I)-apoHPAO-1 contains the precursor amino acid residue Tyr405 in an "on-copper" orientation with its hydroxyl group coordinated to the Cu(I) (Figure 2.3B). The Cu(I) is bound tetrahedrally, ligated by the three conserved histidine residues with Tyr405 serving as a fourth copper ligand at a distance of 2.8 Å. The imidazole groups of the three conserved histidine ligands all sit 2.0-2.1 Å from the bound copper ion. The tyrosine side chain is most likely protonated due to the long distance between the phenolic oxygen and the bound copper.

Previous structural models of HPAO-1 have not included the residues at the enzyme C-terminus due to disorder in the electron density beyond residue 672 in the primary sequence (there are 692 total amino acid residues in native HPAO-1). Electron density corresponding to residues 681-692 has been located in the Cu(I)-apoHPAO-1 structure (Figure 2.4A). This group of resolved residues is packed against the surface of the other monomer adjacent to one of two β-hairpin arms which form the extensive interface between the two protein chains within one dimer (Figure 2.4B). The Cu(I)-apoHPAO-1 structure also contains a second interchain disulfide bond in this region which was previously unmodeled in other HPAO-1 structures (Figure 2.4C). The disulfide bond involves residue Cys690 from one HPAO-1 monomer and residue Cys122 from its partner in the HPAO-1 dimer, forming a covalent connection between the two protein chains.

Figure 2.4 Stereoviews of newly modeled C-terminal residues in Cu(I)-apoHPAO-1 (A) Close-up view of the new residues. One protein monomer from the HPAO-1 homodimer is shown as a grey surface, and the second is shown as a pink cartoon. Newly modeled residues H673 and A684-K692 are shown in stick and colored by atom type (carbon, pink). The $2F_o$-F_c electron density map is shown as blue mesh and contoured to 1σ. (B) Newly modeled residues in Cu(I)-apoHPAO-1 within the context of the HPAO-1 homodimer. An HPAO-1 dimer is shown with one monomer as a grey surface and the other as a pink cartoon. New residues are shown in stick and colored by atom type (carbon, pink) (C) The second disulfide bond in Cu(I)-apoHPAO-1 with $2F_o$-F_c electron density. The HPAO-1 homodimer is shown in cartoon (chain A, grey; chain B, pink). Residues are shown in stick and colored by atom type (for Cys122 in chain A: carbon, grey; for Cys690 in chain B: carbon, pink). The $2F_o$-F_c electron density map is shown as blue mesh and contoured to 1σ.

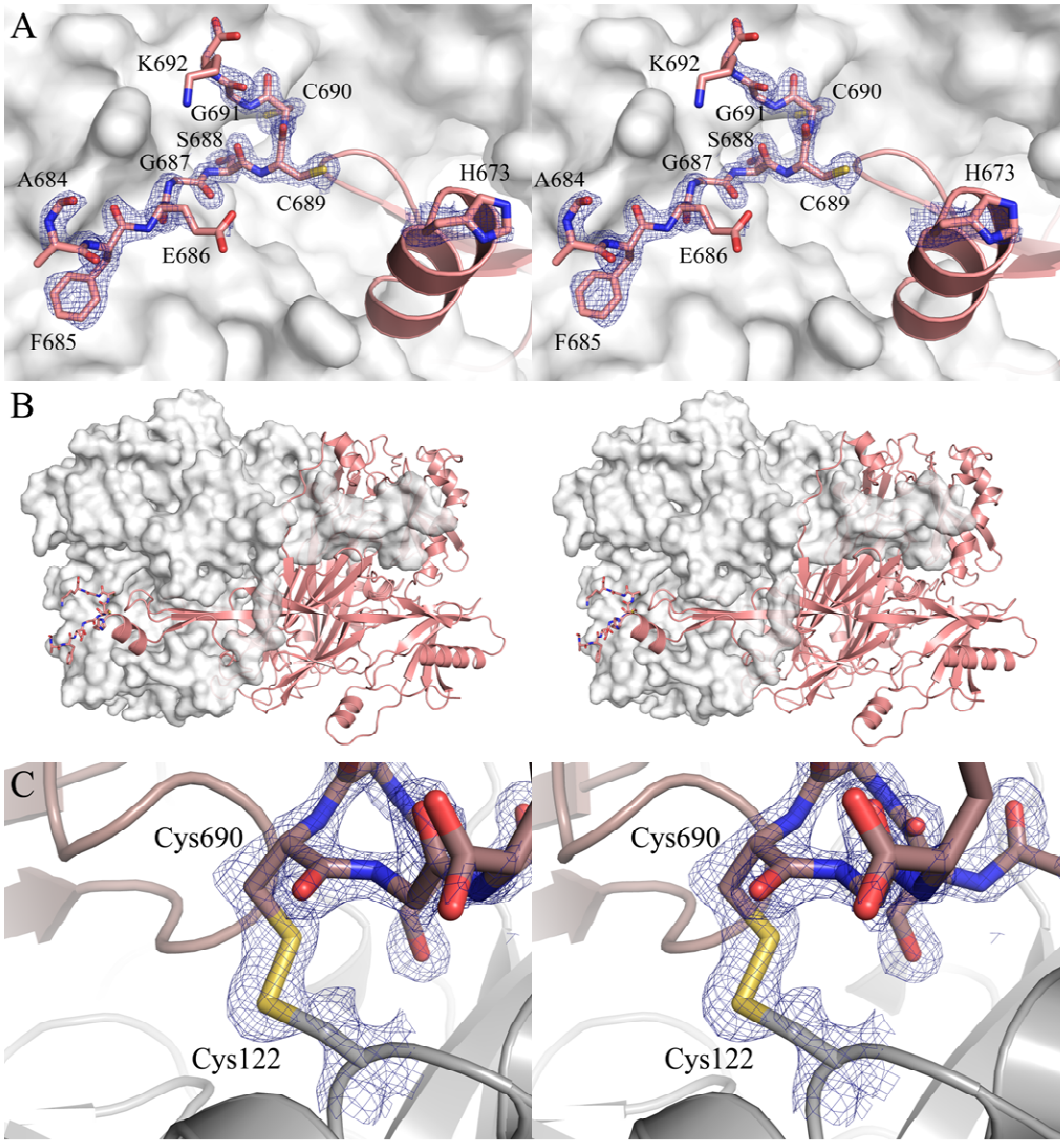

X-ray crystal structure analysis: Co(II)-apoHPAO-1 active site

X-ray diffraction data for an aerobic complex between apoHPAO-1 and Co(II) were collected to a resolution of 1.27 Å, which makes this the highest resolution CAO structure to date (Table 2.2. For the quality of the electron density, see Figure 2.5).

Figure 2.5 Stereoview of Co(II)-apoHPAO-1 active site residues with the $2F_o$-F_c electron density map. Residues are shown in stick and colored by atom type (carbon, grey). The cobalt ion is shown as a pink sphere. Water molecules are shown as small red spheres. The $2F_o$-F_c electron density map is shown as blue mesh and contoured to 1σ.

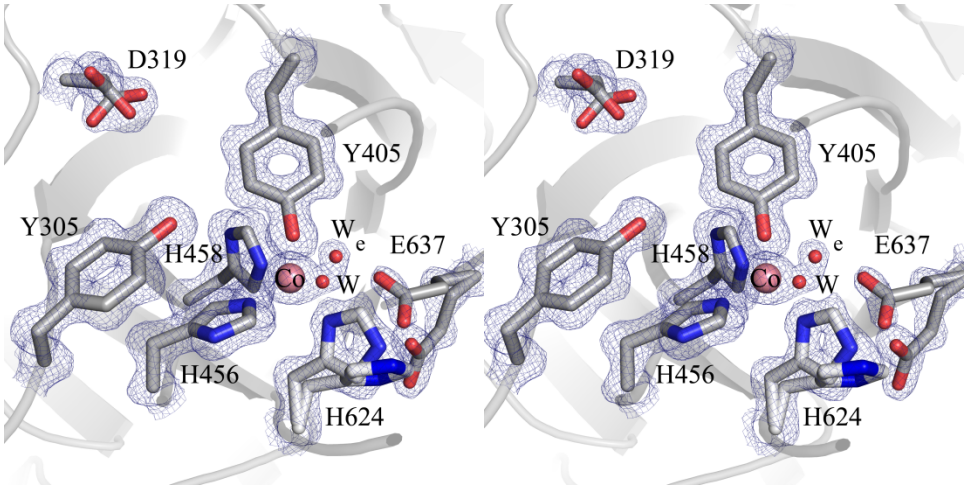

Distances are reported as the range observed across the six polypeptides of the ASU in this crystal form following refinement. The active site of Co(II)-apoHPAO-1 contains cobalt bound at an occupancy of 0.5 (Figure 2.3C). The unmodified precursor tyrosine side chain ligates the cobalt, with its phenolic hydroxyl 2.15-2.20 Å away. The three histidine metal ligands sit with their imidazole groups 2.00-2.20 Å from the bound cobalt. Electron density in the $2F_o$-F_c and F_o-F_c maps indicated the presence of a water molecule acting as an equatorial ligand to the cobalt at a distance of 2.15-2.20 Å (W_e in

Figure 2.3C). Peaks in the F_o-F_c electron density map indicated the presence of a water molecule at an occupancy of 0.5 between the three active site histidine residues that is present when Co(II) is not bound (W in Figure 2.3C). This water molecule is nearly superimposable with that found occupying the metal binding site in the apoHPAO-1 structure (Figure 2.3A) and reflects the partial occupancy of the cobalt. One of the three histidine residues that ligate the active site metal (His624), adopts the alternate conformation seen in the apoHPAO-1 structure with its side chain rotated ~90° around its Cβ-Cγ bond at different occupancies depending on protein chain (chain A, occupancy = 0.3; chain B: occupancy = 0.5; chain C, occupancy = 0.4; chain D, occupancy = 0.3; chain E, occupancy = 0.4; chain F, occupancy = 0.4). The active site catalytic base (Asp319) and residue Glu637 also adopt second conformations in this complex in which their side chains have rotated around the Cβ-Cγ bond. These alternate conformers are present at different occupancies depending on protein chain (for Asp319: all chains, occupancy = 0.30; for Glu637: chain A, occupancy = 0.5; chain B, occupancy = 0; chain C, occupancy = 0.4; chain D, occupancy = 0.5; chain E, occupancy = 0.4; chain F, occupancy = 0.5), and reflect the partial binding of cobalt. This results in the presence of apoHPAO-1 active site features in the electron density as well.

Electron density corresponding to a group of residues near the C-terminus (residues 683-691) was seen in the $2F_o$-F_c and F_o-F_c maps of the Co(II)-apoHPAO-1 structure. These residues are modeled at an occupancy of 0.5, and are superimposable with those modeled in the Cu(I)-apoHPAO-1 structure (Figure 2.4A, B).

2.4 Discussion

Cu(I)-apoHPAO-1 as a physiologically relevant biogenesis intermediate

Copper in its +1 oxidation state can anaerobically bind to apoHPAO-1, and subsequent exposure of this complex to oxygen initiates TPQ formation at a rate 17-fold slower than Cu(II)-mediated biogenesis (*124*). The rate-limiting step in Cu(I)-mediated TPQ biogenesis was determined by X-band electron paramagnetic resonance spectroscopy to be the dissociation of bound superoxide from the metal site formed via the oxidation of Cu(I) to Cu(II) (*124*). After the oxidation of Cu(I) to Cu(II), Cu(I)-mediated biogenesis mechanistically converges with biogenesis initiated by Cu(II), producing indistinguishable native protein both in terms of TPQ content and catalytic rates (*124*).

The cellular location of HPAO-1 is the yeast peroxisome, which has implications for the electronic form of copper available to initiate TPQ biogenesis (*129*). After translation by free cytosolic polyribosomes, proteins containing a peroxisomal targeting sequence are transported into the peroxisomal matrix after passing through a membrane-associated protein complex. The peroxisomal lumen is predicted to contain no free copper, and there are no known copper transporters associated with the organelle. Given the apparent absence of copper in the peroxisome, it is thought that copper incorporation into apoHPAO-1 occurs in the cytosol while the protein is en route to its final cellular destination. Copper uptake in yeast species such as *Saccharomyces cerevisiae* involves the reduction of Cu(II) to Cu(I) by the cell-surface reductases Fre1 and Fre2, so it is

likely that the copper available to bind to apoHPAO-1 in the yeast cytosol is in its cuprous form (*130*).

Samuels et al. note that Cu(I) (as opposed to Cu(II)) binding to apoHPAO-1 in the cytosol could be beneficial for the yeast, as the slower Cu(I)-mediated biogenesis would reduce the amount of peroxide and free aldehyde generated by maturated HPAO-1 whilst in transit to the peroxisome (*124*). Thus, the structure of apoHPAO-1 in an anaerobic complex with Cu(I) may represent the biologically-relevant initial intermediate in terms of metal incorporation and the initiation of TPQ biogenesis for this peroxisomal CAO.

Identification of a second disulfide bond in HPAO-1

The structures of Cu(I)- and Co(II)-apoHPAO-1 contain an additional disulfide bond involving Cys122 and Cys690 that was previously unmodeled in structures of HPAO-1, where the C-terminus that contains Cys690 is disordered. HPAO-1 had previously not been modeled beyond residue Val672 in the primary sequence, with the C-terminal 20 residues missing (*55, 73, 103*). In the Cu(I)- and Co(II)-apoHPAO-1 structures, the positions of residues 673-674 and 682-692 have been determined (Figure 2.4). No electron density corresponding to residues 675-681 was found during refinement, suggesting that these residues remain disordered and are part of a surface-exposed loop. HPAO-1 contains 12 cysteine residues per monomer and, based on the crystal structure of native HPAO-1 (residues 18-672), contains one buried disulfide bond involving Cys338 and Cys364 (*55*). The new disulfide bond identified in the Cu(I)- and Co(II)-apoHPAO-1 structures is located at the interface between protein partners in the

physiological HPAO-1 dimer and serves as a covalent link between monomers (Figure 2.4). Given that the two structures containing this new disulfide bond have been solved in different space groups, it is likely that this interaction is not due to crystal contacts. There is precedent in CAO structures for disulfide bonds that covalently connect the two CAO monomers in the enzyme from *Pisum sativum*, human diamine oxidase, and the human vascular adhesion protein. However, these are found in different areas of the CAO dimer (*52*, *143*). As the disulfide is on the surface it is likely reduced in the cytosol, but in HPAO-1 it could be physiological as the peroxisome is oxidizing (*144*).

Comparisons with other apoCAO structures

Two CAOs have been produced in their metal-free precursor (apo) form: HPAO-1 and AGAO. The structure of apoAGAO has been solved to 2.2 Å, and a comparison of apoAGAO and apoHPAO-1 reveals very similar active site architecture (Figure 2.6) (*6*). Both active sites contain the unmodified precursor tyrosine residue arranged with its side chain hydroxyl pointed toward the vacant metal binding site. The active site of apoHPAO-1 contains a well-ordered water molecule where the copper is normally bound, which is stabilized by hydrogen bonding interactions with the precursor tyrosine residue and two histidine imidazole ligands. In contrast, the metal binding site of apoAGAO is empty; instead, two of the three metal-binding histidine residues (His433 and 592) have each moved ~0.6 Å toward the vacant metal site (Figure 2.6) (*6*). In both apoCAO structures, two of the three metal-binding histidine residues occupy positions identical to those in the native enzyme. The third (His624 in HPAO-1, His592 in AGAO), however,

is present in two conformers, indicating that there is some flexibility in the positioning of this side chain. In apoHPAO-1, the second conformer of His624 is rotated ~90° about its Cβ-Cγ bond, whereas in apoAGAO, the second conformer of His592 is rotated ~75° about its Cα-Cβ bond.

Figure 2.6 Overlay of the apoHPAO-1 and apoAGAO (PDB code 1avk) active sites (*6*). Residues are shown in stick and colored by atom type (HPAO-1: carbon, grey; AGAO: carbon, green). Residue numbering is that of HPAO-1, with equivalent residues in AGAO in brackets. A water molecule from the apoHPAO-1 active site is shown as a small red sphere, and hydrogen bonding interactions in HPAO-1 are indicated by dashed lines. The view is ~90° rotated from the angle used in Figure 2.3.

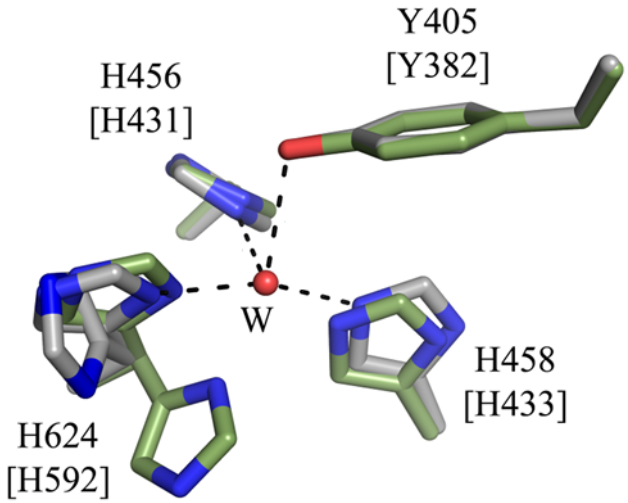

In the presence of oxygen, biogenesis is initiated upon copper binding in the apoCAO active site (*70*). X-ray crystal structures of apoHPAO-1 or apoAGAO in an anaerobic complex with copper have now been solved (*68*). These two structures should contain copper in different oxidation states (although photoreduction was not tracked in the Cu(II)-apoAGAO structure determination), with the HPAO-1 structure containing cuprous copper and the AGAO structure containing cupric copper. A comparison of the Cu(I)-apoHPAO-1 structure with the Cu(II)-apoAGAO complex (both solved to a

resolution of 1.9 Å) reveals that despite the difference in the oxidation state of the bound copper, the two structures exhibit very similar active site architecture (*68*). Both active sites contain the unmodified precursor tyrosine residue oriented with its hydroxyl pointed toward the bound copper. In Cu(II)-apoAGAO, the tyrosine side chain sits with its hydroxyl ~2.5 Å away from the Cu(II) ion (Figure 2.7) (*68*). In Cu(I)-apoHPAO-1, the tyrosine hydroxyl is ~2.8 Å away from the bound Cu(I). Both structures contain the precursor tyrosine residue in its protonated form, as inferred from the long distances between the hydroxyl of the tyrosine and bound copper. Despite the presence of copper at full occupancy, one of the three histidine residues that ligate the copper is present in two conformers in Cu(II)-apoAGAO (His592). These are identical in position to those seen in the structure of apoAGAO (Figure 2.6). In contrast, the corresponding residue in HPAO-1 does not appear to be as mobile, as the electron density indicated that this side chain exists only in the major conformer observed in structures of the native enzyme (His624). Neither of the two copper-bound active sites contains an ordered water molecule ligating the copper in an equatorial position, which has been observed in some polypeptide chains of the native HPAO-1 structure (*103*). It appears that a change in the oxidation state of the bound copper does not significantly alter the active site architecture or the coordination geometry in copper-bound apoCAO. However, as noted earlier, the copper ion oxidation state of the Cu(II)-apoAGAO crystal structure may have changed to Cu(I) during X-ray data collection, as photoreduction was not tracked.

Figure 2.7 Overlay of the Cu(I)-apoHPAO-1 and Cu(II)-apoAGAO (PDB code 1ivu) active sites (*68*). Residues are shown in stick and colored by atom type (HPAO1: carbon, grey; AGAO: carbon, green). Residue numbering is that of HPAO-1, with equivalent residues in AGAO in brackets. Copper ions are shown as gold spheres, and water molecules are shown as small red spheres. Hydrogen bonding interactions in HPAO-1 are indicated by dashed lines, and ligand-metal interactions in HPAO-1 are indicated by solid lines.

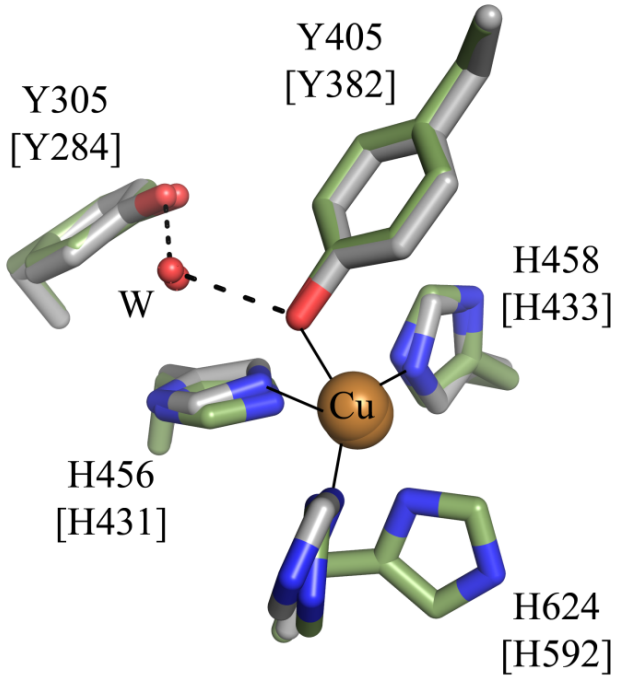

Like Cu(I), zinc is typically coordinated in buried enzyme active sites by four ligands in a tetrahedral geometry (*145*). The structure of apoHPAO-1 in complex with Zn(II) (PDB code 1ekm) solved to 2.5 Å resolution contains bound zinc and active site residues which are nearly superimposable with those of the Cu(I)-apoHPAO-1 structure (Figure 2.8) (*73*). Like Cu(I), Zn(II) binds to the apoHPAO-1 active site in a tetrahedral geometry, and is ligated by the precursor tyrosine residue as well as by the three conserved active site histidine residues. Despite such similar coordination geometry, the binding of zinc in the active sites of CAOs renders the enzyme inert, while copper binding initiates biogenesis (*131*). The specific factors which inhibit zinc-mediated

biogenesis in apoCAO are unclear, but may relate to its filled *d*-orbital electron configuration.

Figure 2.8 Overlay of the Cu(I)-apoHPAO-1 and Zn(II)-apoHPAO-1 (PDB code 1ekm) active sites (*73*). Residues are shown in stick and colored by atom type (Cu(I): carbon, grey; Zn(II): carbon, blue). A Cu(I) ion is shown as a gold sphere, and a Zn(II) ion is shown as a grey sphere. Water molecules are shown as small red spheres, and hydrogen bonding interactions in Cu(I)-apoHPAO-1 are indicated by dashed lines.

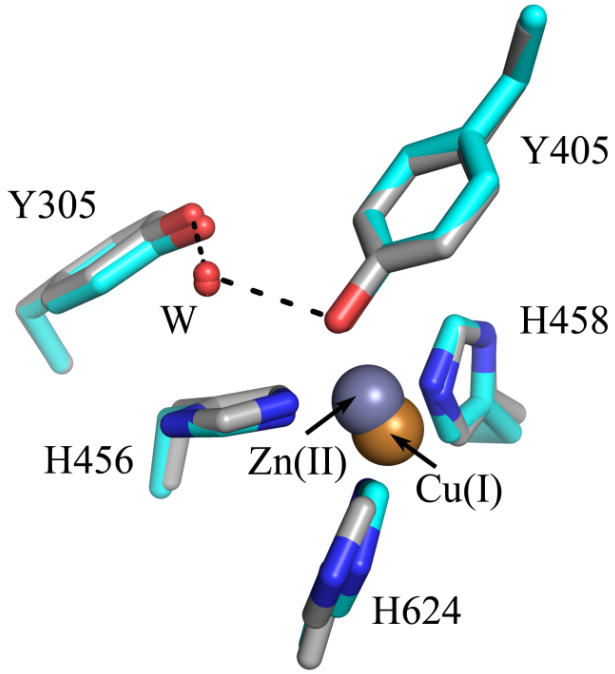

The presence of cobalt in the AGAO active site initiates biogenesis under aerobic conditions, but in HPAO-1 cobalt does not support the production of TPQ. The structures of apoHPAO-1 in complex with Co(II) and an anaerobic Co(II)-apoAGAO complex have been solved to resolutions of 1.27 and 2.0 Å, respectively (*125*). In the case of HPAO-1, the Co(II) complex represents an inert structure, while in AGAO, the anaerobic Co(II) complex is the first intermediate in Co(II)-mediated biogenesis, which produces TPQ identical to that of the native enzyme (*131*). Comparison of the two

cobalt-containing complexes indicates that in these two apoCAOs cobalt binds with distinct geometries (Figure 2.9).

Figure 2.9 Overlay of the Co(II)-apoHPAO-1 and Co(II)-apoAGAO (PDB code 1wmp) active sites (*125*). Residues are shown in stick and colored by atom type (HPAO-1: carbon, grey; AGAO: carbon, green). Co(II) ions are depicted as pink spheres. A water molecule from the Co(II)-apoHPAO-1 active site is shown as a small red sphere. Ligand-metal interactions in HPAO-1 are indicated by solid lines. Residue numbering is that of HPAO-1, with AGAO numbering in brackets.

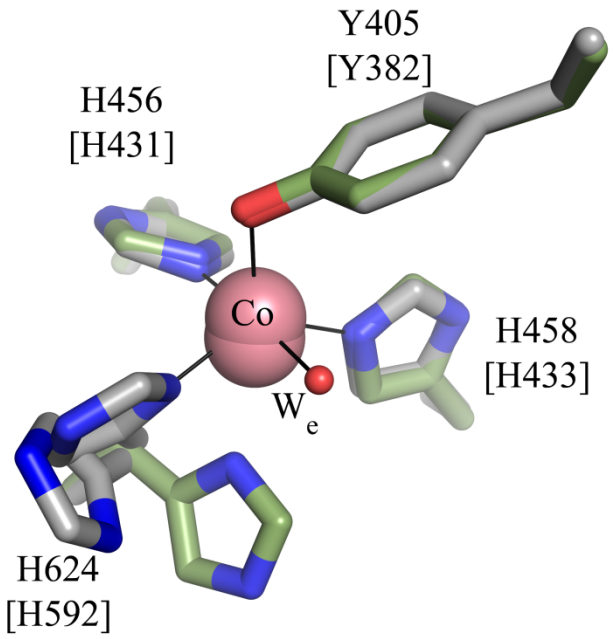

In the case of Co(II)-apoHPAO-1, the cobalt ion is 5-coordinate, binding in a distorted square pyramidal geometry. The species ligating the cobalt include the precursor tyrosine residue, the three conserved active site histidine ligands, and an equatorial water molecule (W_e in Figure 2.9). The structure of apoAGAO in an anaerobic complex with cobalt, however, contains 4-coordinate cobalt in a distorted tetrahedral geometry, ligated by the three active site histidine residues and the precursor tyrosine residue. In addition, the crystal structure of native AGAO in complex with Co(II) has

been solved to a resolution of 2.0 Å (PDB code 1iqx) (*131*). The most pronounced change in the active site of native AGAO upon the replacement of Cu(II) with Co(II) is the conformation of one of the histidine residues which ligate the Co(II). This residue rotates ~60° about the Cα-Cβ bond and occupies a position identical to that in the Co(II)-apoAGAO structure. In contrast to the four-coordinate tetrahedrally bound cobalt ion in Co(II)-apoAGAO, Co(II)-AGAO contains six-coordinate cobalt ligated by the three histidine residues, the axial and equatorial water ligands common to the native structure, and an additional water molecule in an octahedral geometry. Such geometric differences may explain the inefficiency of Co(II)-PSAO to catalyse substrate oxidation in relation to the native Cu(II)-PSAO (*96*). It appears that differences in metal coordination geometry, in conjunction with additional factors such as Lewis acidity and redox potential, coordinate to determine whether a metal can initiate biogenesis as well as sustain efficient catalysis in the mature CAO. Given that cobalt can support TPQ biogenesis in AGAO but not in HPAO-1, differences in cobalt coordination likely influence this process.

CHAPTER 3: STRUCTURAL AND KINETIC ANALYSIS OF SUBSTRATE SPECIFICITY IN TWO COPPER AMINE OXIDASE PARALOGS FROM *Hansenula polymorpha*

Content in this chapter is reprinted with permission from:

Chang, C.M., Klema, V.J., Johnson, B.J., Mure, M., Klinman, J.P., and Wilmot, C.M. (2010) Kinetic and structural analysis of substrate specificity in two copper amine oxidases from *Hansenula polymorpha*, *Biochemistry 49*, 2540-2550.

The structural basis of enzyme substrate specificity is investigated in a pair of CAOs from *Hansenula polymorpha* (HPAO-1 and HPAO-2). The X-ray crystal structure (to 2.0 Å resolution) and steady state kinetic data of the second copper amine oxidase (HPAO-2) are presented for comparison to those of HPAO-1. Despite 34% sequence identity and superimposable active site residues implicated in catalysis, the enzymes vary considerably in their substrate entry channel. The previously studied CAO, HPAO-1, has a narrow substrate channel. In contrast, HPAO-2 has a wide funnel-shaped substrate channel that also contains a side chamber. In addition, there are a number of amino acid changes within the channels of HPAO-2 and HPAO-1 that may sterically impact the ability of substrate to form covalent Schiff base catalytic intermediates and to initiate chemistry. These differences can partially explain the greatly different substrate specificities as characterized by k_{cat}/K_m value differences. In HPAO-1, the k_{cat}/K_m for methylamine is 330-fold greater than for benzylamine, whereas in HPAO-2, benzylamine is the better substrate by 750-fold. In HPAO-2, an inflated $^{D}k_{cat}/K_m$(methylamine) in relation to $^{D}k_{cat}/K_m$(benzylamine) indicates that proton abstraction has been impeded more than substrate release. In HPAO-1, $^{D}k_{cat}/K_m$(S) changes little with the slow substrate and indicates a similar increase in the energy barriers that control both substrate binding and subsequent catalysis. In neither case is k_{cat}/K_m for the second substrate consumed during CAO catalysis, O_2, significantly altered. These results reinforce the modular nature of the active sites of CAOs and show that multiple factors contribute to substrate specificity and catalytic efficiency. In HPAO-1, the enzyme with the smaller substrate binding pocket, both initial substrate binding and proton loss are affected by an

increase in substrate size, while in HPAO-2, the enzyme with the larger substrate binding pocket, the rate of proton loss is differentially affected when a phenyl substituent in the substrate is reduced to the size of a methyl group.

3.1 Background

Copper amine oxidases (CAOs) are virtually ubiquitous in aerobic organisms and catalyse the oxidative deamination of primary amines in the following overall reaction:

$$RCH_2NH_3^+ + O_2 + H_2O \rightarrow RCHO + H_2O_2 + NH_4^+$$

While usually sharing only 20-40% amino acid sequence identity, features of the active sites are almost identical across CAOs from widely varying species. These include the protein-derived enzymatic cofactor 2,4,5-trihydroxyphenylalanine quinone (TPQ), an active site copper, and its three histidine ligands (*58, 146*). The CAO mechanism is ping-pong and proceeds via Schiff base chemistry, which creates a covalent adduct between the amine substrate and the TPQ (Scheme 3.1). A conserved aspartate residue acts as the catalytic base. The release of aldehyde product at the end of the enzymatic reductive half-reaction leaves the cofactor as a two-electron reduced aminoquinol containing a substrate-derived nitrogen atom. In the oxidative half-reaction, the reduced enzyme is converted to a one-electron reduced *N*-semiquinone and then an oxidized iminoquinone through the reduction of molecular oxygen to hydrogen peroxide. This is followed by hydrolysis of the iminoquinone to regenerate the resting TPQ quinone and release ammonium.

Despite these similarities, CAOs from different organisms and cellular locations preferentially react with primary amine substrates ranging from small aliphatic amines to whole peptides. The CAO from *E. coli* (ECAO), for example, prefers aromatic monoamines (*147*), while the first characterized CAO from *Hansenula polymorpha* (HPAO-1) is most active against small aliphatic amines (*122*). The structural basis for

this difference in substrate specificity has remained elusive.

Copper amine oxidases are not unique in their variable substrate specificity. Among other classes of enzymes, e.g., aminotransferases (*148*) and flavin-containing monoamine oxidases (MAOs) (*149*), the basis of isoenzyme specificity has been explored. Protein conformational flexibility has been suggested as a source of substrate specificity in aspartate aminotransferase and aromatic amino acid aminotransferase (*150*), whereas differences in static hydrophobic and aromatic π-π interactions in the substrate binding pocket have been implicated in MAO-A (*151*). It is rare for paralogous enzymes to demonstrate a strong yet inverted discrimination between two different substrates. Thus, most investigations have focused on understanding the relative rates of preferred over poor substrates in a single enzyme, rather than between isoenzymes.

The first described CAO from the methylotrophic yeast *H. polymorpha* (HPAO-1) was heterologously expressed in *Saccharomyces cerevisiae* and purified in 1994 (*122*) and subsequently studied by X-ray crystallography (*55*). Although a peroxisomal protein in its native host organism, it was found in the cytosol of *S. cerevisiae* during recombinant expression (*152*). Characterized as a "methylamine oxidase," HPAO-1 demonstrated much greater activity against methylamine than benzylamine. However, extraction of CAO from *H. polymorpha* grown on benzylamine-enriched media had indicated the presence of a second CAO with a distinct catalytic activity toward benzylamine (*122*). In the case of mammals, multiple CAO isoenzymes, annotated as *AOC1*, *AOC2*, and *AOC3*, have also been established in the human genome (*153*). Comparison of the enzymatic activities of human diamine oxidase (*154*) to human

vascular adhesion protein-1 (*155*) indicates broad though largely non-overlapping substrate specificities. Although these two human enzymes have also been characterized structurally (*19, 52, 53*), their broad substrate specificities make it difficult to rationalize the features that control substrate discrimination.

In this work, a detailed kinetic and crystallographic characterization of a second copper amine oxidase from *H. polymorpha* (HPAO-2) is presented for comparison with HPAO-1. In particular, k_{cat}/K_m data indicate a marked reversal of substrate selectivity between the two isoenzymes when their activities are interrogated with a small aliphatic vs. an aromatic amine. Using the X-ray crystal structure of HPAO-2 reported here to compare to that of HPAO-1, the structural origins of this divergent substrate specificity can be deciphered. Residue changes between HPAO-1 and HPAO-2 that likely play roles in determining substrate specificity have been identified close to the active site and are discussed in the context of the available kinetic parameters and corresponding isotope effects.

3.2 Methods

Cloning; protein expression, purification, and characterization; and kinetic measurements

Cloning of *hpao-2* from *H. polymorpha* was performed by Minae Mure, and protein expression, purification, and kinetic measurements were carried out by Cindy Chang at the University of California, Berkeley. Detailed methods for these are included in Appendix A of this work.

HPAO-2 crystallization

HPAO-2 in 50 mM potassium phosphate (pH 7.2) was buffer exchanged into 20 mM HEPES (pH 7.0) and concentrated to 23 mg/mL for crystallization. HPAO-2 crystals were grown by sitting drop vapor diffusion using a 1:1 volume ratio (6 μL total) of purified HPAO-2 and a mother liquor solution (0.5-0.75 M potassium sodium tartrate tetrahydrate in 0.10 M phosphate (pH 6.0-7.5)) at 20°C. Crystals grew as clusters, and physical manipulation was necessary to separate individual crystals. Prior to be flash-frozen in liquid nitrogen, crystals were soaked in 25% high-purity glycerol (Hampton Research) mixed with mother liquor taken directly from the crystallization well for 5 min.

Diffraction data collection, structure determination, and refinement

X-ray diffraction data were collected from a single crystal at 100 K using an undulator source (wavelength of 0.979 Å) and an ADSC Quantum 315r detector at the Advanced Photon Source, Argonne National Laboratory (beamline 19-ID, SBC-CAT).

Data were processed using HKL2000 and SCALEPACK (*133*). Molecular replacement was conducted using PHASER and MOLREP from the CCP4 suite (*135*) with a polyalanine truncated search model based on a previously deposited HPAO-1 model (PDB entry 2oov) (*103*).

An initial model was built into the experimental electron density, and manual adjustments were made in COOT (*136*). Model refinement was performed using REFMAC with 5% of the data excluded from the refinement to enable calculation of R_{free} (*137*). ARPWaters was used to place water molecules into the model at peaks greater than 3.0σ in the $2F_o$-F_c electron density map (*156*). Cycles of manual model building and refinement were performed until peaks in the F_o-F_c electron density map did not make structural sense and appeared to be within the level of noise.

3.3 Results

Characterization of HPAO-2 and comparison to HPAO-1

Cell extracts after induction for 24 h contained a band at ~72 kDa that is absent in the non-transformed control yeast cell extracts. The size of the protein corresponds to the estimated size of HPAO-2 calculated from the primary sequence. After purification, the resulting protein constituted >90% of the total protein, as observed by SDS-PAGE (Figure 3.1).

Figure 3.1 10% SDS-PAGE gel of HPAO-2. Lanes 1-4: 100 μg protein loaded per lane. (1) cell lysate, (2) post Q-sepharose, (3) post S-300, (4) Bio-Rad Broad range ladder (150, 100, 75, 50, 37, 25, 20 kDa fragments visible). Substantial purification of HPAO-2 is evident from the relative intensities of HPAO-2 to other minor contaminating bands in moving from lane 1 to lane 3.

The net effect of the purification protocol was to increase the amount of HPAO-2 relative to the contaminant bands. Some of the contaminant bands also stained on a

nitroblue tetrazolium blot, indicating probable breakdown products of HPAO-2 (data not shown). HPAO-1 migrates slightly faster by SDS-PAGE, suggesting an overall smaller primary structure; however the DNA-derived primary protein sequence of HPAO-1 predicts a protein slightly larger than HPAO-2. Post-translational modifications may account for this difference as HPAO-2 has an additional predicted glycosylation site. Concentrated purified HPAO-2 was a vibrant peach color, characterized by a broad shoulder in the UV/visible region around 480 nm (Figure 3.2).

Figure 3.2 UV/visible spectra of 20 μM HPAO-2 before (—-) and after (- - -) incubation for 5 min with 100 μM phenylhydrazine HCl in 100 mM potassium phosphate buffer (pH 7.2) at 25°C. The inset shows 20 μM HPAO-2 before incubation with phenylhydrazine HCl magnified to show a shoulder at 480 nm, as observed for other TPQ-containing enzymes.

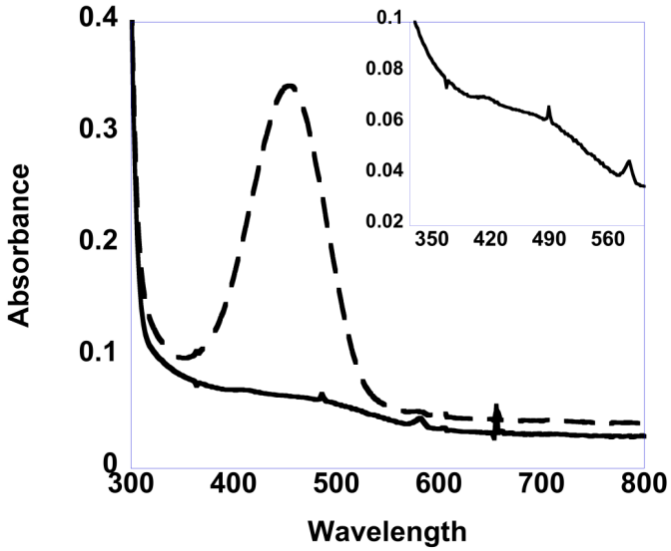

N-terminal sequencing of the protein matched the expected N-terminus from the HPAO-2 DNA sequence, except for the absence of the initial Met (Figure 3.3). The N-

terminus of HPAO-1 is longer by 20 amino acids and contains a peroxisomal targeting sequence (Figure 3.3).

Figure 3.3 Comparison of the DNA-derived N-terminal sequences of HPAO-2 and HPAO-1, including a peroxisomal signaling sequence (underlined) in HPAO-1, and the experimental N-terminal sequence of HPAO-2.

HPAO-1	MERLRQIASQATAASAAPARPAHPLDPLSTAEIKAA
HPAO-2	----------MVHPYDPISDAELQLT
N-Term Seq:	----------VHPYDPISDAELQLT

The presence of a quinone cofactor was tested by both quinone stain and phenylhydrazine assay. Nitroblue tetrazolium staining resulted in a purple band similar to that observed with HPAO-1 (data not shown). Reaction with phenylhydrazine resulted in the rapid formation of a peak in the region seen previously with other CAOs (~450 nm) corresponding to the phenylhydrazone (Figure 3.2). The rate of phenylhydrazone formation in HPAO-2 ($87 \pm 3\ s^{-1}$) is $>10^4$-fold faster than that of HPAO-1 ($7.8 \times 10^{-3} \pm 7.0 \times 10^{-4}\ s^{-1}$). Typical yields of phenylhydrazone correspond to ~50% of the subunit concentration.

The copper content of purified protein was measured by elemental analysis. Initial analyses indicated 2 moles of copper per monomer. However, after overnight dialysis against 1 mM EDTA, followed by dialysis against 0.1 M potassium phosphate buffer (pH 7.2), the expected level of one copper atom per monomer was observed. The presence of the loosely bound second copper did not affect enzyme turnover rates, as kinetic measurements performed with the dialyzed enzyme yielded rates that were the

same as those with non-dialyzed enzyme sample (Table 3.1). Thus, there appears to be an adventitious metal binding site that plays no role in catalysis.

Table 3.1 Comparison of k_{cat} values in EDTA-dialyzed vs. non-dialyzed HPAO-2 samples.

	benzylamine (150 μM)	methylamine (5 mM)
HPAO-2 / (HPAO-2 + EDTA)	$1.9 \pm 1 \times 10^{1}$ / $1.9 \pm 1 \times 10^{1}$	1.69 ± 0.07 / 1.9 ± 0.1

Kinetic properties

The near-unity $^{D}k_{cat}$ values observed for HPAO-2 with both substrates indicate that proton abstraction is not significantly rate-limiting with either substrate (Table 3.2). The lower limit for the rate constant reflecting the proton abstraction step is thus defined by the respective k_{cat} values. Conversely, HPAO-1 has an elevated $^{D}k_{cat}$ for the slower substrate benzylamine ($^{D}k_{cat}$ (benzylamine) equals 5.9, whereas $^{D}k_{cat}$ (methylamine) equals 1.7), pointing to a higher relative energy barrier for proton loss from the poor substrate relative to other steps following substrate binding. The overall turnover rate (k_{cat}) for benzylamine is also down 94-fold relative to that for methylamine. Stopped-flow kinetic studies of HPAO-1 have confirmed the oxidative half-reaction is the major determinant of rate during turnover with methylamine (*112*).

Overall, the changes in k_{cat} between the different amine substrates are smaller than the changes in k_{cat}/K_m(S) (Table 3.2). The second-order rate constant reflects turnover under low substrate conditions and varies by 750-fold between the two substrates for HPAO-2. The change in k_{cat}/K_m(S) between substrates observed with HPAO-1 is similar,

but somewhat smaller (330-fold). As such, HPAO-2 shows a clear preference for bulkier aromatic amines, and HPAO-1 shows a preference for short aliphatic amines. These differences in k_{cat}/K_m(S) originate from substrate-dependent rate differences in one or more steps that occur between binding of substrate to the enzyme up to and including the first irreversible step (Scheme 3.1).

Scheme 3.1 Proposed reaction mechanism for HPAO-1, indicating intermediates along the pathway.

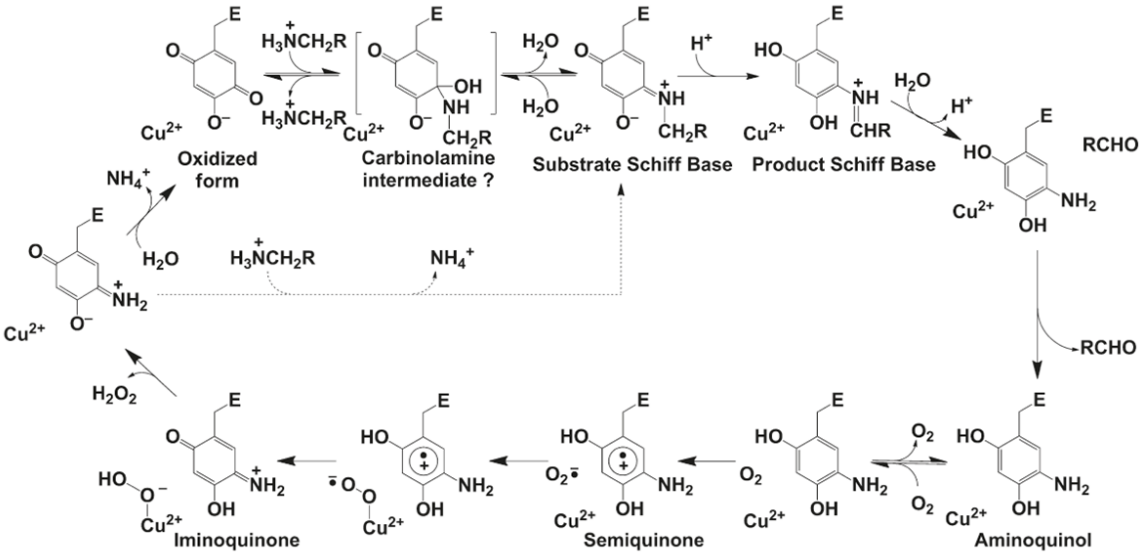

In contrast, $k_{cat}/K_m(O_2)$ changes little between the two substrates and two isoenzymes (Table 3.2). This suggests that steps from oxygen binding through the irreversible oxygen reduction step vary little between the two substrates, as expected for the ping-pong mechanism proposed for HPAO-1 (Scheme 3.1). The small reduction in $k_{cat}/K_m(O_2)$ for methylamine turnover (as compared to that of benzylamine in HPAO-2) could suggest oxygen binding to an enzyme form that has retained formaldehyde and is

unreactive to O_2 until the product is released. Bound aldehyde product has been shown to significantly impede the oxidative half-reaction in ECAO crystals, where the restraints imposed by the lattice lead to very slow product release (*106*).

Table 3.2 Steady state kinetic parameters for HPAO-1 and HPAO-2 at 25°C in 100 mM potassium phosphate (pH 7.2) with the ionic strength maintained at 300 mM with potassium chloride. BeAm = benzylamine, MeAm = methylamine

	k_{cat} (s^{-1})	k_{cat}/K_m(S)[a] (M^{-1} s^{-1})	k_{cat}/K_m(O_2)[b] (M^{-1} s^{-1})	$^{D}k_{cat}$	$^{D}k_{cat}/K_m$(S)
			HPAO-2		
BeAm	8.1 ± 0.2	(9 ± 1) × 10^5	(4.7 ± 0.6) × 10^5	1.00 ± 0.04	2.0 ± 0.3
MeAm	2.18 ± 0.06	(1.2 ± 0.1) × 10^3	(1.6 ± 0.3) × 10^5	1.36 ± 0.08	18.5 ± 0.1
			HPAO-1		
BeAm	(6.6 ± 0.3) × 10^{-2}	(9 ± 1) × 10	(8.1 ± 2.1) × 10^4	5.9 ± 0.7	3 ± 1
MeAm[c]	6.2 ± 0.2	(3.0 ± 0.6) × 10^4	(4 ± 1) × 10^5	1.7 ± 0.1	4.3 ± 0.2

[a]Amine substrate. [b]Measured at saturating amine substrate and varying oxygen levels. This led to some variation in ionic strength: HPAO-2, μ = 250 mM with benzylamine and μ = 300 mM with methylamine; HPAO-1, μ = 257 mM with benzylamine and μ = 250 mM with methylamine. [c]Data from ref (*112*); experimental conditions identical to those herein, except at pH 7.0 instead of pH 7.2.

Comparison of isotope effects on k_{cat}/K_m(S) on the two isoenzymes with both substrates demonstrates that the extent of rate limitation by proton abstraction differs on steps in the reductive half-reaction. Isotope effects on k_{cat}/K_m(S) with HPAO-2 indicate that proton abstraction is clearly more rate-limiting for methylamine than benzylamine, as $^{D}k_{cat}/K_m$(S) equals 2.0 for benzylamine and 18.5 for methylamine (Table 3.2). The increase in the contribution of the proton abstraction step to k_{cat}/K_m is likely due to an increase in the free energy barrier for proton abstraction, rather than a decrease in the

barrier for methylamine binding (Scheme 3.2A), as this substrate is smaller than the preferred substrate benzylamine and thus should have no trouble accessing the active site.

Scheme 3.2 Proposed free energy diagrams that represent k_{cat}/K_m(S) in (A) HPAO-2 or (B) HPAO-1.

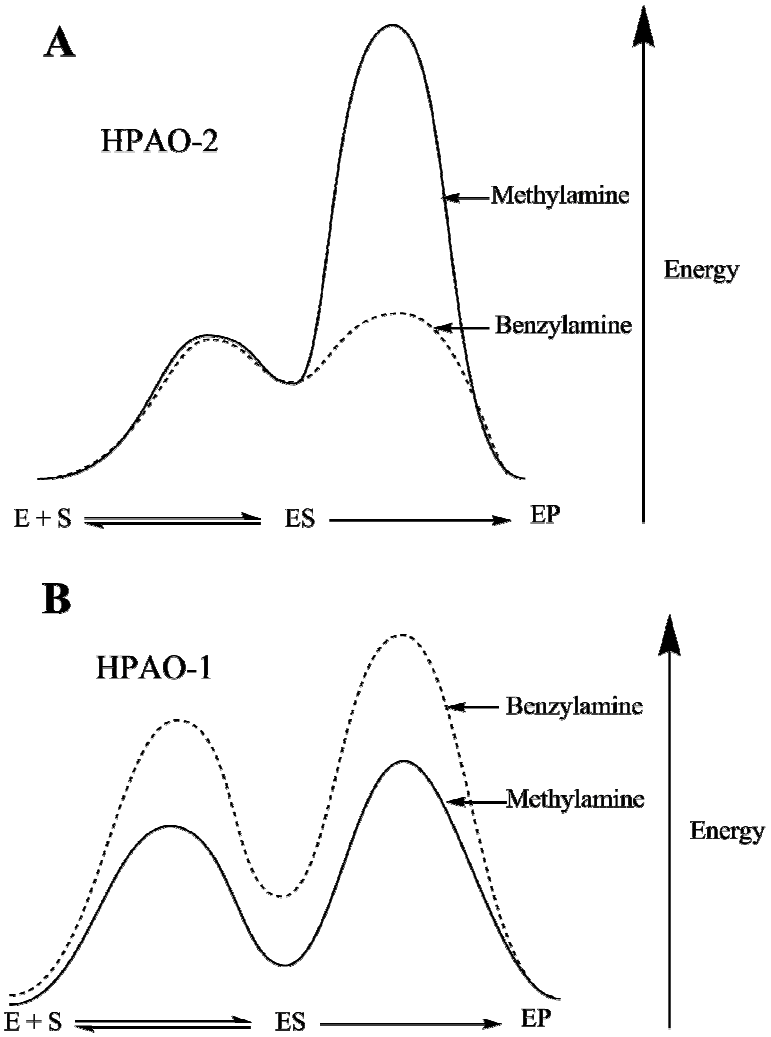

In the case of HPAO-1, the similar $^{D}k_{cat}/K_m$ values (3.0 for benzylamine vs. 4.3 for methylamine (Table 3.2)) indicate that proton abstraction is similarly rate-limiting with

respect to substrate binding for both substrates, despite the large reduction in rate when using benzylamine as the substrate. This implies that *both* substrate binding/release and proton abstraction are affected to a similar extent (Scheme 3.2B).

The impact of pH on catalysis has also been examined for HPAO-2 (using benzylamine as the substrate) for comparison to that of HPAO-1 (using methylamine as the substrate) (*100*). As summarized in Figure 3.4, the pH optima for both k_{cat}/K_m(S) and k_{cat} are ~8-8.2 and similar to that of HPAO-1 (*100*).

Figure 3.4 HPAO-2 pH profiles of (A) k_{cat}/K_m(benzylamine) (pK_{a1} = 6.6, pK_{a2} = 9.7), and (B) k_{cat} (pK_{a1} = 6.0, pK_{a2} = 7.6, pK_{a3} = 8.9).

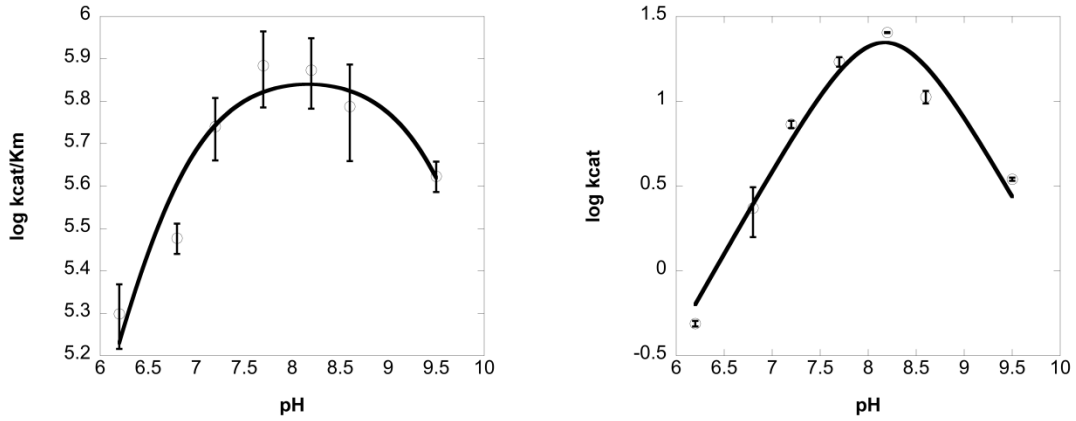

The fact that these pH optima are elevated above pH 7 is consistent with the fact that HPAO-1 is found in the *S. cerevisiae* peroxisome, which has a pH of 8.2 (*157*). The intracellular location of HPAO-2 is unknown; however, the absence of an extended N-terminus in relation to HPAO-1 suggests the site of function may be cytosolic (Figure 3.3).

Crystal structure of HPAO-2 in comparison to that of HPAO-1: overall fold and active site

Table 3.3 contains the data collection, processing, and refinement statistics for HPAO-2 to a resolution of 2.0 Å. Final R_{work} and R_{free} values are 14.5 and 19.1%, respectively (for the quality of the electron density, see Figure 3.5).

Table 3.3 X-ray crystallographic data collection, processing, and refinement statistics for HPAO-2.

Data collection and processing statistics	
detector type	ADSC Quantum 3154
beamline and source	19-ID SBC-CAT, Advanced Photon Source
temperature (K)	100
space group	*C*2
unit cell dimensions	a = 288.5 Å, b = 91.1 Å, c = 151.1 Å, β = 117.2°
no. of molecules in the unit cell, Z	6
wavelength (Å)	0.9785
resolution (Å)[a]	50.00-2.00 (2.07-2.00)
no. of unique reflections	210228
completeness (%)[a]	90.6 (69.3)
R_{merge}[a,b]	0.089 (0.319)
$I/\sigma I$[a]	13.34 (3.0)
redundancy[a]	3.5 (3.1)
Crystallographic refinement and model statistics	
resolution range (Å)[a]	37.4-2.00 (2.06-2.01)
no. of reflections in the working set[a]	200161 (10684)
no. of reflections in the test set[a]	10514 (539)
R_{work} (%)[a,c]	14.5 (21.9)
R_{free} (%)[a,d]	19.1 (27.3)
no. of non-hydrogen atoms	
no. of amino acid residues	1899
no. of protein atoms	15321
no. of solvent molecules	3199
no. of Cu(II) ions	3
no. of other atoms	91
rmsd from ideal geometry	
bond lengths (Å)	0.026
bond angles (°)	2.0
Ramachadran plot	
energetically favored regions (%)	89.2
additionally allowed regions (%)	10.4

Table 3.3, continued. X-ray crystallographic data collection, processing, and refinement statistics for HPAO-2.

Ramachandran plot	
generously allowed regions (%)	0.2
disallowed regions (%)	0.2
average *B* factor (Å^2)	
main chain	24.4
side chain	26.3
ligands	43.8
solvent atoms	44.2

[a]Numbers in parentheses refer to the highest resolution shell. [b]R_{merge} = $\Sigma_{hkl}\Sigma_i|I_{hkl,I} - \langle I_{hkl}\rangle|/\Sigma_{hkl}\Sigma_i I_{hkl,I}$, where I is the observed intensity and $\langle I\rangle$ is the average intensity for multiple measurements. [c]R_{work} = $\Sigma||F_o| - |F_o|/\Sigma|F_o|$, where $|F_o|$ is the observed structure factor amplitude and $|F_c|$ is the calculated structure factor amplitude for 95% of the data used in refinement. [d]R_{free} based on 5% of the data excluded from refinement.

Figure 3.5 Stereoview of the $2F_o$-F_c electron density quality (contoured at 1.5σ) within the HPAO-2 β-sheet core. The model associated with the electron density is drawn explicitly in stick and colored green. The rest of the HPAO-2 model is drawn as green ribbon.

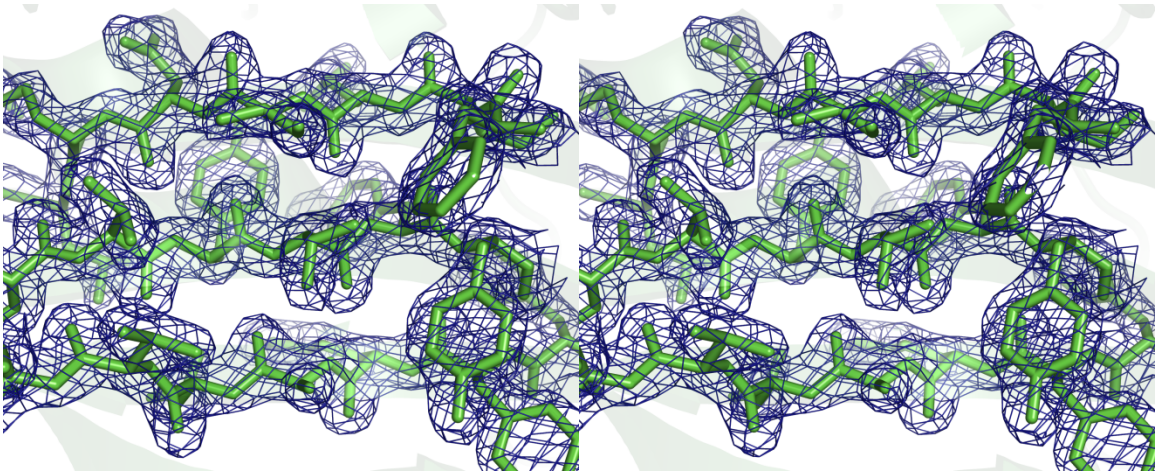

Three polypeptide chains, or 1.5 physiological HPAO-2 dimers, were seen in the crystallographic asymmetric unit (ASU) in space group *C*2. The overall structure of the HPAO-2 dimer is identical in fold to that of HPAO-1 and other CAOs (Figure 1.3) (*6*, *19*,

52-55, 57-60). Superimposition of the HPAO-2 and HPAO-1 homodimers yields a root-mean-square deviation (rmsd) for main chain atoms of 0.99 Å.

HPAO-2 consists of three domains arranged along its primary sequence (D2-D4). The amine oxidase from *E. coli* contains an additional protruding "stalk" domain (D1) at the N-terminus that is not present in the other CAO crystal structures (*58*). Two small α/β domains (D2 and D3) are formed by the N-terminal portion of HPAO-2, while the larger catalytic domain (D4) is composed of the C-terminal portion of the chain. As seen in HPAO-1, the catalytic domain (D4) of HPAO-2 contains a complex antiparallel β-sandwich fold (*55*). Two β-hairpin arms protrude from each monomer and form part of the intricate interaction within the HPAO-2 homodimer. Some CAOs from other sources, such as *E. coli*, pea seedling, and human kidney, bind a calcium or manganese ion at an additional site on the periphery of the protein (*19, 58, 59, 154*). Like HPAO-1, no evidence of this second metal binding site was observed in the HPAO-2 crystal structure (*55*). Unusually, an adventitious second copper ion is present in HPAO-2 samples following initial protein purification. Even though the protein used in crystallization had not been dialyzed against EDTA, which removes this loosely bound copper, there was no evidence in the electron density to indicate where this site may be located within the protein. HPAO-2 contains eight cysteine residues per monomer, but only two form a disulfide bond (Cys321 and Cys347). In HPAO-1, the two equivalent cysteine residues (12 cysteine residues in total) also form one of two disulfide bonds seen in HPAO-1 (Cys338 and Cys364) (*55*).

The HPAO-2 active site is deeply buried within the protein interior. The two active sites within the functional HPAO-2 homodimer each contain a TPQ cofactor (42.2 Å between the Cα atom of each TPQ cofactor) and a cupric ion (34.7 Å between copper ions in the dimer) coordinated by three conserved histidine ligands in a distorted square pyramidal geometry (Figure 3.6). Two well-ordered water molecules are ligated to the copper ion: one sits in an axial position (W_a) bridging the O2 atom of TPQ and the copper, and the other in an equatorial position (W_e) nearly planar with Cu(II) and the nitrogen atoms of its three histidine ligands (Figure 3.6). This latter solvent position is variably occupied in different CAO crystal structures and when modeled has a higher average B-factor than the axial water. W_e was clearly observed in all three subunits within the crystallographic ASU of the HPAO-2 electron density, whereas it was only modeled in two of the six subunits in the HPAO-1 structure ASU; thus, this water molecule appears to be more labile in HPAO-1 than HPAO-2 (*103*).

The electron density for TPQ clearly indicates that >90% of the active sites in the crystal contain fully formed TPQ (Figure 3.6), even though treatment of the protein preparation used in crystallization with phenylhydrazine indicated only ~50% TPQ was present. However, the observation of only 50% TPQ could arise from half-site reactivity, which is known to occur in other CAOs, and as indicated in the crystal structure, the true TPQ content could actually be closer to 100% (*80, 107, 111*). Alternatively, enzyme with TPQ in both subunits may have selectively crystallized from the mother liquor. The TPQ cofactor adopts a single orientation with its O2 atom closest to the copper center and O5 atom closest to the conserved catalytic base, Asp302. It is thus poised for substrate attack

at the C5 atom of TPQ to form the substrate Schiff base intermediate and represents a conformation competent for catalysis termed “off-copper”. There is no evidence of the “on-copper” conformation in which the O4 atom of TPQ is directly ligated to the copper, displacing the axial water ligand (W_a). This conformation is considered not competent for catalysis as the C5 is inaccessible to amine substrate but is often present in CAO crystal structures, including HPAO-1 where it forms ~30% of the TPQ conformers (*103*).

Figure 3.6 Active site of HPAO-2 with $2F_o$-F_c electron density. Residues are shown in stick and colored by atom type (carbon, green). Hydrogen bonds are indicated by dashed lines. Ligand-metal interactions are indicated by solid lines. The copper ion is shown as a gold sphere, and water molecules are depicted as small red spheres (W_a indicates the axial water ligand to the copper and W_e indicates the equatorial water ligand). The $2F_o$-F_c electron density contoured at 1.5σ is shown as blue mesh.

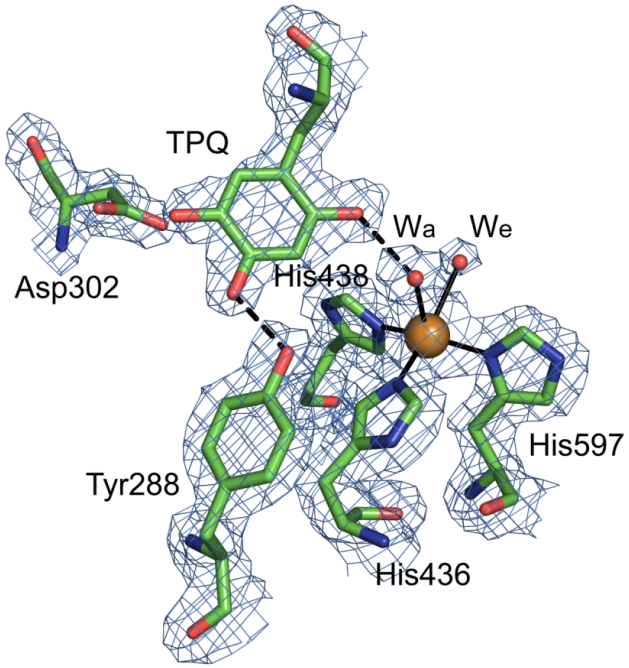

Crystal structure of HPAO-2 in comparison to HPAO-1: substrate amine entry channel

Although the residues important for chemistry are structurally identical between HPAO-2 and HPAO-1, their substrate channels differ considerably. HPAO-2 has a broad, funnel-shaped substrate entry channel compared to HPAO-1 (Figure 3.7).

Figure 3.7 Surface representation of the substrate entry channels in (A) HPAO-2 and (B) HPAO-1. TPQ and the "gating" tryptophan residue are drawn in stick and colored by atom type ((A) carbon, green; (B) carbon, blue), and copper is depicted as a gold sphere.

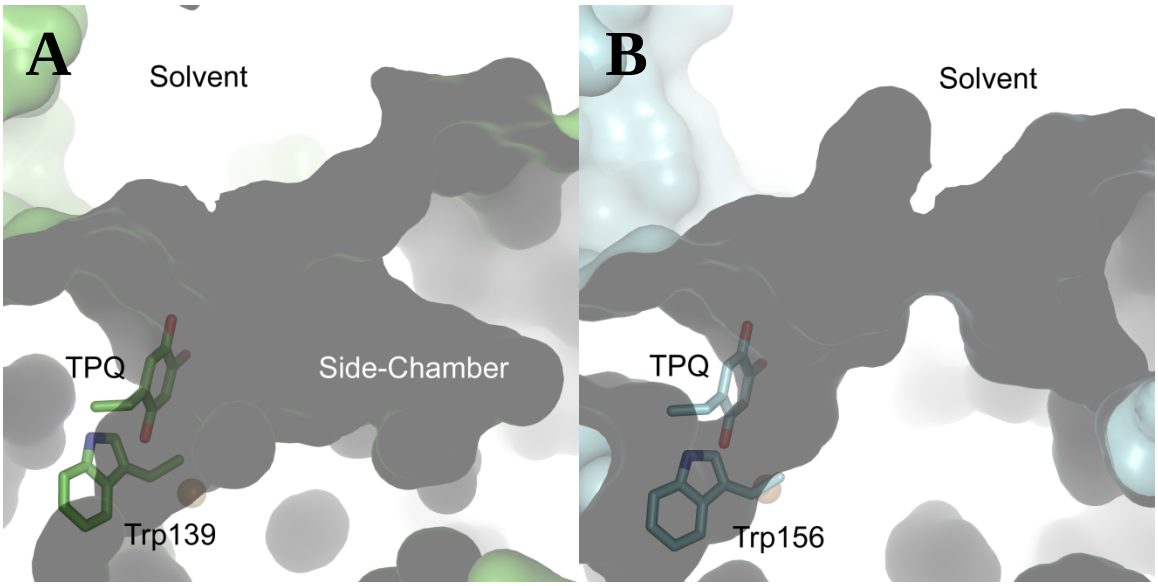

The widening of the HPAO-2 channel mouth is primarily due to a two-residue deletion in the loop of the β-hairpin arm from the other monomer that reaches across close to the active site (red in Figure 1.3). This arm contains a conserved His (residues 359 and 376 in HPAO-2 and HPAO-1, respectively) that forms a hydrogen bond to the conserved acidic residue following TPQ in the protein sequence. In HPAO-1, the loop is

defined by the Arg380-Asp-Asn-Phe-Ala-Thr385 sequence, whereas in HPAO-2, the Phe and Ala residues are deleted to give a four-residue β-hairpin turn consisting of Arg363, Thr364, Asn365, and Val366 (orange in Figure 3.8). Interestingly, HPAO-2 also has a side chamber just below the mouth of the main channel, which is sufficiently large to accommodate and retain a bulkier aromatic substrate like benzylamine or the outgoing product of its reaction, benzaldehyde (Figures 3.7 and 3.9).

Figure 3.8 Stereo overlay between key residues in HPAO-2 and HPAO-1 that define the substrate channel. Only HPAO-2 residues are numbered, and the side chains are colored as specified in the text. The structurally corresponding residues in HPAO-1 are drawn as white sticks, except in the case of the red HPAO-2 side chains that define the side chamber, which is absent in HPAO-1. The fold of HPAO-2 is depicted as a green ribbon.

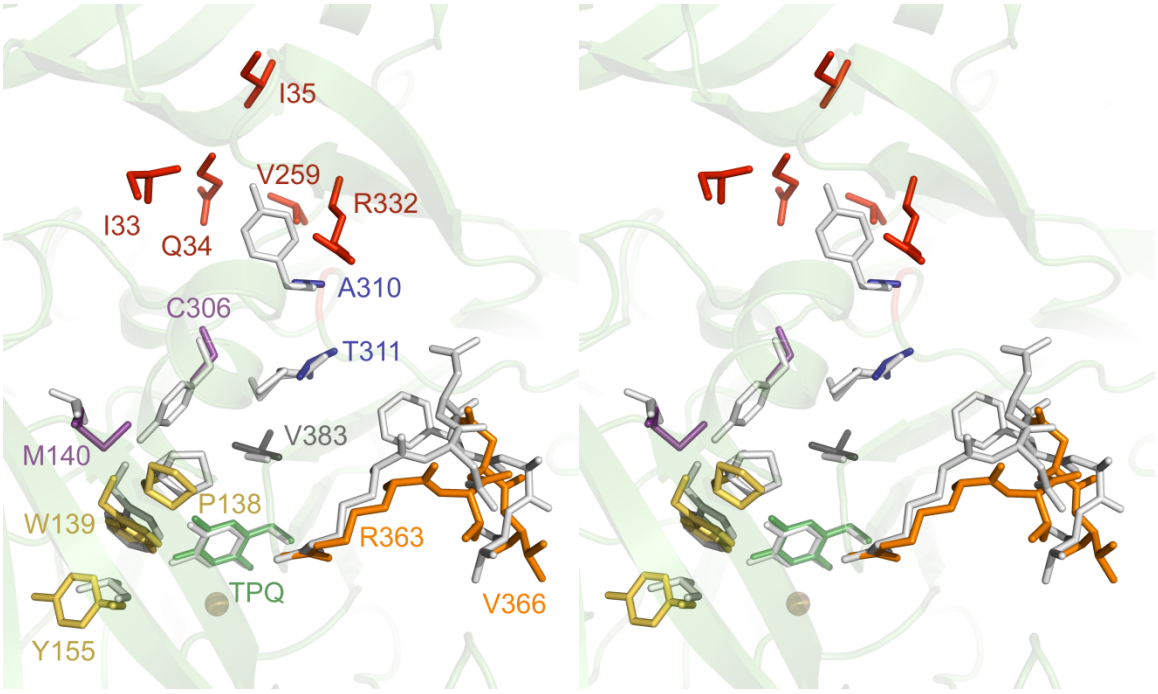

The chamber is accessed by a mouth that widens out to a diameter of 5.1 Å and is 5.4 Å deep. There are three small pockets at its deepest point which present backbone polar groups (Ile33, Gln34, and Ile35) that could form hydrogen bonds to a substrate amine group (red in Figure 3.8, and Figure 3.9). One side of the chamber is hydrophobic, which is formed by the alkyl chain of Arg332, Val259, and Ala310, and would enable a favorable interaction with an aromatic moiety (red except Ala310 which is blue in Figure 3.8, and Figure 3.10B). Interestingly, the opposite wall contains a high density of oxygen atoms, which gives a slight negative electrostatic potential to this side of the chamber.

Figure 3.9 Surface representation of the side-chamber located in the HPAO-2 entry channel. View looking into the side-chamber from the substrate entry channel. The protein surface is colored by atom type (carbon, light grey). TPQ is shown in stick and colored by atom type (carbon, green).

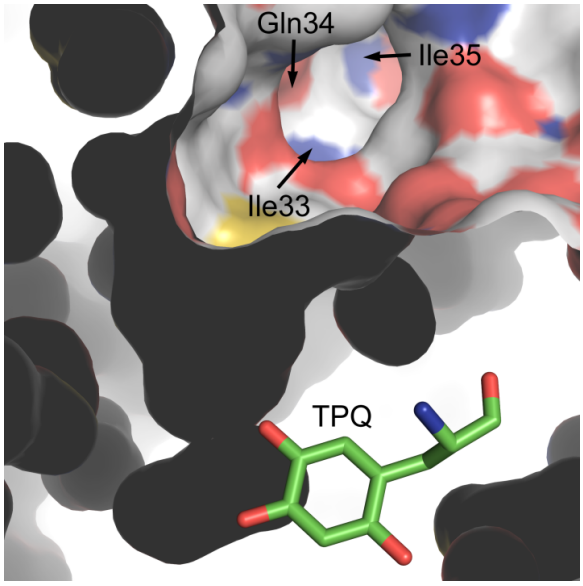

Figure 3.10 Surface representation of the side chamber located in the HPAO-2 entry channel. (A) Slice through the side-chamber. (B) Panel (A) with benzylamine modeled in the side chamber. The protein surface is colored by atom type (carbon, light grey). TPQ and amino acid side chains are drawn in stick colored by atom type (carbon, green). The molecular surface is colored by atom type (carbon, grey). The model of benzylamine is drawn in stick and colored by atom type (carbon, grey). The view in panels (A) and (B) is rotated about the vertical approximately 90° from the view in Figure 3.9.

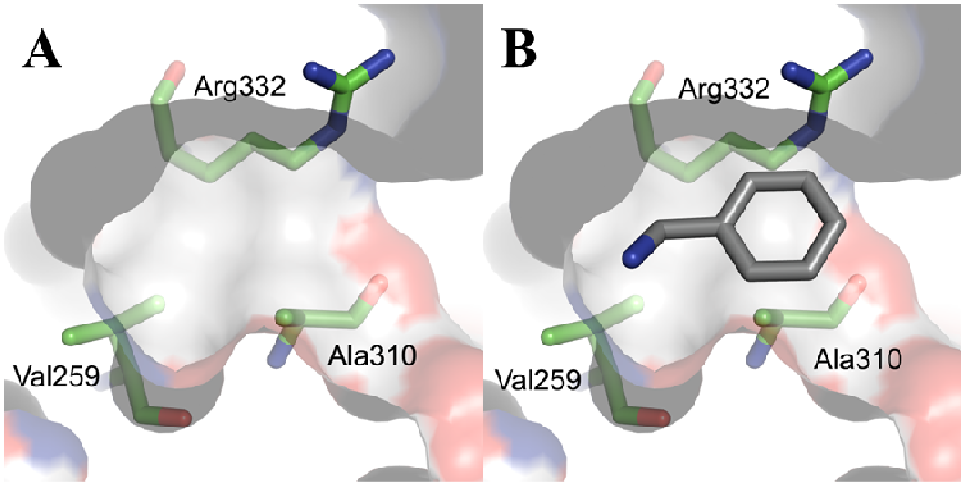

Between the side chamber and the active site, there are two key sequentially adjacent residue side chain changes that widen the HPAO-2 channel from that of HPAO-1 (Ala310 and Thr311 in HPAO-2, compared to Tyr327 and Met328 in HPAO-1) (Table 3.4, blue in Figure 3.8).

Table 3.4 Residue changes between HPAO-2 and HPAO-1 that likely impact the accommodation of substrate and catalytic intermediate structures.

HPAO-2	HPAO-1
Met140	Thr156
Tyr155	Leu174
Cys306	Tyr323
Ala310	Tyr327
Thr311	Met328
Val383	Ala402

At the base of the substrate entry channel, where the substrate undergoes chemistry to form the product, there is a conserved tryptophan residue in HPAO-2 and -1 (Trp139 and Trp156, respectively (Figure 3.7 and yellow in Figure 3.8)) that in other CAOs is generally a Tyr or Phe (*6, 52-55, 57-59*). This residue has been termed a "gate" to the active site (*6*). It has two major conformers: one blocking access to TPQ (normally observed in resting state CAO crystal structures, although the side chain can also be disordered) and the other rotated out of the way (observed in Schiff base intermediates generated in an active site base mutant and suicide inhibitor complexes that mimic Schiff base intermediates) (*53, 80, 105, 158*). Interestingly, the gate hypothesis does not appear to pertain to mammalian CAOs. The corresponding tyrosine residues in structures of CAO from bovine plasma, human diamine oxidase, and human vascular adhesion protein-1 are in an intermediate position halfway between the "open" and "closed" conformations (*19, 52-54*). Due to HPAO-2 and HPAO-1 having the larger Trp amino acid at this position, the "gate" is always open in these structures, and has B-factors that are equivalent to those of surrounding residues indicating a lower mobility than in other CAOs. However, the angle of the Trp side chain is different between the two enzymes, and the main chain is shifted such that the channel in HPAO-1 is more constricted than in HPAO-2 (Figure 3.7). This appears to primarily result from the substitution of Leu174 in HPAO-1 for Tyr155 in HPAO-2 (Table 3.4 and yellow in Figure 3.8). This residue does not directly form part of the channel wall but sits behind the five-membered ring of Trp156, pushing it into the channel in HPAO-1. The conserved Pro residue that is N-terminal to the Trp in both structures rigidifies the main chain, reducing the possibility of

compensating flexibility in the channel (yellow in Figure 3.8). On the other side of the channel, the main chain is also moved inward in HPAO-1, constricting the channel compared to HPAO-2. This is again a "knock-on" effect due to a two residue insertion into the tip of the β-hairpin that reaches across from the other monomer of the homodimer and was discussed above (orange in Figure 3.8). HPAO-1 has a two-residue insertion (Phe383-Ala384) compared to HPAO-2, and it is the side chain of Phe383 that pushes the main chain containing Ala402 (Val383 in HPAO-2) into the substrate channel (Table 3.4 and colored dark gray in Figure 3.8). Although Val383 is a larger side chain than Ala402, the displacement of the main chain places the end of these two residue side chains at the same place, but the effect N-terminal to these residues is an overall displacement constricting the HPAO-1 channel. The coincident positioning of the end of the side chains of Val383 in HPAO-2 and Ala402 in HPAO-1 appears to have an important role, as TPQ is sequentially close to this position (HPAO-2, position 386; HPAO-1, position 405) and the structures become coincident immediately C-terminal to Val383 or Ala402.

Finally, there are two side chain changes between HPAO-2 and HPAO-1 within the substrate entry channel that would interact with bulky R groups during the reductive half-reaction; in HPAO-2, Met140 and Cys306 have replaced Thr157 and Tyr323, respectively, in HPAO-1 (Table 3.4 and magenta in Figure 3.8).

3.4 Discussion

HPAO-2 is the second copper amine oxidase to be isolated and characterized from *H. polymorpha*. The marked change in substrate specificity is largely manifested in k_{cat}/K_m, which is 750-fold greater for benzylamine than methylamine. Complementarily, the k_{cat}/K_m values for the previously studied CAO from the same organism, HPAO-1, are opposite in specificity. Hence, the isolation and characterization of two copper amine oxidases from the same organism with 67% sequence homology and 34% sequence identity, but inverted substrate specificities, begin to address the nature of substrate specificity in these kinetically diverse enzymes.

The substrate entry and binding pockets of the two enzymes are clearly very structurally different as determined by comparison of the X-ray crystal structures (Figure 3.7). The wider mouth of the entry channel of HPAO-2 would be more likely to capture and funnel the larger benzylamine from bulk solvent into the heart of the enzyme. In HPAO-1, the channel is almost as narrow at its entrance as it is close to the active site. This would restrict the orientations in which bulky aromatic substrates could enter the channel, which is likely to reduce the probability of their capture.

In HPAO-2, there is a defined side-chamber off the mouth of the amine entry channel (Figure 3.9). This chamber could easily accommodate benzylamine, and contains three pockets at its deepest part of the chamber with polar groups that could form hydrogen bonds with the amine group of substrate (Figure 3.10A). This could be considered a holding area or “anteroom” that increases the local concentration of substrate near the active site. It is also possible that binding of substrate into this side

chamber away from the main portion of the entry channel could facilitate movement of the product out of the enzyme. Interestingly, there has been another anteroom identified in CAOs that is proposed to have a similar function, but in this case for substrate O_2 (*54*, *57*, *103*)). This anteroom lies on the opposite side of the copper from the amine entry channel and is structurally conserved among CAOs. In contrast, the amine anteroom appears to be a particular feature of HPAO-2 and is unlikely to play a significant role in the kinetics of the enzyme.

The large changes in k_{cat}/K_m between the substrates of both enzymes suggest that substrate binding at the site of chemistry plays a role in determining substrate preference. However, selection against the smaller substrate methylamine for HPAO-2 cannot depend on sterics alone, since the substrate binding pocket could accommodate both substrates. During catalysis, the formation of tetrahedral intermediates is postulated through nucleophilic attack on C5 of cofactor, as in the initial attack of amine to form the substrate Schiff base (Scheme 3.1). TPQ in its active "off-copper" conformation sits in a wedge-shaped environment in which the C2-C3 side of the ring forms tight packing interactions with the protein, while the C5-C6 side of the ring does not. This additional space next to C5 is proposed to be important for the accommodation of tetrahedral intermediates during nucleophilic attack (*79*). The C5 environment is controlled primarily by two invariant residues, the aspartate catalytic base and the asparagine residue N-terminal to TPQ (position 385 in HPAO-2 and position 404 in HPAO-1). The headgroup of the Asn residue packs against one face of the TPQ ring, meaning that amine

attack can occur only from the other face of the ring that lies by the catalytic base (Figure 3.11).

Figure 3.11 The active site of HPAO-2 showing the protein residues (Asp302 and Asn385) which lie on either side of the TPQ ring. Protein residues are colored by atom type (carbon, green). Asp302 and Asn385 are drawn as space-filling spheres. TPQ and the histidine residues ligating the copper are shown in stick, and the copper ion is shown as a gold sphere. The fold of HPAO-2 is depicted as a green ribbon.

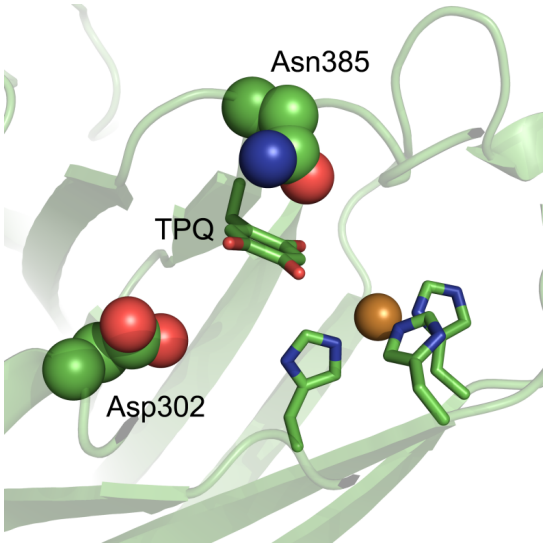

The importance of Asn404 in orienting the TPQ cofactor has been demonstrated. Mutation of this residue to alanine in HPAO-1 leads to the accumulation of the product Schiff base upon reaction with methylamine (*76*). However, for bulkier substrates such as benzylamine, the orientation of amine attack and the accommodation of subsequent Schiff base intermediates are controlled by the next sphere of residues that line the entry channel just outside the catalytic active site. Two key residues are spatially positioned with a large/small side chain pattern being reversed in the two enzymes; Met140 and Cys306 in HPAO-2 are replaced with Thr157 and Tyr323, respectively, in HPAO-1 (Table 3.4, magenta in Figure 3.8, and Figure 3.12). This has the effect of moving the position of a small pocket such that bulkier R groups can access the HPAO-2 active site.

Benzylamine, as a substrate, is unusual in that its product Schiff base is fully conjugated and thus planar, and the shape of the HPAO-2 substrate channel by the active site is more complementary to this species than that of HPAO-1 (Figure 3.12).

Figure 3.12 Model of the product Schiff base of benzylamine with TPQ. Residues from the crystal structures are drawn in stick colored by atom (HPAO-2: carbon, green; HPAO-1: carbon, cyan). The modeled product Schiff base is drawn in stick and colored by atom type (carbon, dark grey).

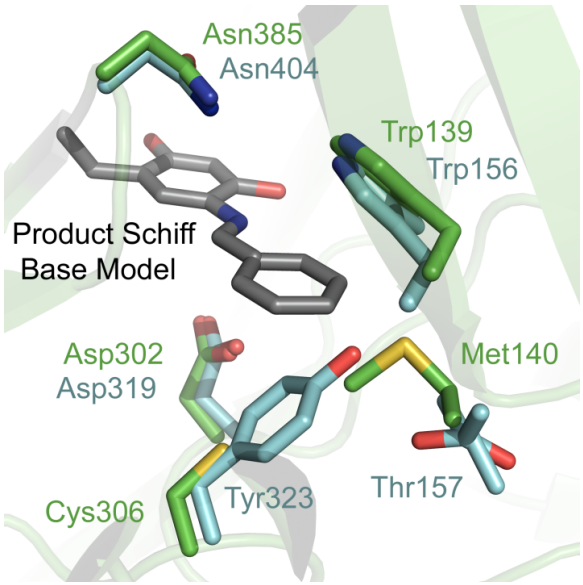

In HPAO-2, the effect of substrate deuteration on k_{cat}/K_m is of particular value in understanding the reduced reactivity with methylamine, specifically the large $^{D}k_{cat}/K_m$ for methylamine as compared to the more optimal substrate, benzylamine. The magnitude of the methylamine $^{D}k_{cat}/K_m$ (18.5 ± 0.1) is very close to the intrinsic isotope effect for CAOs (*159*), implying that proton abstraction has become rate-limiting for the poor substrate. The origin of the reduced k_{cat}/K_m(S) value is thus attributed in part to an impaired proton abstraction step (Scheme 3.2A). Considering the shape complementarity for benzylamine in the entry channel of HPAO-2, a preferential decrease in the rate of

proton abstraction is likely due to difficulty in achieving precise alignment between the methylamine substrate Schiff base and the active site base. It was also possible that the faster benzylamine rate could reflect an increased level of conjugation in its resulting carbanion-product Schiff base complex. However, a comparison of k_{cat}/K_m(S) for the oxidation of aromatic phenylethylamine (2.6×10^5 $M^{-1}s^{-1}$) at the nonconjugated C1 position to the benzylamine value (Table 3.2) indicates a similar or elevated value.

Although the HPAO-1 and HPAO-2 structures overlay exactly with regard to the positions of the catalytic base (an aspartate), "off-copper" TPQ, and the ordered water molecules between them, TPQ appears to have a lower mobility in HPAO-2 than in HPAO-1. This is supported by the fact that in the three subunits of the crystallographic ASU of HPAO-2 there is no evidence of the on-copper conformer of TPQ, whereas in four of the six subunits in the HPAO-1 structure, there is a substantial proportion of on-copper TPQ. The side chain B-factors for the cofactor and the surrounding residues, normalized to the overall B-factor of each structure, also support the idea that TPQ is less mobile in HPAO-2 than in HPAO-1. This feature may exacerbate the ability of HPAO-2 to orient the reactive carbon of the methylamine Schiff base with the aspartate catalytic base. We note that there is some isotope effect on k_{cat}/K_m for benzylamine with HPAO-2, indicating that proton abstraction contributes to k_{cat}/K_m for this substrate as well as for methylamine. It is, therefore, very likely that additional factors contribute to the 10^3-fold rate reduction with methylamine oxidation by HPAO-2.

In the case of HPAO-1, similar $^{D}k_{cat}/K_m$ values are observed for both substrates, while the second-order rate constant is reduced ~330-fold for benzylamine. The most

likely explanation is that both proton abstraction and substrate binding/release are slowed when the enzyme is challenged with the larger substrate (Scheme 3.2B). The increase in rate limitation by proton abstraction for benzylamine is also reflected in $^{D}k_{cat}$, which is elevated relative to that of methylamine ($^{D}k_{cat}$ (benzylamine) = 5.9, whereas $^{D}k_{cat}$ (methylamine) = 1.7). In previous studies of HPAO-1 with methylamine, three partially rate-determining steps have been documented that include aldehyde release, transfer of the first electron to oxygen, and hydrogen peroxide and/or ammonium release (*112*). The loss of a proton from the C1 atom of the substrate Schiff base must contribute significantly to the decreased rate of turnover with benzylamine, since all steps after oxygen binding are common to both substrates and therefore cannot account for the difference in turnover rates (Scheme 3.1).

Significantly, the differences in $k_{cat}/K_m(S)$ are not mirrored in $k_{cat}/K_m(O_2)$. The oxygen binding and reactivity sites, copper, and copper ligands on the two enzymes are structurally similar. All the residues that define the O_2 anteroom close to the copper are different between HPAO-1 and -2, but the nature of the area is still hydrophobic (Table 3.5).

Table 3.5 Residue changes which define the O_2 anteroom.

HPAO-2	HPAO-1
Ala406	Leu425
Phe595	Ile622
His612	Ile639
Val404	Ile423
Phe460	Leu440

This is true in other CAOs, where the residues comprising the O_2 anteroom are not conserved but the hydrophobic nature of the pocket is maintained (*54, 103, 117, 118*). Hence, the kinetic and structural data suggest a modular structure for both HPAOs, in which changes at the amine substrate site are not propagated to the pocket where oxygen undergoes reaction. Furthermore, the similar $k_{cat}/K_m(O_2)$ values for both isoenzymes, regardless of substrate, support the ping-pong mechanism proposed for HPAO-1 (Scheme 3.1). The stark contrast between the substrate-dependent changes in $k_{cat}/K_m(S)$ and the substrate-independent $k_{cat}/K_m(O_2)$ highlights the independence of the oxygen binding and reduction sites from the structural determinants affecting amine kinetics.

3.5 Conclusions

In this study, the origins of substrate specificity in the copper amine oxidases from *Hansenula polymorpha* designated HPAO-1 and HPAO-2 have been investigated. From the newly determined crystal structure of HPAO-2 in comparison with that of HPAO-1, we can begin to see how the narrow binding channel of HPAO-1 may predispose that CAO isoenzyme to reaction with smaller aliphatic amines via changes in substrate binding energies. However, selection against the smaller aliphatic substrate in the wide funnel-like substrate binding channel of HPAO-2 cannot be due to sterics alone. A significant increase in $^{D}k_{cat}/K_m$ values for the poorer methylamine substrate relative to the preferred substrate indicates that proton abstraction has become rate-determining with methylamine. Impairment in the positioning of the methylamine substrate Schiff base in HPAO-2 affords the most likely explanation for the increase in $^{D}k_{cat}/K_m(S)$ while the reduction in the absolute magnitude of $k_{cat}/K_m(S)$ likely arises from numerous factors. Conversely, in HPAO-1, both the binding of substrate and the release of product, as well as the proton abstraction step, appear to be hindered under catalysis with the bulkier aromatic amine. This combination of kinetic and structural characterization reveals the multiplicity of factors that enter into the discrimination between large and small substrates at the active sites of a pair of paralogous enzymes which catalyze identical chemical reactions.

CHAPTER 4: UNDERSTANDING AMINE SUBSTRATE SPECIFICITY THROUGH STRUCTURAL ANALYSIS OF *Hansenula polymorpha* COPPER AMINE OXIDASE-1 SUBSTRATE COMPLEXES

The CAO catalytic mechanism is ping-pong, and can be divided into two half-reactions: a reductive half-reaction, in which the active site TPQ cofactor is reduced with the oxidation of a primary amine, and an oxidative half-reaction, in which reduced TPQ is re-oxidized with the concomitant reduction of molecular oxygen to hydrogen peroxide. The reductive half-reaction proceeds via Schiff base chemistry, in which a primary amine substrate first attacks the C5 carbonyl of TPQ, forming a series of covalent intermediates. The X-ray crystal structures of copper amine oxidase-1 from the yeast *Hansenula polymorpha* (HPAO-1) in complex with methylamine, ethylamine, and benzylamine prepared in an anaerobic chamber have been solved to resolutions of 1.89, 2.18, and 2.25 Å, respectively. These structures reveal the three amine substrates bound at the back of the active site near the site of catalysis. In the ethylamine- and benzylamine-HPAO-1 complexes, the bound substrate is coincident with TPQ in its two-electron reduced aminoquinol form. The structure of HPAO-1 treated with methylamine contains a complex mixture amongst the polypeptide chains of either (A) the substrate Schiff base intermediate and aminoquinol in conjunction with bound methylamine, or (B) formaldehyde and the protonated iminoquinone. Rearrangements of particular amino acid side chains within the substrate channel and specific protein-substrate interactions provide insight into substrate specificity in HPAO-1. These changes begin to account for this CAO's kinetic preference for small, aliphatic primary amines over the aromatic amines or whole peptides preferred by some of its homologs.

4.1 Background

The CAO family of enzymes, which are responsible for the oxidation of primary amines to their corresponding aldehydes, are found in nearly every aerobic organism, including bacteria, yeast, plants, fungi, and animals. This ubiquity is echoed in the wide range of primary amines which can act as substrates, and consequently in the variety of biological functions attributed to these enzymes. In prokaryotes, CAOs allow for the use of primary amines as a sole carbon and/or nitrogen source during metabolism (*160-162*). The functions of CAOs from eukaryotic sources are more complex, with proposed roles including the production of second messenger compounds involved in the cross-linking of cell wall components and wound healing in plants (*163-165*) as well as the regulation of glucose uptake and inflammatory lymphocyte extravasation in mammals (*119, 166*). The products generated during CAO catalysis can be highly cytotoxic, in particular formaldehyde, which has been implicated in protein crosslinking correlated with cellular damage in late-diabetic vascular complications and atherosclerosis (*121*).

Catalysis in CAOs proceeds by means of a ping-pong mechanism, which can be divided into two half-reactions (Scheme 4.1): a reductive half-reaction in which a primary amine substrate is oxidized to its corresponding aldehyde with the concomitant reduction of the organic quinocofactor TPQ, and an oxidative half-reaction in which TPQ is re-oxidized with the reduction of O_2 to H_2O_2 and the release of an ammonium ion:

Scheme 4.1 The two half-reactions of CAO catalysis. E represents the enzyme, and $RCH_2NH_3^+$ represents all primary amine substrates.

reductive half-reaction: $E_{ox} + RCH_2NH_3^+ \rightarrow E_{red} + RCHO$

oxidative half-reaction: $E_{red} + O_2 + H_2O \rightarrow E_{ox} + H_2O_2 + NH_4^+$

The CAO catalytic mechanism is described in detail in Chapter 1 of this work. Briefly, catalysis begins with a nucleophilic attack on the C5 atom of oxidized TPQ by a primary amine (A in Scheme 4.2). This covalently links the two species through generation of a substrate Schiff base intermediate (B in Scheme 4.2). An invariant aspartate residue abstracts a proton from the C1 atom of the substrate. This produces a product Schiff base species (D in Scheme 4.2) by way of a carbanionic intermediate (C in Scheme 4.2). The rapid hydrolysis of the product Schiff base releases the corresponding aldehyde, leaving TPQ in a two-electron reduced aminoquinol form (E in Scheme 4.2) and marking the end of the reductive half-reaction.

The oxidative half-reaction involves the re-oxidation of reduced TPQ coupled with the reduction of molecular oxygen to hydrogen peroxide. Following the release of the free aldehyde product at the end of the reductive half-reaction, the aminoquinol/Cu(II) couple exists in equilibrium with a semiquinone radical/Cu(I) couple (E and F in Scheme 4.2, respectively). The reduction of molecular oxygen generates an oxidized iminoquinone intermediate and hydrogen peroxide (G in Scheme 4.2). Finally, hydrolysis of the iminoquinone releases an ammonium ion and regenerates oxidized TPQ (A in Scheme 4.2). Alternatively, when substrate levels are high the iminoquinone can react with another amine substrate, liberating an ammonium ion and producing the substrate Schiff base (B in Scheme 4.2).

Scheme 4.2 Proposed CAO catalytic mechanism. $RCH_3NH_3^+$ is representative of all primary amine substrates.

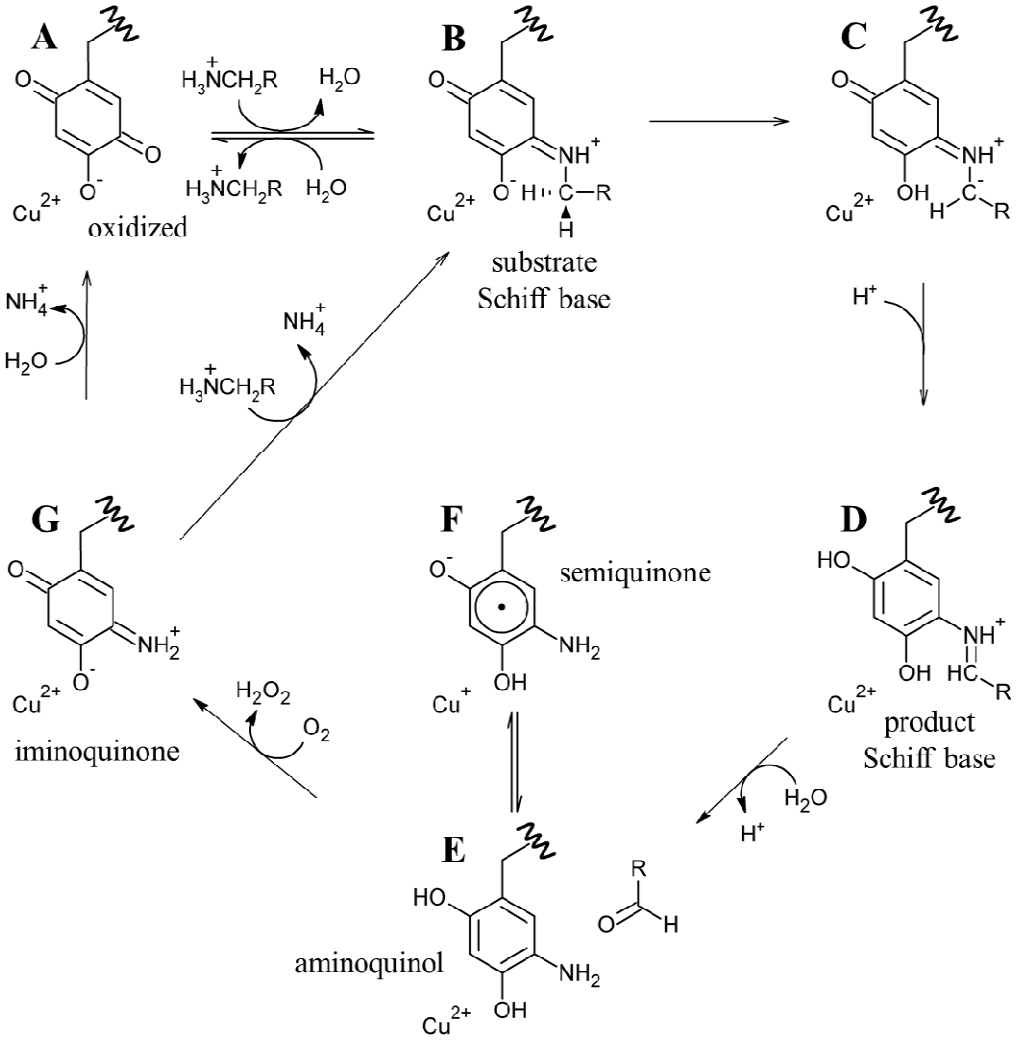

Despite well-conserved active site residues that carry out identical chemistry, members of the CAO family of enzymes are known to react with a great variety of primary amine substrates, ranging from methylamine to whole proteins. Substrate preferences in CAOs vary by source and cellular location. Work using CAOs isolated from *Escherichia coli* (ECAO) and *Arthrobacter globiformis* (AGAO), for instance, have established these enzymes' preference for primary aromatic monoamines such as

phenylethylamine or tyramine (*58*). Two CAO paralogs isolated from the yeast *Hansenula polymorpha* (HPAO-1 and HPAO-2) demonstrate strongly opposite preferences for small aliphatic amines such as ethylamine or methylamine (HPAO-1) as opposed to the bulkier aromatic amine benzylamine (HPAO-2), and are described in Chapter 3 of this work (*56*). Vascular adhesion protein-1 (VAP-1), one of three functional CAO isoforms expressed in humans, is active against much larger amine substrates and regulates lymphocyte adhesion and rolling along vascular surfaces to sites of cellular inflammation through its activity against free amine groups from membrane-bound VAP-1 counter-receptors (*24*).

Lacking in the study of substrate specificity in CAOs thus far is a structural investigation of a single CAO reduced by multiple primary amines that have undergone kinetic characterization. In order to explore the structural factors that influence substrate specificity in HPAO-1, crystals of the native protein have been reduced in an anaerobic chamber with methylamine, ethylamine, or benzylamine before flash-freezing, and structures of the resulting complexes have been solved by X-ray crystallography. A comparison of HPAO-1 in complex with all three amine substrates with the structure of native HPAO-1 provides insight into specific substrate-protein interactions involving residues located within the amine substrate channel and active site. These are considered within the context of steady state kinetic data available for the reaction with all three amines. Additionally, the structures of the aminoquinol, substrate Schiff base intermediate formed with methylamine, and protonated iminoquinone are reported.

4.2 Methods

Protein expression and purification

Native HPAO-1 protein was heterologously expressed in *Saccharomyces cerevisiae* and purified as previously described (*103*).

HPAO-1 crystallization and substrate soaks

Following purification, HPAO-1 protein was buffer-exchanged into 50 mM HEPES, pH 7.0 and concentrated to 13 mg/mL for crystallization. Crystals were grown by the hanging drop vapor diffusion method as described previously (*55*). The ratio of protein to crystallization solution (8-9% w/v polyethylene glycol 8000 in 0.22-0.25 M potassium phosphate, pH 6) in the hanging drops was 1:1 (6 µL total). Drops were seeded after 24 hours of equilibration using a streak-seeding technique and mature HPAO-1 crystals as seed donors (*132*). Cube-shaped crystals that were pink in color formed within 3-4 days.

Trays containing crystals of native HPAO-1 were brought into an anaerobic glove box (Belle Technology) and allowed to equilibrate for at least one week. Solutions used for crystal soaking and cryoprotection were brought into the glove box immediately after passing N_2 gas over the container headspace while stirring for >30 min in septa-covered bottles. Individual HPAO-1 crystals were soaked in an artificial crystallization solution containing methylamine HCl, ethylamine HCl, or benzylamine HCl. A range of amine concentrations and soak times were used for substrate soaks in order to optimize the

diffraction quality of the crystals as well as the occupancy of the amine substrate in the complex. All crystals were visually colorless after ~10 seconds following exposure to methylamine, ethylamine, or benzylamine; however crystals were left for longer periods than this to ensure that all residual O_2 remaining in the crystallization drop had been consumed, and that HPAO-1 had stabilized and contained the aminoquinol. The reduced HPAO-1 crystals were then soaked in a crystallization solution containing 25% glycerol mixed with well solution for ~5-10 seconds for cryoprotection before flash-freezing in N_2(l). The conditions used to form each of the complexes reported here were: 10 mM methylamine HCl for 1 hour, 10 mM ethylamine HCl for 2 hours, or 5 mM benzylamine HCl for 5 minutes.

Single crystal UV/visible microspectrophotometry

HPAO-1 crystals which had been anaerobically reduced with methylamine, ethylamine, or benzylamine before flash-freezing were subjected to single crystal UV/visible microspectrophotometry before and after X-ray diffraction data collection using a UV/visible single crystal microspectrophotometer from 4DX-ray Systems (system AB).

X-ray diffraction data collection, processing, and structure solution

X-ray diffraction data for the methylamine-, ethylamine-, and benzylamine-HPAO-1 complexes (see Table 4.1 for data collection, processing, and refinement statistics) were collected from single crystals at 100K at the Advanced Photon Source, Argonne National Laboratory (methylamine-HPAO-1: beamline 19-ID, SBC-CAT; ethylamine- and benzylamine-HPAO-1: beamline 23-ID, GM/CA-CAT). Diffraction data were collected to resolutions of 1.89, 2.18, and 2.25 Å for the methylamine-, ethylamine-, and benzylamine-HPAO-1 complexes, respectively, and processed using SCALEPACK and HKL2000 (*133*).

The structure of the methylamine-HPAO-1 complex was solved by difference Fourier, using the structure of native HPAO-1 as a starting model (PDB code 2oov with solvent atoms, ligands, and the side chain of residue 405 removed from each of six polypeptide chains) (*103*). The ethylamine- and benzylamine-soaked HPAO-1 crystals were found to be non-isomorphous with previously deposited structures of native HPAO-1. For phase determination of the benzylamine-HPAO-1 complex, molecular replacement was conducted using PHASER from the CCP4 suite with a search model based on a polypeptide dimer from the previously deposited native HPAO-1 structure (PDB code 2oov with solvent atoms, ligands, and the side chain of residue 405 removed from each protein chain) (*103, 167*). The structure of HPAO-1 in complex with ethylamine was then solved by difference Fourier using programs in the CCP4 suite with the entire (six polypeptide chains) benzylamine-HPAO-1 complex (with solvent atoms,

ligands, and the side chain of residue 405 removed from each polypeptide chain) as a starting model (*135*).

X-ray crystal structure refinement

The initial coordinates for each structure were first subjected to rigid body refinement using REFMAC in the CCP4 suite (*137*). Water molecules were incorporated into the coordinates of all three structures at positions with peaks >3.0σ in the corresponding $2F_o$-F_c electron density maps. Multiple cycles of manual model building using COOT followed by refinement using REFMAC were completed based on peaks in the corresponding $2F_o$-F_c and F_o-F_c electron density maps (*136, 137*). Copper ions were assigned to the strongest peaks in the electron density maps, which correspond with the well-established copper binding site in CAOs.

When TPQ occupies an "off-copper" position in the native HPAO-1 structure (see Figure 1.4A), an ordered water molecule ligates the copper in an axial position. In all chains of the three HPAO-1 substrate complexes, a water molecule was first modeled at this position based on strong peaks in the $2F_o$-F_c and F_o-F_c electron density maps. After refinement, persistent positive peaks in the F_o-F_c difference electron density map in conjunction with very low B-factors (~2 $Å^2$) indicated that water was electronically insufficient to account for the density at this position in all polypeptide chains of the methylamine-HPAO-1 complex as well as chains A, B, E, and F of the ethylamine-HPAO-1 complex and chains A, B, E, and F of the benzylamine-HPAO-1 complex. Two additional ligands were systematically modeled at this position in the active site and

subjected to test refinements. These were hydrogen peroxide, which has previously been visualized bound side-on to the copper in crystal structures of ECAO (*106*), and a Cl^- ion after consideration of the chemical species with which HPAO-1 crystals were in contact during crystal growth, soaks, and harvesting. Test refinements against these two alternate axial copper ligands and B-factor analysis were used to determine the identity of the appropriate species in each polypeptide chain of the three substrate complexes.

In all polypeptide chains of the three substrate-HPAO-1 complexes, the active site cofactor could be clearly modeled in its "off-copper" conformation, with no electron density suggesting any "on-copper" component (see Figure 1.4A). Based on single crystal UV/visible absorption spectra, which were bleached, the cofactor was modeled in its aminoquinol form in all polypeptide chains of the ethylamine- and benzylamine-HPAO-1 complexes (PDB residue TYQ) (*106*).

After inspection of the hydrogen bonding network in the active sites of the methylamine-HPAO-1 complex, the aminoquinol was modeled in chains C, D, and F at an occupancy of 0.5 (PDB residue TYQ), which reflects the presence of the substrate Schiff base form of cofactor at partial occupancy (discussed below), and in chain E at an occupancy of 1. Careful inspection of the electron density corresponding to the cofactor in chains A and B revealed that the cofactor is likely present in its iminoquinone form at full occupancy, which was modeled into these two polypeptide chains (PDB residue TYY) (*106*).

After initial refinement of the methylamine-HPAO-1 complex, the $2F_o$-F_c and F_o-F_c electron density maps clearly showed unaccounted connective electron density

extending from the C5 carbonyl of the cofactor in chains C, D, and F indicating a covalently linked species. A model of the substrate Schiff base intermediate formed upon reaction with methylamine was built using Sketcher, and library files were generated using the program LIBCHECK within the CCP4 suite. A previously deposited Schiff base species was used as a starting model (PDB residue ESB), which was manually edited to reflect the use of methylamine as the substrate (*116*).

The structures of methylamine, formaldehyde, ethylamine, and benzylamine were built into the appropriate polypeptide chains based on peaks in the $2F_o$-F_c and F_o-F_c, electron density maps which indicated substrate or product bound in the back of the active site. The positions of the terminal functional groups of the substrate/product moieties (amine or aldehyde functional group, respectively) relative to nearby amino acid side chains, the cofactor, and the active site water network were used to assign the likely identity of the ligand through differences in allowable hydrogen bonds and geometry. Additional cycles of manual model building and refinement were carried out in all three structures until peaks in the F_o-F_c electron density maps were at the level of noise.

4.3 Results

Overall fold of the HPAO-1 substrate complexes

X-ray diffraction data for HPAO-1 in complex with methylamine, ethylamine, and benzylamine were collected and refined to 1.89, 2.18, and 2.25 Å resolutions with final R_{work} values of 0.120 (R_{free} = 0.167), 0.156 (R_{free} = 0.196) and 0.169 (R_{free} = 0.231), respectively (see Table 4.1 for data collection, processing, and refinement statistics).

Table 4.1 X-ray diffraction, processing, and refinement statistics for methylamine-, ethylamine-, and benzylamine-HPAO-1 complexes.

substrate	methylamine	ethylamine	benzylamine
detector type	ADSC Quantum 315r	MARmosaic 300 CCD	MARmosaic 300 CCD
beamline	19-ID, SBC-CAT	23-ID, GM/CA-CAT	23-ID, GM/CA-CAT
temperature (K)	100	100	100
space group	$P2_1$	$P2_1$	$P2_1$
unit cell dimensions $a \times b \times c$, (Å); β (°)	103.5, 223.0, 103.5; 95.8	104.4, 232.8, 105.1; 96.7	104.2, 233.7, 105.1; 96.6
no. of molecules in the unit cell, Z	3	3	3
resolution (Å)[a]	50.00-1.89 (1.96-1.89)	50.00-2.18 (2.22-2.18)	50.00-2.25 (2.29-2.25)
no. of unique reflections	360,368	257,277	232,595
completeness (%)[a]	98.0 (96.7)	100.0 (100.0)	98.8 (97.7)
R_{merge} (%)[a,b]	0.053 (0.159)	0.108 (0.457)	0.089 (0.324)
$I/\sigma(I)$	22.9 (8.0)	10.0 (1.7)	9.8 (1.8)
redundancy[a]	3.2 (3.0)	3.8 (3.6)	4.3 (4.1)
refinement resolution range (Å)[a]	49.0-1.89 (1.94-1.89)	49.0-2.18 (2.24-2.18)	48.9-2.25 (2.31-2.25)
no. of reflections in the working set[a]	342,159 (24,025)	244,276 (16,892)	220,912 (16,116)
no. of reflections in the test set[a]	18,137 (1,244)	12,922 (875)	11,654 (793)

Table 4.1, continued. X-ray diffraction, processing, and refinement statistics for methylamine-, ethylamine-, and benzylamine-HPAO-1 complexes.

substrate	methylamine	ethylamine	benzylamine
R_{work} (%)[a,c]	0.120 (0.145)	0.150 (0.243)	0.169 (0.258)
R_{free} (%)[a,d]	0.167 (0.199)	0.201 (0.296)	0.230 (0.332)
rmsd from ideal geometry			
bond lengths (Å)	0.020	0.016	0.023
bond angles (°)	1.71	1.59	1.95
Ramachadran plot			
energetically favored regions (%)	95.6	95.2	94.6
allowed regions (%)	4.1	4.2	4.7
outliers (%)	0.3	0.6	0.7

[a]Numbers in parentheses refer to the highest-resolution shell. [b]R_{merge} = $\Box_{hkl}\Box_i\Box I_{hkl,I}$ - $\langle I_{hkl}\rangle\Box/\Box_{hkl}\Box_i I_{hkl,I}$, where I is the observed intensity and $\langle I\rangle$ is the average intensity for multiple measurements. [c]R_{work} = $\Box\Box F_o\Box$ - $\Box F_o\Box/\Box\Box F_o\Box$, where $\Box F_o\Box$ is the observed structure factor amplitude and $\Box F_c\Box$ is the calculated structure factor amplitude for 95% of the data used in refinement. [d]R_{free} based on 5% of the data excluded from refinement.

Phases for the methylamine-HPAO-1 complex were determined using difference Fourier with the structure of native HPAO-1 as a starting model (PDB code 2oov with solvent atoms, ligands, and the side chain of residue 405 removed from each polypeptide chain) and programs within the CCP4 suite (*103*, *135*). The ethylamine- and benzylamine-HPAO-1 complexes are non-isomorphous with native HPAO-1 (Table 4.2).

Table 4.2 Unit cell parameters for native HPAO-1 and substrate-HPAO-1 complexes.

structure	space group	unit cell lengths (Å)	β angle (°)
native HPAO-1	$P2_1$	a = 104.15, b = 223.08, c = 104.25	95.77
methylamine-HPAO-1	$P2_1$	a = 103.52, b = 223.03, c = 103.47	95.75
ethylamine-HPAO-1	$P2_1$	a = 104.41, b = 232.83, c = 105.12	96.66
benzylamine-HPAO-1	$P2_1$	a = 104.24, b = 233.71, c = 105.05	96.57

Consequently, molecular replacement was used to calculate phases for the benzylamine-HPAO-1 complex using a polypeptide dimer from the coordinates of native HPAO-1 as a search model (PDB code 2oov with solvent atoms, ligands, and the side chain of residue 405 removed from each of two polypeptide chains) (*103*). The resulting benzylamine-HPAO-1 structure was then used to calculate phases for the ethylamine-HPAO-1 complex using difference Fourier. All three substrate-HPAO-1 complexes contain six polypeptide chains comprising three physiological dimers within the asymmetric unit (ASU) in space group $P2_1$. The overall fold is nearly identical to that of the native enzyme, with superimposition of corresponding main chain atoms with those of native HPAO-1 (PDB code 2oov) yielding root-mean-square deviations (rmsd) of 0.15, 0.36, and 0.43 Å for the methylamine-, ethylamine-, and benzylamine-HPAO-1 complexes, respectively (*103*). All three structures adopt the archetypal overall CAO fold, which can be described in terms of three domains arranged along the primary sequence (see Figure 1.3 and Chapter 1 for a discussion of the CAO overall fold). Any significant structural differences between the three substrate-HPAO-1 complexes and the structure of native HPAO-1 are limited to specific regions of the enzyme.

Substrate binding in the HPAO-1 active site

Peaks in the $2F_o$-F_c and F_o-F_c electron density maps immediately following phase calculation and rigid body refinement indicated the presence of either substrate amine or product aldehyde bound in the back of the active site in all protein chains located in the ASU of all three structures. In polypeptide chains C, D, E, and F of the methylamine-

HPAO-1 complex and all six polypeptide chains of both the ethylamine- and benzylamine-HPAO-1 complexes, the terminal functional group of the substrate/product species is involved in hydrogen bonding interactions with an ordered water molecule (W2 in panels A, C, and D of Figure 4.1) as well as with the side chain of Asp319 and the N5 atom of the aminoquinol ((A) methylamine-HPAO-1, (C) ethylamine-HPAO-1, and (D) benzylamine-HPAO-1 in Figure 4.1).

Because an aldehyde functional group possesses two lone pairs and thus cannot be involved in three hydrogen bonds, the species bound in the back of the active site was determined to be the corresponding amine substrate in chains C, D, E, and F of the methylamine-HPAO-1 complex and all protein chains of the ethylamine- and benzylamine-HPAO-1 complexes. Additionally, after refinement the electron density indicated a species in the ethylamine-HPAO-1 complex with an angle between the three non-hydrogen atoms of ~104-111°, and a non-coplanar species in the benzylamine-HPAO-1 complex with its terminal functional group rotated out of the plane of the phenyl ring by 18-40° (angles reported as the range across six polypeptide chains in the ASU). This supports the assignment of these peaks as ethylamine and benzylamine because in the case of acetaldehyde, the angle between the three non-hydrogen atoms is expected to be 120°, and in the case of benzaldehyde, the aldehyde functional group is expected to be coplanar with the phenyl ring.

Figure 4.1 Active sites of (A) methylamine-, (B) formaldehyde-, (C) ethylamine-, and (D) benzylamine-containing HPAO-1 complexes. Residues and substrate/product species from polypeptide chains C, A, A, and E in panels (A), (B), (C), and (D), respectively, are shown in stick and colored by atom type (carbon, grey). Water molecules are shown as small red spheres, copper ions are shown as gold spheres, and chloride ions are shown as green spheres. Hydrogen bonding is indicated by dashed lines, and metal-ligand interactions are indicated by solid lines. Electron density from the $2F_o$-F_c electron density maps is shown as blue mesh and contoured to 1σ.

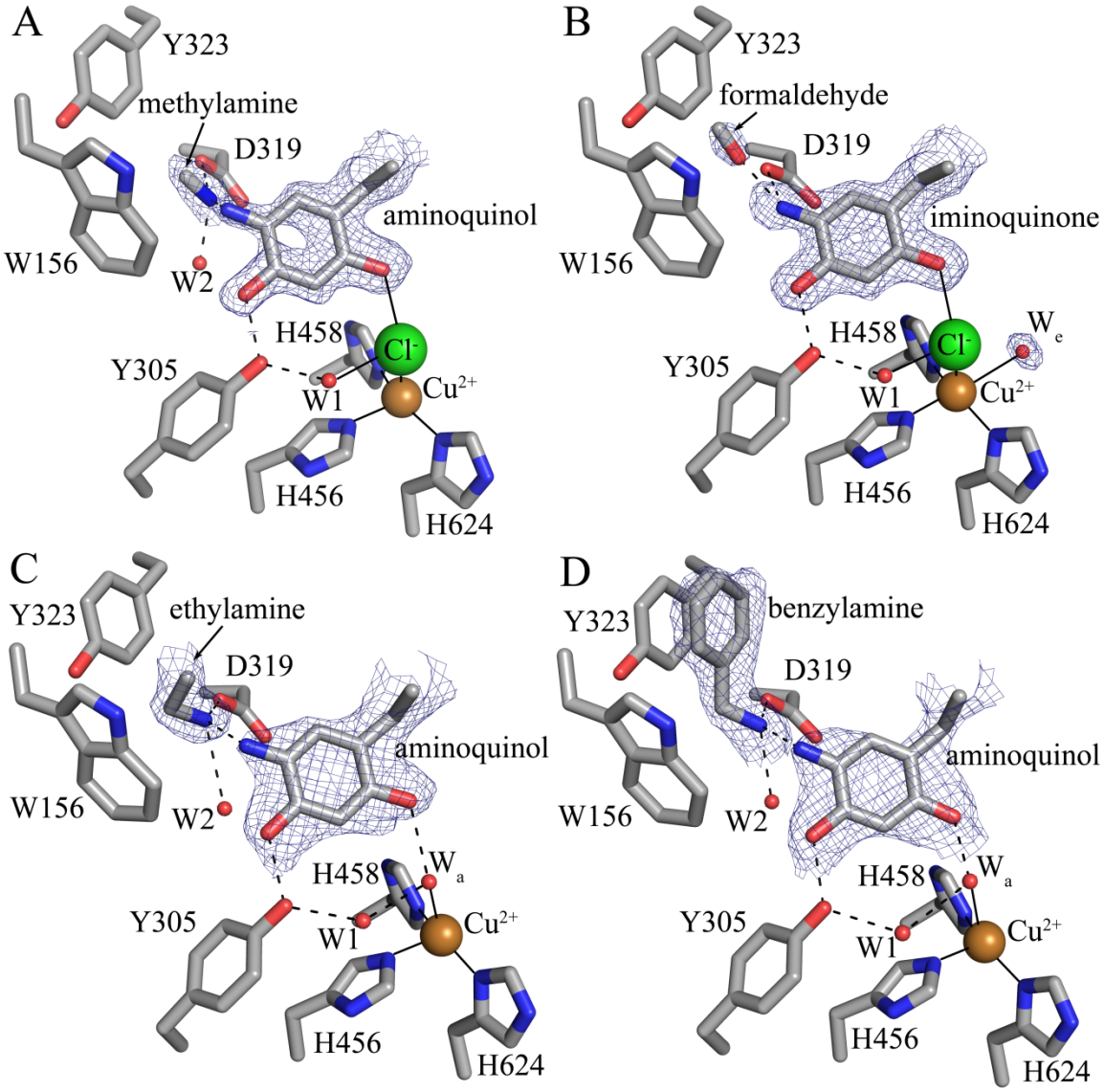

Chains A and B of the methylamine-reduced HPAO-1 structure do not contain electron density indicating a third hydrogen bonding partner for the substrate/product species, making the assignment of this species in the back of the active sites in these two polypeptide chains difficult. The substrate/product species in these chains have been tentatively modeled as formaldehyde product, based on the assignment of protonated iminoquinone cofactor in those two chains, which is discussed later. There is precedent for the presence of the iminoquinone form of cofactor in conjunction with aldehyde product bound in the back of the active site in a steady-state crystal structure of ECAO (*106*).

Distances between the functional groups of the three amine substrates/formaldehyde and other active site components are reported as the range across the appropriate polypeptides in the ASU of each structure (see Table 4.3 for the composition of individual active sites). The methylamine-HPAO-1 complex contains methylamine bound with its amine group 2.0-2.7 Å from the N5 atom of the aminoquinol, 2.4-3.4 Å from the carboxylate of Asp319, and 3.0-3.4 from an ordered water molecule in chains C, D, E, and F (Figure 4.1A), or formaldehyde bound with its aldehyde group 2.1-2.2 Å from the N5 atom of the iminoquinone in chains A and B (Figure 4.1B). The large range of interaction distances in the chains best modeled with methylamine likely reflects the aminoquinol disorder that is evident in the averaged electron density (Figure 4.1A), and the difficulty in accurately placing methylamine (effectively a diatomic in terms of visible electron density).

In all polypeptide chains of HPAO-1 in complex with ethylamine, the amine group of ethylamine sits 2.5-2.8 Å from the N5 atom of the aminoquinol, 2.6-2.9 Å from the carboxylate of Asp319, and 3.0-3.3 Å from an ordered water molecule (Figure 4.1C). The structure of HPAO-1 in complex with benzylamine contains benzylamine substrate bound with its amine group 2.3-2.7 Å from the N5 atom of the aminoquinol, 2.6-2.9 Å from the carboxylate of Asp319, and 2.5-3.3 Å from an ordered water molecule in all six polypeptide chains (Figure 4.1D). Chains D and E of the methylamine-HPAO-1 complex and chains A and F of the benzylamine-HPAO-1 complex contain substrate bound <2.5 Å from the aminoquinol, which indicates a shared proton.

In all three substrate-HPAO-1 structures, the amine substrates are bound in a hydrophobic pocket adjacent to TPQ with their amine groups pointed toward atom C5 of the cofactor, which is the site of nucleophilic attack during catalysis. Four polypeptide chains in the methylamine-reduced HPAO-1 complex contain methylamine in either one (chain D) or two (chains C, E, and F) alternate positions as indicated by peaks in the F_o-F_c electron density map. Methylamine has been modeled in the one binding position that is common to these four active sites, but the additional methylamine binding sites in chains C, E, and F are not systematic, and peaks in the electron density are too weak to support modeling this second methylamine position with confidence.

All six polypeptide chains within the ASU of the ethylamine-HPAO-1 complex contain ethylamine modeled at a single binding site (Figure 4.1C). In Chain E of the ethylamine-HPAO-1 complex, an ordered water molecule, which is not visualized in the native enzyme, is seen near the methyl group of ethylamine at a distance of 3.5 Å. The

presence of negative peaks in the F_o-F_c electron density map coincident with the modeled ethylamine, in addition to positive peaks in the F_o-F_c electron density map present at 5.5-7σ located adjacent to this species in all of the ethylamine-HPAO-1 active sites, suggests a partially-occupied second ethylamine binding site. This indicates positional mobility associated with ethylamine binding in the active site; however the electron density is not clear enough to model this alternate position with confidence.

The benzylamine molecules in all six polypeptide chains in the ASU of the benzylamine-HPAO-1 complex are present in only one position at the back of the active site (Figure 4.1D). Low B-factors and the absence of difference electron density in the F_o-F_c map indicate that benzylamine is bound at full occupancy at only one site in all six polypeptide chains. Benzylamine is positioned such that its phenyl ring is involved in a parallel displaced π-π stacking interaction with Tyr323, as well as a perpendicular π-π interaction with Trp156. The distances between atoms in the phenyl rings of benzylamine and Tyr323 are ~3.5-4.0 Å, which is consistent with a stabilizing aromatic interaction (*168, 169*). Likewise, the position of benzylamine relative to the side chain of Trp156 is similar to that seen in other examples of perpendicular aromatic stabilization, with the centers of the phenyl ring in benzylamine and the six-membered ring of Trp156 located 5.4-5.9 Å apart (*168, 169*).

Table 4.3 Features in the substrate-HPAO-1 complex active sites. SSB = substrate Schiff base, A = axial copper ligand, E = equatorial copper ligand, * = multiple possible binding sites. Occupancies are listed in parentheses.

substrate	chain	likely electronic form of cofactor	chain	copper ligands	chain	species bound in active site
methylamine	A	iminoquinone (1)	all	A = Cl^-	A	formaldehyde (1)
	B	iminoquinone (1)		E = H_2O	B	formaldehyde (1)
	C	aminoquinol (0.5) SSB (0.5)			C	methylamine (0.5)*
	D	aminoquinol (0.5) SSB (0.5)			D	methylamine (0.5)
	E	aminoquinol (1)			E	methylamine (1)*
	F	aminoquinol (0.5) SSB (0.5)			F	methylamine (0.5)*
ethylamine	all	aminoquinol (1)	A	A = H_2O_2	A	ethylamine (1)*
			B	A = H_2O_2	B	ethylamine (1)
			C	A = H_2O E = H_2O	C	ethylamine (1)*
			D	A = H_2O	D	ethylamine (1)*
			E	A = H_2O_2 E = H_2O	E	ethylamine (1)
			F	A = H_2O_2	F	ethylamine (1)*
benzylamine	all	aminoquinol (1)	A	A = H_2O_2	all	benzylamine (1)
			B	A = H_2O_2		
			C	A = H_2O E = H_2O		
			D	A = H_2O		
			E	A = H_2O_2		
			F	A = H_2O_2		

Active site features of the substrate-HPAO-1 complexes

Copper binding

The HPAO-1 active site lies deeply buried within the protein interior, and is formed by residues from domains D3 and D4 (see Figure 1.3 for the arrangement of CAO domains within the protein dimer). In all polypeptide chains within the ASU of the three substrate-HPAO-1 complexes, copper is bound at full occupancy by four ligands, including the imidazole groups from a conserved trio of histidine residues at distances of

2.0-2.1, 1.9-2.2, and 1.9-2.1 Å for His456, His458, and His624, respectively (Figure 4.1). Additionally, strong electron density indicating an equatorial water molecule acting as the fifth copper ligand can be seen in all chains of the methylamine-HPAO-1 complex at a distance of 2.5-2.9 Å, as well as in chains C and E of the ethylamine-HPAO-1 structure at distances of 2.5 and 3.0 Å, respectively, and chain C of the benzylamine-HPAO-1 structure at a distance of 2.6 Å.

In the structure of native HPAO-1, a water molecule ligates the bound copper in an axial position when TPQ is in the "off-copper" conformation and indirectly links the O2 atom of TPQ and the bound copper through hydrogen bonding. A water molecule was first modeled at this position in all protein chains of the three substrate-HPAO-1 complexes based on peaks in the $2F_o$-F_c and F_o-F_c electron density maps. Persistent positive peaks in the F_o-F_c difference electron density maps and very low B-factors (~2 $Å^2$) after refinement indicated that in all chains of the methylamine-HPAO-1 structure; chains A, B, E, and F of the ethylamine-HPAO-1 structure; and chains A, B, E, and F of the benzylamine-HPAO-1 structure, water is electronically insufficient and unable to account for the electron density at this position. Test refinements were therefore conducted after modeling hydrogen peroxide or a Cl^- ion at this position in the appropriate polypeptide chains. Hydrogen peroxide has been seen bound at this position in other CAO structures, and its presence would indicate low levels of oxygen present in the anaerobic glove box most likely from the crystallization drop solution (*106*). Additionally, the chemical compounds used for substrate soaks with all three amines were hydrochloride salts, so Cl^- was chosen for test refinements and modeled as a

potential axial copper ligand as well. Analyses of the electron density maps after refinement as well as the resulting B-factors associated with each ligand were used to assign the identity of the axial copper ligand in each structure (Table 4.3; electron density associated with test refinements in chain A of the methylamine-HPAO-1 structure and chain E of the ethylamine-HPAO-1 structure is shown in Figure 4.2).

The methylamine-HPAO-1 complex was found to contain a Cl^- ion ligating the copper in an axial position in all protein chains at a distance of 2.5-2.7 Å from the copper (Figure 4.1A, Figure 4.2D, Table 4.3). The ethylamine-HPAO-1 complex contains a mixture of water molecules or side-on hydrogen peroxide at this position within different polypeptide chains in the ASU (water, W_a in Figure 4.1B; H_2O_2 in Figure 4.2G; Table 4.3). Water is bound 2.6-2.7 Å from the copper in chains C and D, and a side-on hydrogen peroxide is bound with both oxygen atoms 2.5-3.0 Å from the copper in chains A, B, E, and F, which are typical for bound hydrogen peroxide (distances are reported as the range across the appropriate polypeptide chains in the ASU) (Table 4.3). Finally, the benzylamine-HPAO-1 complex was found to contain a side-on hydrogen peroxide in chains A, B, E, and F with both oxygen atoms bound at a distance of 2.7-3.3 Å from the copper, and water ligating the bound active site copper in an axial position at a distance of 2.7-2.8 Å in chains C and D, which is similar to that of the native enzyme (W_a in Figure 4.1C, Table 4.3). The presence of a side-on hydrogen peroxide in these polypeptide chains indicates that low levels of oxygen were present at some point during crystal handling, soaking, and/or freezing in the anaerobic glove box. The assignment of predominantly aminoquinol rather than iminoquinone is based on the featureless

UV/visible spectra of the crystals (protonated iminoquinone: λ_{max} ~ 350 nm; deprotonated iminoquinone: λ_{max} ~ 450 nm). Some turnover must have occurred but it appears that substrate amine has been able to react with the iminoquinone to generate aminoquinol with product H_2O_2 still present (Scheme 4.1). Hydrogen peroxide release is known to be rate-limiting in crystals of ECAO [21].

Figure 4.2 Structures of the active site of chain A of the methylamine-HPAO-1 complex with (A) no ligand, (B) water (W_a), (C) H_2O_2, or (D) a Cl^- ion modeled as the axial copper ligand; or chain A of the ethylamine-HPAO-1 complex with (E) nothing, (F) water (W_a), or (G) H_2O_2 modeled as the axial copper ligand. Residues in all panels and the peroxide in panels (C) and (G) are shown in stick and colored by atom type (carbon, grey). Copper ions in all panels are shown as gold spheres, a chloride ion in panel (D) is shown as a green sphere, and water molecules in panels (B) and (F) are shown as a small red spheres. The $2F_o$-F_c electron density maps after refinement against the corresponding species are shown as blue mesh and contoured to 1σ. The F_o-F_c electron density maps after refinement are shown as green or red mesh and contoured to +3.5 or -3.5σ, respectively.

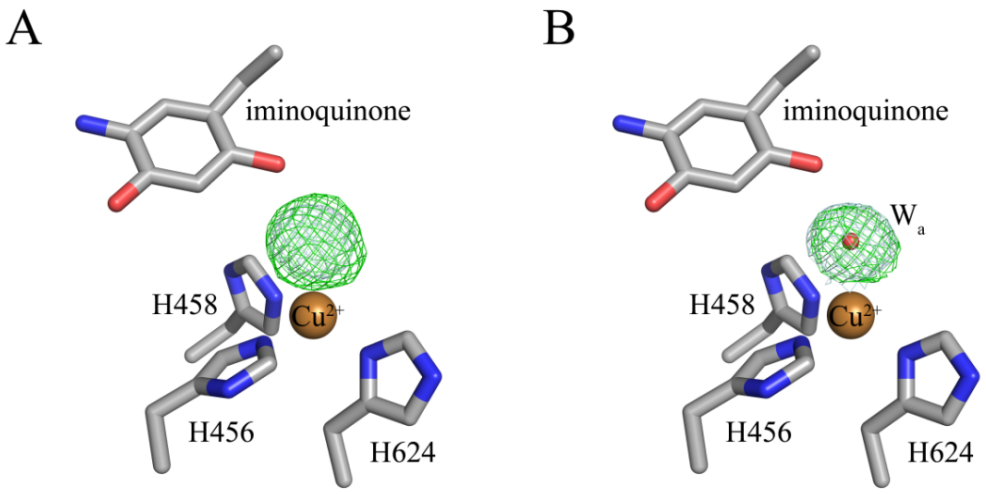

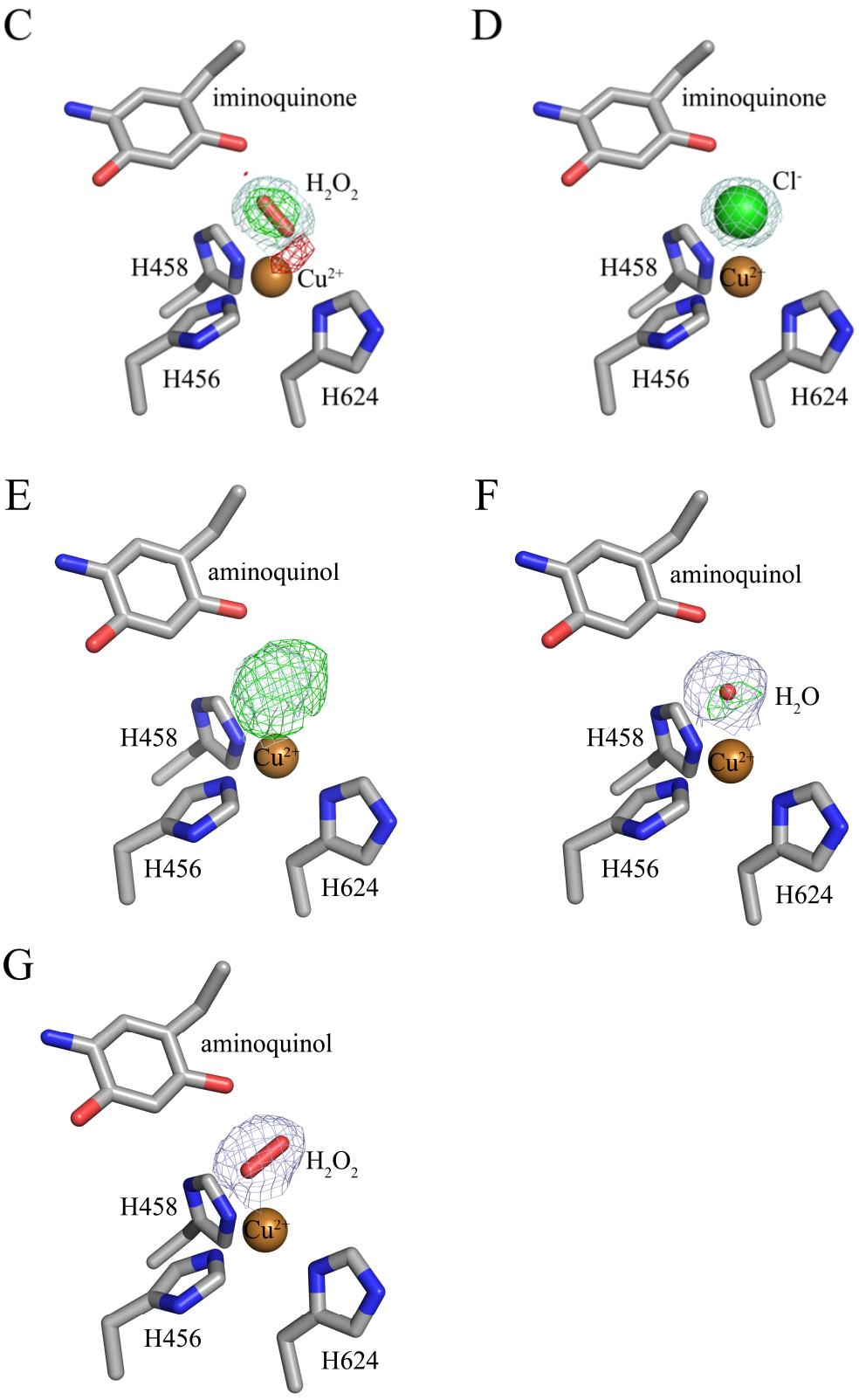
C
iminoquinone
H_2O_2
H458
Cu^{2+}
H456
H624
D
iminoquinone
Cl^-
H458
Cu^{2+}
H456
H624
E
aminoquinol
H458
Cu^{2+}
H456
H624
F
aminoquinol
H_2O
H458
Cu^{2+}
H456
H624
G
aminoquinol
H_2O_2
H458
Cu^{2+}
H456
H624

Electronic form of the cofactor in the substrate-HPAO-1 complexes

The active site cofactor could be clearly modeled in its "off-copper" conformation in all six polypeptide chains of the three structures. In the native enzyme, the "off-copper" conformation, which represents a catalytically productive state, denotes TPQ with its C5 carbonyl directed toward the substrate entry channel. In this position, TPQ is not a direct ligand to the copper but instead interacts with copper via an axial water molecule. No electron density was found to indicate the presence of cofactor in its unproductive "on-copper" conformation, in which the O4 atom is a direct ligand to the copper. This contrasts with the native HPAO-1 structure, in which four of six polypeptide chains in the ASU contain a mixture of "off-copper" and "on-copper" TPQ conformations (*103*). Single crystal UV/visible spectroscopy using crystals which were anaerobically treated with methylamine, ethylamine, or benzylamine showed only a small shoulder feature at ~310 nm but were otherwise bleached as compared to spectra of the native enzyme, which is consistent with the presence of cofactor in its two-electron reduced aminoquinol form (for representative spectra for native and methylamine-reduced HPAO-1, see Figure 4.3, Figure 4.4).

Figure 4.3 Single crystal UV/visible microspectrophotometry of a native HPAO-1 crystal (red) and a native HPAO-1 crystal which has been treated with methylamine (MeAm) (black). A dashed lined indicates λ = 480 nm.

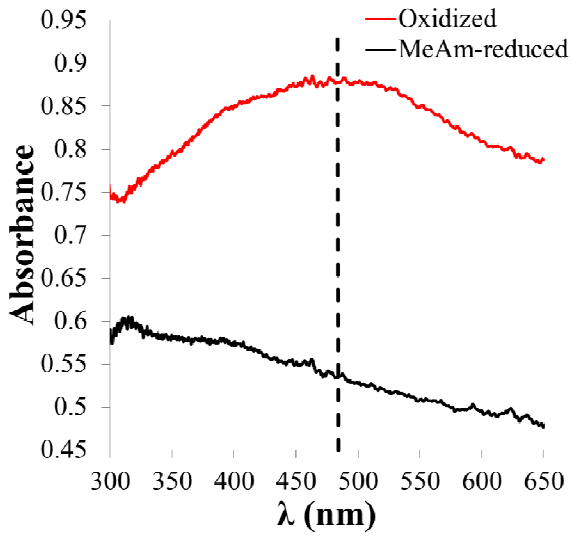

In chains A and B of the methylamine-HPAO-1 complex, the cofactor is rotated ~22° around its Cα-Cβ bond toward Asp319 as compared to the conformation of TPQ in native HPAO-1, and interacts directly with Asp319 at a distance of 2.8 Å. These chains also contain unusually strong electron density for an equatorial water ligand (Figure 4.1B). The active sites of these two polypeptide chains, including the position of the cofactor and equatorial water, are nearly superimposable with another structure of methylamine-treated HPAO-1 known to contain the protonated iminoquinone based on a weak absorbance feature at 350 nm (Bryan Johnson, unpublished data) (Figure 4.4). This structure was formed at higher O_2 concentrations, and five out of the six active sites contain protonated iminoquinone. Although in this study there is no absorbance feature indicative of the protonated iminoquinone in the crystal UV/visible spectrum (Figure 4.3), a tentative assignment of protonated iminoquinone has been made based on the

similarity between these structures and the pH of the crystals (6.0). The lack of a clear 350 nm absorbance feature may be due to the much smaller fraction of cofactor (two out of the six active sites) proposed to contain this species. Based on the assignment of the cofactor as the protonated iminoquinone, the species bound at the back of the active sites of chains A and B of the methylamine-HPAO-1 complex is likely formaldehyde, which contains two lone pairs and is capable of acting as a hydrogen bond acceptor.

Figure 4.4 Different electronic forms of TPQ proposed to be in the methylamine-HPAO-1 complex.

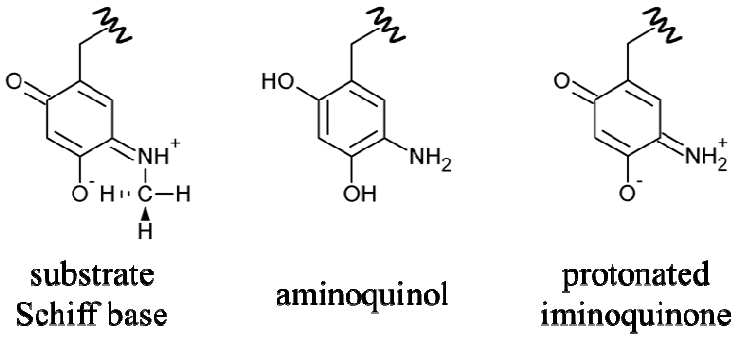

Persistent peaks in the $2F_o$-F_c and F_o-F_c electron density maps continuous with electron density at the N5 atom of the aminoquinol in the methylamine-HPAO-1 complex indicated the presence of a covalent Schiff base intermediate in chains C, D, and F which is coincident with methylamine bound at partial occupancy (Figure 4.5). Based on the hydrogen bonding networks in chains C, D, and F of the methylamine-HPAO-1 structure, it was determined that the substrate Schiff base and not the product Schiff base is present (Figure 4.4). The coordinates and library files for the structure of the substrate Schiff base formed with methylamine were manually built based on a Schiff base ligand (PDB residue ESB) and altered to reflect the correct identity of the substrate (*116*). This

substrate Schiff base ligand was built into the appropriate chains of the methylamine-HPAO-1 structure. Subsequent test refinements determined the ratio of methylamine/aminoquinol to the substrate Schiff base to be ~50:50 (Figure 4.5).

Figure 4.5 Structure of the substrate Schiff base in chain D of the methylamine-HPAO-1 complex in conjunction with bound methylamine. Residues are shown in stick and colored by atom type (carbon, grey). The F_o-F_c electron density map after the initial round of rigid body refinement (before the substrate Schiff base or methylamine had been built into the structure) is shown as green mesh and contoured to +3.5σ.

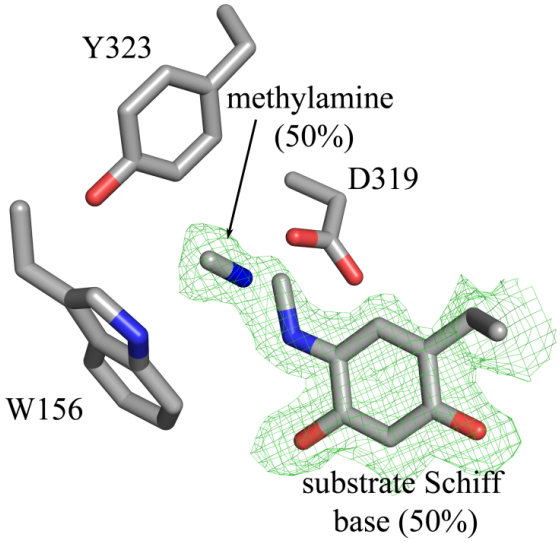

Changes in the HPAO-1 substrate channel associated with substrate binding

The structural changes in HPAO-1 following anaerobic treatment with the three amine substrates are localized to a conserved channel which leads from the enzyme surface to the deeply buried CAO active site (a distance of ~18 Å in HPAO-1) (*55*). The CAO amine substrate channel is defined by a series of secondary structural elements at different depths relative to the enzyme surface. The entrance to this channel is delineated by a surface-exposed helix which lies across its edge (*60*). Ethylamine or benzylamine binding resulted in the movements of residues Leu116-Cys122 located within this helix

away from the center of the amine substrate channel (green (ethylamine) and blue (benzylamine) in Figures 4.6 and 4.7). In contrast, residues from this helix in the methylamine-HPAO-1 complex have moved towards the channel when compared to those of the native enzyme (orange (methylamine-reduced) in Figures 4.6 and 4.7).

Figure 4.6 Concerted helical movement following methylamine, ethylamine, or benzylamine treatment of HPAO-1 as compared to native HPAO-1. Helices are shown as Cα traces and colored as follows: native HPAO-1, black; methylamine-HPAO-1, orange; ethylamine-HPAO-1, green; benzylamine-HPAO-1, blue. TPQ and its three histidine ligands from the native structure are shown in stick and colored by atom type (carbon, grey). The active site Cu(II) ion is shown as a gold sphere.

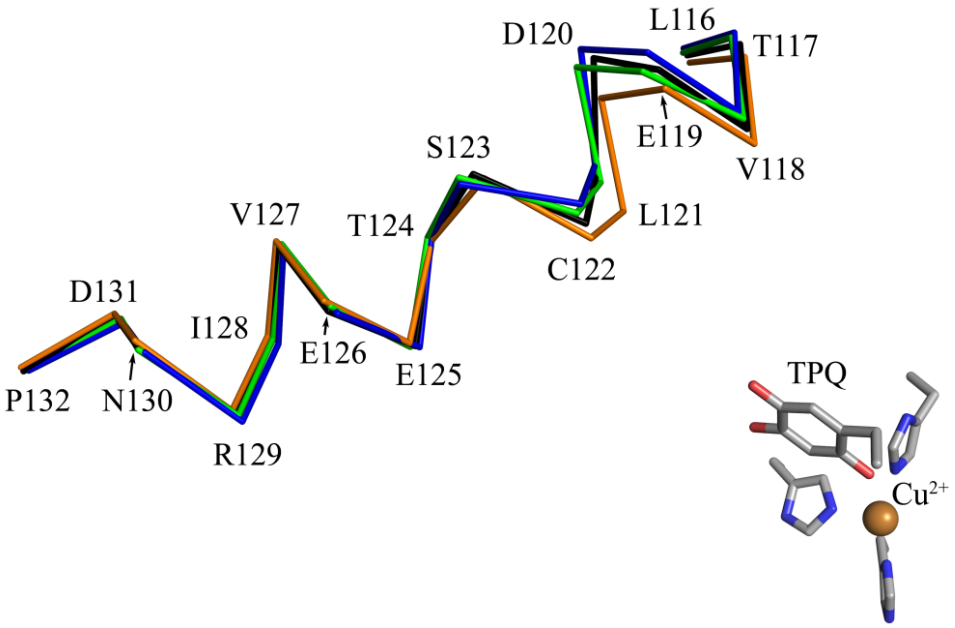

Lying closer to the deeply buried HPAO-1 active site, the side chain of residue Met328 has rotated ~120° around its Cβ-Cγ bond in the ethylamine- and benzylamine-HPAO-1 structures, which further expands the width of the substrate channel relative to that of the native enzyme (green (ethylamine) and blue (benzylamine) in Figure 4.7). In the case of the methylamine-HPAO-1 structure, this residue adopts the conformation

visualized in the native enzyme, with its side chain positioned such that the substrate channel at this depth is narrower than that of the ethylamine- and benzylamine-HPAO-1 structures (gold (methylamine) in Figure 4.7). Additionally, the side chain of Tyr323, which has been proposed to influence substrate specificity in HPAO-1, is rotated ~30° away from the active site in the ethylamine- and benzylamine-HPAO-1 complexes relative to its position in native HPAO-1 (green (ethylamine) and blue (benzylamine) in Figure 4.7) (*56*).

Figure 4.7 Stereoview of structural changes in the amine substrate channel following substrate binding. Residues are shown in stick and colored by structure and by atom type (native HPAO-1: carbon, grey; methylamine-HPAO-1: carbon, gold; ethylamine-HPAO-1: carbon, green; benzylamine-HPAO-1: carbon, blue). TPQ from native HPAO-1 is shown in stick and colored by atom type (carbon, grey). Asterisks indicate side chains which come from the other monomer of the homodimer. The overall fold of native HPAO-1 is shown as a semi-transparent grey cartoon.

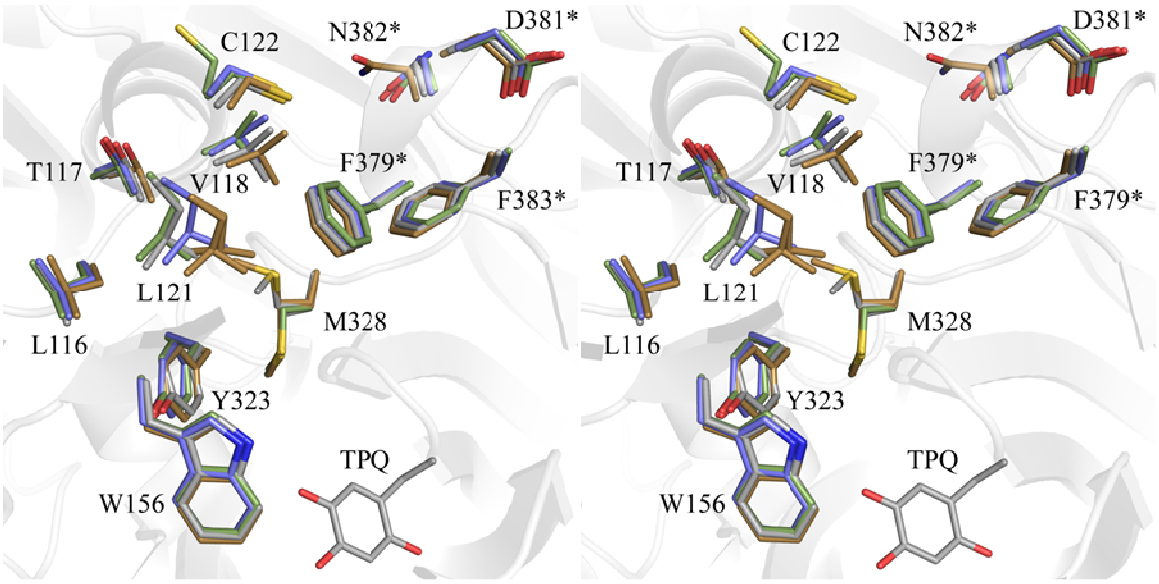

The back wall of the active site of one CAO monomer is partially formed by residues from domain D3 of the other monomer in the protein dimer. These residues are derived from a loop connecting a pair of β-strands that pack tightly against the other monomer to form a β-hairpin "arm" (red in Figure 1.3). In the structures of HPAO-1 in complex with ethylamine and benzylamine, the side chains of residues Phe379*, Asp381*, Asn382*, and Phe383* from this loop (* = from the other polypeptide in the dimer) have shifted away from the center of the substrate channel (green (ethylamine) and blue (benzylamine) in Figure 4.7). This movement, in conjunction with movements of the specific amino acid side chains mentioned previously, results in the general broadening of the amine substrate channel in the ethylamine- and benzylamine-HPAO-1 complexes (panels (C) (ethylamine) and (D) (benzylamine) in Figure 4.8). In contrast, residues Phe379*, Asp381*, and Phe383* have shifted closer to the active site in the methylamine-HPAO-1 complex (gold in Figure 4.7). Also, residue Asn382* adopts an alternate conformation in the methylamine-HPAO-1 complex resulting from a ~60° rotation around the Cα-Cβ bond. These motions, along with movements in the additional amino acid side chains shown in Figures 4.6 and 4.7, result in the constriction of the amine substrate channel upon methylamine binding in HPAO-1 (panel B in Figure 4.8).

Figure 4.8 Side view of the surface of the substrate entry channel in (A) native HPAO-1, (B) methylamine-HPAO-1, (C) ethylamine-HPAO-1, and (D) benzylamine-HPAO-1. Structures are shown as a molecular surface and colored grey. TPQ, iminoquinone, and aminoquinol moieties are shown in stick and colored by atom type (carbon, grey).

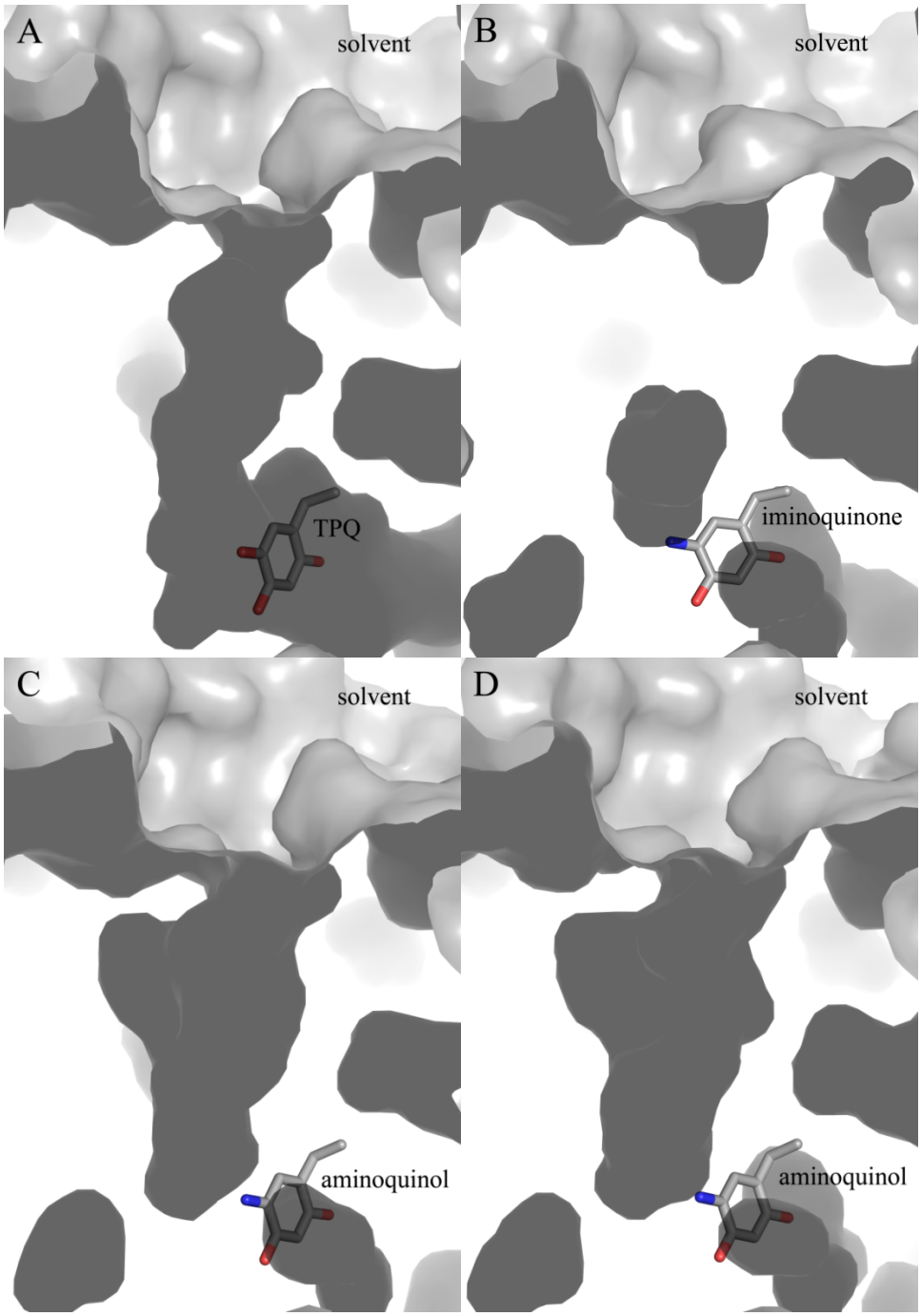

4.4 Discussion

Are the ping-pong kinetics of HPAO-1 in solution disrupted in crystallo?

The disruption of ping-pong kinetics has been observed in ECAO crystals aerobically undergoing turnover with 2-phenylethylamine, which revealed a steady-state structure in which product aldehyde was found at the back of the amine substrate channel in conjunction with H_2O_2 bound at the copper (PDB code 1d6z) (gold in Figure 4.9) (*106*).

Figure 4.9 Overlay of the active sites of HPAO-1 in complex with benzylamine (chain D) and a steady-state structure of ECAO in complex with product phenylacetaldehyde and H_2O_2 (chain A, PDB code 1d6z) (*106*). Residues are shown in stick and colored by atom type (HPAO-1: carbon, grey; ECAO: carbon, gold). Hydrogen bonds in the HPAO-1 structure are indicated by dashed lines. Residues labels are those of HPAO-1, with labels for the ECAO structure in brackets.

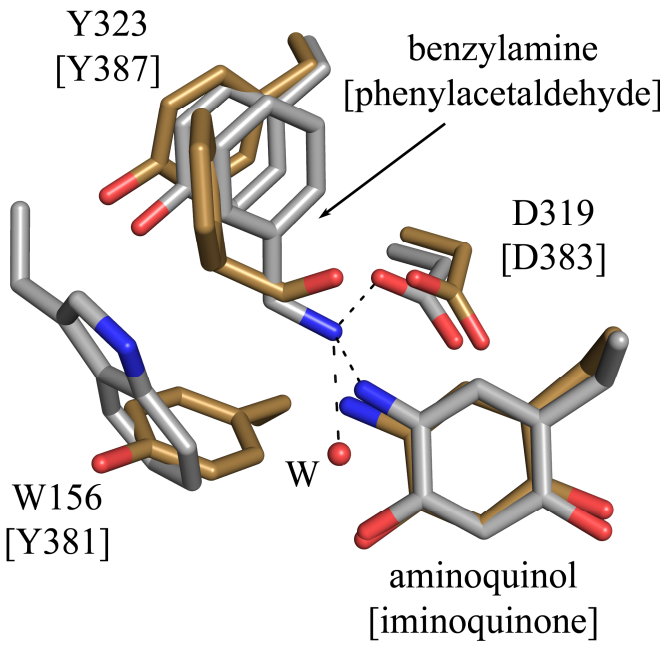

It was proposed that in solution, dynamic motion of domains D3 and D4, which both contribute residues that form the amine substrate channel, is key to product dissociation from the ECAO active site. Intermolecular contacts appear to slow aldehyde release in crystallo and disrupt the ping-pong kinetics normally seen in solution, resulting in the accumulation of product aldehyde and H_2O_2 in the active site. The presence of hydrogen peroxide concurrent with cofactor in its two-electron reduced aminoquinol form, or the tentative assignment of aldehyde product formed during the reductive half-reaction concurrent with the iminoquinone, suggests that the same could be true of the three substrate-HPAO-1 complexes (Figure 4.1). However, although consistent with the data here it is not conclusive due to the differing conditions (anaerobic vs. aerobic) and tentative nature of the formaldehyde assignment.

Structural determinants of substrate specificity in HPAO-1

The CAO family of enzymes possesses only ~20-40% sequence homology but displays a high level of structural similarity regardless of enzyme source, particularly in the overall fold as well as the residues which perform chemistry at the enzyme active site. These conserved residues include TPQ, a strictly conserved tyrosine residue that stabilizes the position of TPQ during both biogenesis and catalysis, three histidine residues that ligate the active site copper ion, and an invariant aspartate residue that acts as a general catalytic base. Given the wide variety of functional roles played by CAOs depending on source and cellular location, substrate selectivity is critical and appears to be controlled by several factors. Not surprisingly, the overall shape and size of the CAO

amine substrate channel correlates with its preferred substrates. CAOs which display the highest activity against bulkier or branched amines contain a correspondingly broad and solvent-exposed substrate channel, while those that show a preference for smaller amines have a more restricted substrate channel. The crystal structures of CAOs from *Aspergillus nidulans* (ANAO) and *Pichia pastoris* (PPLO), for example, reveal amine substrate channels so wide that there is unimpeded access to the active site from bulk solvent (see Figure 1.11) (*57, 60*). This correlates well with the documented ability of these CAOs to deaminate peptidyl lysine residues. The HPAO-1 substrate channel is relatively narrow compared to some of its CAO counterparts (see Figure 1.11). This reduces the number of orientations with which a substrate can approach the active site, thus the likelihood of binding and subsequent catalysis with a bulky substrate such as benzylamine is reduced.

A comparison of the steady-state kinetic parameters k_{cat} and k_{cat}/K_m for the HPAO-1-catalyzed oxidation of methylamine, ethylamine, and benzylamine reveals that HPAO-1 is an effective methylamine and ethylamine oxidase but does not efficiently oxidize benzylamine (Table 4.4) (*56, 100*). Ethylamine is the most efficient known substrate for HPAO-1 (Table 4.4). The overall turnover rate and second order rate constant for the reaction with methylamine are similar to those obtained with ethylamine. However, the values of k_{cat} and k_{cat}/K_m for reaction with benzylamine are reduced ~300-fold and ~580-fold, respectively, relative to the oxidation of ethylamine. Data describing the kinetic isotope effect for the reaction with benzylamine are available, and the values for $^{D}k_{cat}$ and $^{D}k_{cat}/K_m$ (S) (5.9 ± 0.7 and 3 ± 1, respectively) indicate that proton

abstraction and substrate binding are similarly rate-limiting during the reaction with benzylamine (*56*). In contrast, kinetic isotope effect data available for the reaction with methylamine report values for $^{D}k_{cat}$ and $^{D}k_{cat}/K_m$ of 1.7 and 4.3, respectively, which suggest that methylamine binding, but not proton abstraction, is rate-limiting during HPAO-1 catalysis with methylamine.

Table 4.4 Steady state kinetic parameters for the oxidation of methylamine, ethylamine, or benzylamine by HPAO-1.

substrate	k_{cat} (s^{-1})	k_{cat}/K_m(S) ($M^{-1}s^{-1}$)	$^{D}k_{cat}$	$^{D}k_{cat}/K_m$ (S)
methylamine	6.2 ± 0.2 [a]	(3.0 ± 0.6) × 10^4 [a]	1.7 ± 0.1 [a]	4.3 ± 0.2 [a]
ethylamine	20 [b]	5.2 × 10^4 [b]	ND	ND
benzylamine	(6.6 ± 0.3) × 10^{-2} [a]	(9 ± 1) × 10^1 [a]	5.9 ± 0.7 [a]	3 ± 1 [a]

[a] Data from ref. (*56*); experimental conditions: 100 mM potassium phosphate (pH 7.2) with ionic strength maintained at 300 mM with potassium chloride; [b] Data from ref. (*170*); experimental conditions: 100 mM potassium phosphate, ionic strength 175 mM.

The structures of HPAO-1 in complex with three amine substrates provide insight into specific substrate-protein interactions that precede the nucleophilic attack on atom C5 of TPQ that initiates catalysis. Non-mammalian CAOs contain an aromatic residue (typically a Phe or Tyr) at the intersection of the enzyme active site and the amine substrate channel. This residue has been proposed to adopt two conformations and either allow or block substrate access to the active site through the rotation of its Cβ-Cγ bond. In the two CAOs that have been structurally characterized from *Hansenula polymorpha*,

however, this so-called “gating residue” is a tryptophan, and has only been observed in an “open” conformation. Furthermore, the HPAO-1 and HPAO-2 gating residues are derived from β-sheet 2.1 from domain D3, one of two small α/β domains N-terminal to the larger catalytic domain D4. Despite the highly conserved overall fold amongst members of the CAO family of enzymes, all other structurally characterized aromatic gating residues originate from a loop that connects the two β-sheet sandwich motifs in domain D4.

In CAOs like ECAO or AGAO which efficiently oxidize aromatic amines, the gating residue has been proposed to facilitate the reaction with aromatic amines such as 2-phenylethylamine or tyramine through interactions between the aromatic rings (*171*). These interactions are thought to assist in aligning aromatic substrates such that their amine groups are poised for nucleophilic attack on the C5 atom of TPQ at an optimal distance and angle (gating residues: Tyr381, gold (ECAO) and Tyr296, purple (AGAO) in Figure 4.10). In contrast, the corresponding residue in the HPAO-1 primary sequence is an alanine. A comparison of the hydrophobic region near the C5 carbonyl of HPAO-1 with that of ECAO and AGAO reveals that in HPAO-1 the location of this pocket is shifted relative to TPQ and the catalytic base where the initial nucleophilic attack and subsequent proton abstraction take place. In addition to potential interactions with residue Trp156 in HPAO-1, which is situated for a perpendicular π-π interaction with an aromatic substrate, Tyr323 is well-positioned for a parallel displaced π-π interaction with an aromatic substrate as well (grey in Figure 4.10).

Figure 4.10 Overlay of the native HPAO-1 (PDB code 2oov), ECAO (PDB code 1qaf), and AGAO (PDB code 1ivx) active sites displaying the conformation of the aromatic "gating residue" relative to TPQ. Residues are shown in stick and colored by enzyme source (HPAO-1: carbon, grey; ECAO: carbon, gold, AGAO: carbon, purple). Copper ions are shown as gold spheres. Residue numbering is for HPAO-1, with that of ECAO and AGAO, respectively, in brackets. Hydrogen bonds in HPAO-1 are indicated by dashed lines, and ligand-metal interactions in HPAO-1 are indicated by solid lines.

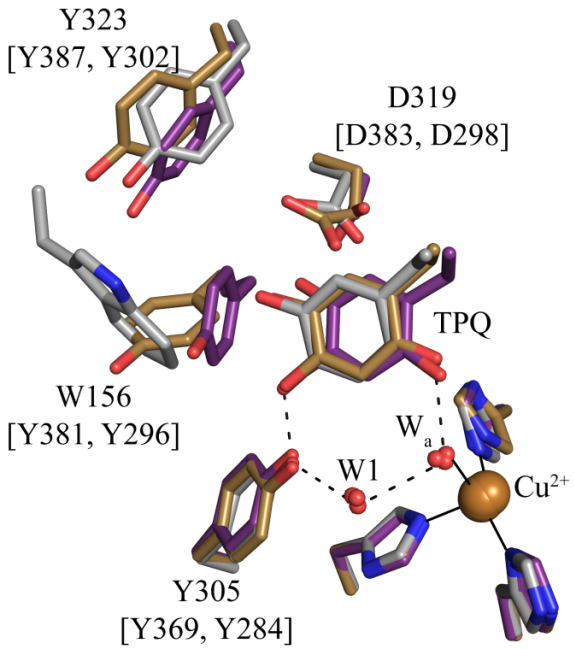

The interaction between two aromatic species, such as the phenyl ring of benzylamine with residues Trp156 and Tyr323 in HPAO-1, is associated with a small but favorable change in free energy (*168*). These interactions could influence the efficiency of catalysis with an aromatic substrate depending on the angle and distance between the amine group of the substrate and TPQ. In HPAO-1 the steps known to be rate-limiting imply that residues in the hydrophobic pocket in which the phenyl ring of benzylamine binds are not optimal for an efficient nucleophilic attack on the C5 atom, and that the substrate Schiff base formed with benzylamine is not well positioned relative to Asp319, hindering proton abstraction. This is consistent with the observation that the electron

density for bound benzylamine supports the presence of only one substrate conformation. In contrast, peaks in the electron density of the F_o-F_c maps of methylamine- and ethylamine-HPAO-1 indicate that these two substrates bind in multiple positions within the active site, suggesting that bound benzylamine is more restricted in the positions it can adopt than methylamine or ethylamine. In addition, the accommodation of tetrahedral intermediates postulated to form during catalysis would be more difficult with benzylamine as the amine substrate as opposed to methylamine (*79*).

Following ethylamine or benzylamine binding, the HPAO-1 active site is made more accessible due to the movement of specific amino acid side chains at different depths relative to the enzyme surface which help widen the substrate entry channel. These include a surface-exposed helix (Leu116-Cys122); residues Tyr323 and Met328; and residues Phe379*, Asp381*, Asn382*, and Phe383*, which all move further from the active site following substrate binding (Figure 4.7). A recent investigation of specific structural changes in AGAO associated with the formation of substrate Schiff base analogs with three hydrazine inhibitors has been conducted (*172*). The structural changes associated with the binding of these inhibitors include movements in the side chains of residues Phe105, Tyr302, and Leu358* in AGAO, resulting in an "induced-fit" effect (*172*). These residues are homologous with those found to move upon binding of the physiological substrates methylamine, ethylamine, and benzylamine in HPAO-1 (Phe105, Tyr302, and Leu358* in AGAO are equivalent to Leu121, Tyr323, and Arg380* in HPAO-1, respectively). Additionally, docking studies conducted with a truncated, soluble form of VAP-1 (sVAP-1) have implicated residues Phe389 and Tyr384 as

important in determining substrate specificity due to predicted interactions with bound aromatic substrates (*173*). Interestingly, Phe389 in sVAP-1 corresponds to Tyr323 in HPAO-1, and although it is derived form a different part of the primary sequence, the side chain of Tyr384 in sVAP-1 occupies the same space as Trp156 in HPAO-1.

In contrast to ethylamine and benzylamine binding, methylamine binding in HPAO-1 results in the constriction of the amine substrate channel, demonstrating that the effect of substrate binding on the conformations of residues lining the substrate channel depends on the identity of the amine substrate. Although methylamine and ethylamine are more structurally similar to one another than to benzylamine, there are likely differences in the way that these substrates interact with the HPAO-1 active site and subsequently differences in the stabilization of resultant intermediates. For example, a kinetic study of catalysis in the E406N HPAO-1 mutant reported the mechanism-based inactivation of the mutant enzyme when reacted with methylamine, but not ethylamine or benzylamine (*99*). The authors suggest that the product Schiff base formed with methylamine is able to rotate into an "on-copper" position in E406N HPAO-1, but is unable to do so when reacted with the larger ethylamine or benzylamine due to steric hindrance. Although this study was conducted using mutant enzyme and there is no evidence in the methylamine-HPAO-1 complex for an on-copper species, these results illustrate that the addition of even a single methylene group in the amine substrate can have significant mechanistic consequences. Interestingly, in the methylamine-HPAO-1 complex, a Cl^- ion is found to ligate the active site copper in an axial position in all polypeptide chains. This has not previously been visualized in CAO structures, and is not

seen in the substrate-HPAO-1 complexes formed with ethylamine or benzylamine. The small size of methylamine and its corresponding catalytic intermediates appear to allow enough conformational flexibility of the cofactor during catalysis for Cl^- to bind at the active site, which is likely to occur at a time when the O4 atom of the cofactor is not negatively charged. The presence of chloride as a metal ligand is predicted to arrest the catalytic reaction, as dioxygen species are known to bind at the same position relative to copper and it is unlikely that these species would displace the negatively charged chloride ion bound to the positively charged copper.

A structural analysis of HPAO-1 in complex with three amine substrates has identified specific amino acid residues lining the amine substrate channel that move upon substrate binding. These either widen or constrict the channel at different depths relative to the deeply buried CAO active site depending on the identity of the amine substrate. In addition, the conformations of specific amino acid side chains that may interact directly with the amine substrate before its nucleophilic attack on TPQ appear to influence substrate specificity as well by altering the efficiency with which primary amines can interact with catalytically-relevant residues in the CAO active site. Species-specific differences in the positions of these side chains likely play a role in substrate selection, helping to generate the broad substrate specificity seen across the CAO family of enzymes.

CHAPTER 5: ONGOING WORKS

5.1 *Hansenula polymorpha* copper amine oxidase mutants that alter substrate specificity

In Chapter 3 of this work, the crystal structure of a second CAO from the yeast *Hansenula polymorpha* (HPAO-2) in addition to an analysis of steady state kinetic data pertaining to the reaction of both HPAO-1 and HPAO-2 with two different amine substrates are presented. HPAO-1 preferentially reacts with small aliphatic substrates such as methylamine, while HPAO-2 displays a kinetic preference for larger aromatic amines such as benzylamine (*56*). Kinetic data available for the oxidation of both substrates by these two CAO paralogs, along with a comparison of the crystal structures of native HPAO-1 and HPAO-2, suggests that multiple features control substrate specificity. These include the overall shape and size of the substrate channel and specific amino acid substitutions that impact the accommodation of intermediates formed during catalysis (Table 3.4).

A model of the product Schiff base intermediate formed with benzylamine in HPAO-1 and HPAO-2 demonstrates that residues Cys306 and Met140 in HPAO-2 (green in Figure 5.1) appear better suited for reaction with benzylamine than the corresponding residues in HPAO-1 (Tyr323 and Thr157) (cyan in Figure 5.1). For this reason, it was proposed that a switch in the identity of these residues may affect substrate preference in these two CAOs.

Complementary single site mutants have been prepared in both CAOs from *Hansenula polymorpha* (Cindy Chang, University of California, Berkeley) (*174*). In HPAO-1, Tyr323, which is thought to hinder the accommodation of catalytic

intermediates formed during reaction with aromatic amines, has been mutated to the corresponding amino acid in HPAO-2 (a cysteine) (Y323C HPAO-1). In HPAO-2, the corresponding cysteine residue in HPAO-2 (Cys306) has been mutated to a tyrosine (C306Y HPAO-2). This position in the primary sequence is thought to influence substrate specificity in these two CAO paralogs because it helps define a hydrophobic pocket postulated to bind amine substrates during catalysis, which is shifted relative to TPQ depending on the enzyme source.

Figure 5.1 Model of the product Schiff base of benzylamine with TPQ in HPAO-1 and HPAO-2. Residues from the crystal structures are drawn in stick and colored by atom type (HPAO-2: carbon, green; HPAO-1: carbon, cyan). The modeled product Schiff base is drawn in stick and colored by atom type (carbon, dark grey). Figure from (*56*).

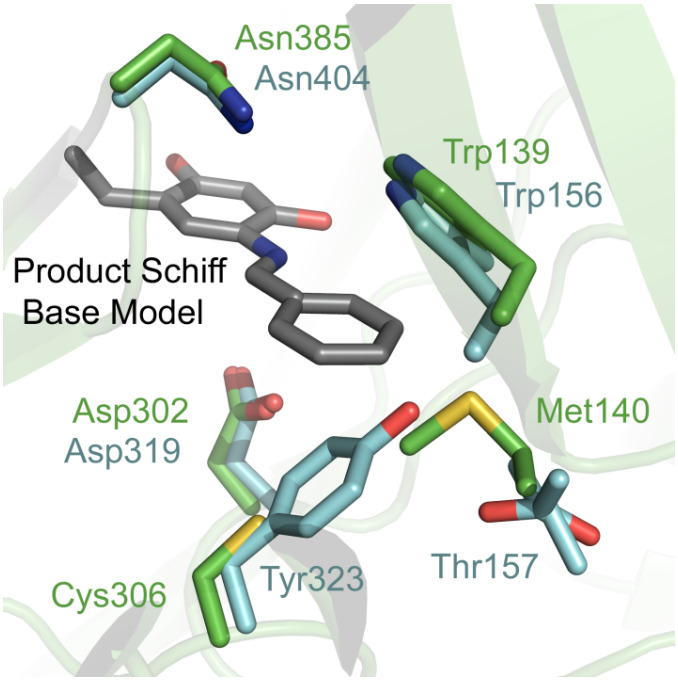

Steady state kinetic data for the reaction of both mutants with benzylamine and methylamine have been collected (Cindy Chang, University of California, Berkeley) (*174*) (Table 5.1). In the case of HPAO-1, the mutation of Tyr323 to a cysteine results in an increase in the second order rate constant by 30-fold or a decrease in the second order rate constant by 150-fold for reaction with benzylamine or methylamine, respectively. The reaction of HPAO-2 in which Cys306 has been mutated to a tyrosine residue reveals a decrease in the second order rate constant by 4-fold or 12-fold for the reaction with benzylamine or methylamine, respectively.

Table 5.1 Steady state kinetic data for native HPAO-1, Y323C HPAO-1, native HPAO-2, and C306Y HPAO-2 when reacted with benzylamine or methylamine.

	k_{cat} (s^{-1})	k_{cat}/K_m (amine) ($M^{-1}s^{-1}$)	fold change in k_{cat}/K_m(amine) ($M^{-1}s^{-1}$) for mutant vs. native enzyme
Benzylamine			
native HPAO-1[a]	0.055 ± 0.007	$4 \pm 1 \times 10^1$	
Y323C HPAO-1[b]	0.91 ± 0.04	$1.2 \pm 0.2 \times 10^3$	+30
native HPAO-2[a]	4.5 ± 0.2	$1.4 \pm 0.1 \times 10^5$	
C306Y HPAO-2[b]	5.1 ± 0.2	$3.8 \pm 0.7 \times 10^4$	-4
Methylamine			
native HPAO-1[c]	6.2 ± 0.2	3.2×10^4	
Y323C HPAO-1[b]	0.54 ± 0.02	$2.2 \pm 0.2 \times 10^2$	-150
native HPAO-2[a]	0.72 ± 0.3	$1.6 \pm 0.2 \times 10^2$	
C306Y HPAO-2[b]	0.148 ± 0.006	13 ± 2	-12

Data from refs. [a] (*56*), [b] (*174*), [c] (*112*)

Given the multiple factors governing substrate specificity in CAOs, it is not surprising that the mutation of a single amino acid residue in HPAO-1 and HPAO-2

results in only modest changes in steady state kinetic parameters. For both substrates, the change in k_{cat} is larger for the Y323C HPAO-1 mutant than the C306Y HPAO-2 mutant, suggesting that this mutation has some (~10-fold) impact on chemistry. In addition, modest changes in k_{cat}/K_m for the reaction of both mutants with both substrates suggest that while this position is involved in substrate binding and the accommodation of reaction intermediates formed with amine substrates possessing different R groups (a methyl group vs. a phenyl group), additional structural factors that confer substrate specificity are at work as well.

In order to examine the structural basis for these modest changes in substrate specificity, the X-ray crystal structures of the two mutant enzymes, HPAO-1 Y323C and HPAO-2 C306Y, are currently being pursued. Attempts to crystallize the two mutants using the crystallization conditions for both of the native enzymes did not yield crystals of either mutant. Once suitable crystallization conditions have been established, the crystal structures of the two mutant HPAO proteins will be solved. In addition, the structures of mutant proteins that have been anaerobically reduced with methylamine and benzylamine will be solved for comparison with the respective native enzymes.

5.2 *Hansenula polymorpha* copper amine oxidase-1 aniline derivatives

TPQ is produced in a copper- and oxygen-dependent fashion from an endogenous tyrosine residue in a process termed biogenesis. A proposed TPQ biogenesis mechanism is outlined in Chapter 1 of this work (see Scheme 1.1). The ligation of a precursor tyrosine side chain to the bound active site copper ion is thought to activate the phenolic ring for monooxygenation by prebound O_2. A ligand-to-metal charge transfer (LMCT) species between the tyrosine and copper is proposed to form after a conformational change in the tyrosine side chain following O_2 binding in a nearby hydrophobic pocket (B→C in Scheme 1.1). This movement, followed by deprotonation of the tyrosine side chain, activates the phenolic ring for the initial monooxygenation event which produces dopaquinone (F in Scheme 1.1).

In order to study the factors governing the initial copper binding step in biogenesis, HPAO-1 proteins with the site-specific incorporation of an aniline amino acid (or *p*-amino phenylalanine, pAF) at two active site tyrosine positions have been expressed and purified (Figure 5.2). These residues include the strictly conserved precursor tyrosine residue that is converted to TPQ (Tyr405) as well as a conserved active site tyrosine residue known to regulate cofactor production by stabilizing the phenolic ring in a productive conformation during biogenesis (Y305) (*75*).

The aniline amino acid is a powerful tool for probing enzymatic reactions that involve redox-active tyrosine residues because its side chain cannot be deprotonated in a biologically-relevant pH range (pK_a = 4.6 and 10.1 for aniline and tyrosine, respectively) yet it has a similar reduction potential at neutral pH (E° = 1.0 and 0.9 V vs. NHE for

aniline and tyrosine, respectively) (Figure 5.2) (*175-178*). This difference in pK_a allows for an investigation of the factors which control the formation of the LMCT species formed following copper binding.

Figure 5.2 Structures of *p*-amino phenylalanine (aniline amino acid) and tyrosine.

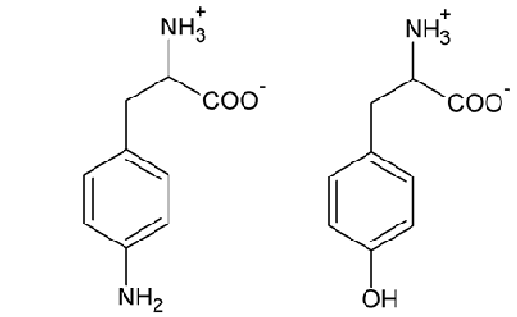

aniline amino acid (*p*-amino phenylalanine) tyrosine

The insertion of pAF into the primary sequence of HPAO-1 takes advantage of novel orthogonal aminoacyl-tRNA synthetase/tRNA pair technology developed to impart new or enhanced chemical properties to enzyme active sites (*179*). This particular method involves the manufacturing of organisms or cell lines that encode not only the 20 traditional amino acids but additional modified residues as well. Several systems have been used to explore this technology, including *E. coli*, yeast, and mammalian cells. A diverse set of unnatural amino acids have successfully been incorporated into yeast proteins, including a phenylalanine residue with acetyl, propargyloxyl, iodo, benzoyl, or azido groups substituted at the *para* position of the phenyl ring; *o*-methyltyrosine; *o*-nitrobenzyl groups incorporated into cysteine and serine residues; dansylalanine; and

methylhistidine (*180-183*). Because these unnatural amino acids are genetically encoded, they are incorporated into synthesized proteins with the same fidelity as the 20 canonical amino acids.

In order to incorporate *p*-amino phenylalanine into HPAO-1, directed evolution in *Saccharomyces cerevisiae* has been conducted by a two-step selection mechanism (Schultz lab, the Scripps Research Institute). This process produced yeast clones which exclusively aminoacylate a tRNA designed to suppress a blank codon with *p*-amino phenylalanine, and thus can incorporate *p*-amino phenylalanine into a synthesized protein during translation (*179*).

HPAO-1 proteins with pAF incorporated into two strictly conserved positions in the primary sequence that encode a tyrosine residue have been expressed and purified using the native HPAO-1 purification protocol (Albert Lang, University of California, Berkeley) (*103*). Upon the aerobic or anaerobic reconstitution of Y405pAF or Y305pAF HPAO-1 proteins with copper, a broad absorbance feature centered at λ_{max} = 450 nm appears in the UV/visible spectrum (Albert Lang, personal communication) (Figure 5.3). This feature is present at a range of pH values but is strongest at more basic pHs with maximal levels at pH 9.0. Additionally, preliminary electron paramagnetic resonance (EPR) data indicates a radical signal for both Y405pAF and Y305pAF when reconstituted with copper (Albert Lang, personal communication). An extinction coefficient for 4-methylaniline radical cation absorbing at ~450 nm has been observed at ~7,800 $M^{-1}cm^{-1}$ (*176*). Using this as an estimate for the extinction coefficient of the Y405pAF and Y305pAF species, a proportion of ~12% radical cation in Y405pAF and ~24% radical

cation in Y305pAF can be calculated. This is roughly equivalent to the yield of TPQ produced when apoHPAO-1 is reconstituted with copper (~30-35%) (*77*).

Figure 5.3 Solution UV/visible spectra of (A) Y405pAF HPAO-1 and (B) Y305pAF HPAO-1 before (black line) and after (red line) aerobic reconstitution with Cu(II) (Albert Lang, personal communication).

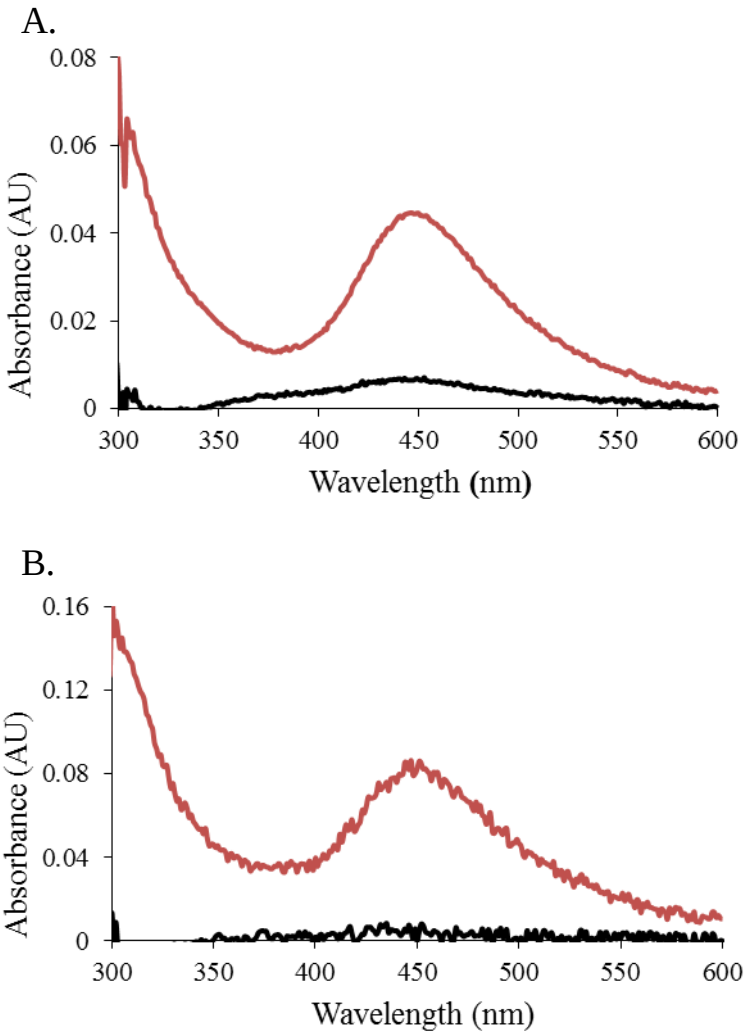

The incubation of Y405pAF or Y305pAF HPAO-1 proteins with phenylhydrazine does not result in the formation of a characteristic absorbance peak indicating the

presence of a hydrazone adduct, indicating that either (a) no TPQ is produced upon reconstitution with Cu(II) or (b) TPQ is not available for reaction with phenylhydrazine (Albert Lang, personal communication). In addition, both proteins are unreactive with the amine substrates ethylamine or benzylamine (Albert Lang, personal communication).

In order to structurally investigate the species in Y405pAF and Y305pAF HPAO-1 that gives rise to the absorbance feature at 450 nm, the X-ray crystal structures of Y405pAF and Y305pAF HPAO-1 in complex with Cu(II) are currently being pursued. The crystal structure of Y405pAF HPAO-1 in complex with Cu(II) has been solved to a resolution of 1.57 Å and is described below.

5.2.1 Methods

Protein preparation and crystallization

Y405pAF HPAO-1 protein was expressed and purified in *Saccharomyces cerevisiae* as previously described by Albert Lang at the University of California, Berkeley (*122*). Before reconstitution with Cu(II), Y405pAF HPAO-1 protein was buffer exchanged into 50 mM HEPES, pH 7.0. The protein was incubated in a solution of 50 mM HEPES, pH 7.0 containing a 1:1 molar ratio of $CuSO_4$ (final protein concentration of 10 mg/mL) for 1 hr before crystallization.

Crystals of Y405pAF HPAO-1 were grown by hanging drop vapor diffusion using a 1:1 volume ratio of purified protein and the crystallization solution (2-6 μL total volume; 7.0-8.5% w/v polyethylene glycol 8000, 0.25-0.28 M potassium phosphate, pH 7.0). These conditions are similar to those used for the crystallization of native HPAO-1 and metal-free apoHPAO-1. Although the absorbance feature in the aniline-substituted HPAO-1 proteins at 450 nm is strongest at higher pH values (9.0) (Albert Lang, personal communication), attempts to grow diffraction-quality crystals of Y405pAF HPAO-1 at a pH above 7.0 were unsuccessful. After equilibrating for ~24 hrs, drops were seeded with a streak-seeding technique using a native HPAO-1 crystal as seed donor (*132*). Colorless crystals grew to full size after 7-9 days. Once formed, crystals were transferred every other day into a new drop of crystallization solution at an increasingly higher pH (pH was increased by 0.5 for each transfer) until a final pH of 9.0 was reached. Y405pAF HPAO-1 crystals at a variety of final pH values were soaked in 25% glycerol mixed with well solution for ~5-10 sec for cryoprotection before flash-freezing in N_2(l).

Data collection and refinement

Diffraction data collection, processing, and refinement statistics for the structure of Y405pAF HPAO-1 in complex with Cu(II) from a crystal harvested at pH 7.0 are given in Table 5.2. Diffraction data were collected at the Advanced Photon Source in Argonne, IL (beamline 23-ID, General Medical Sciences and National Cancer Institute Collaborative Access Team (GM/CA-CAT)) to a resolution of 1.57 Å and processed using HKL2000 and SCALEPACK (*133*). Y405pAF HPAO-1 protein was found to crystallize in space group $C222_1$, which is different than that of native HPAO-1, which crystallizes in space group $P2_1$. Molecular replacement using the program PHASER in the CCP4 suite with an HPAO-1 monomer from the native structure as a search model (PDB code 2oov with solvent molecules, metal, and the side chain of TPQ removed) was used to solve the Y405pAF HPAO-1 structure (*103, 135*). Manual model building was performed using COOT, and refinement was carried out using the program REFMAC in the CCP4 suite (*136, 137*). The structure of pAF was incorporated into each polypeptide chain (PDB residue HOX) based on peaks in the $2F_o$-F_c and F_o-F_c electron density maps. Cycles of manual model building continued until peaks in the F_o-F_c electron density were at the level of noise.

5.2.2 Preliminary results

X-ray diffraction data, processing, and refinement statistics for Y405pAF HPAO-1 in complex with Cu(II) are listed in Table 5.2. The structure of Y405pAF HPAO-1 contains three polypeptide chains, or 1.5 physiological dimers, in the ASU in space group $C222_1$. It is nearly identical in overall fold to that of native HPAO-1, with superimposition of corresponding main chain atoms resulting in a root-mean-square deviation (rmsd) of 0.31 Å (*103*). Y405pAF HPAO-1 adopts the archetypal CAO overall fold and is arranged in three domains located along the primary sequence, with all significant structural differences between it and the native HPAO-1 structure located at the active site.

Distances and occupancies are reported as the range observed across the three polypeptides in the ASU following refinement. The active site of Y405pAF HPAO-1 contains copper bound at an occupancy of 0.8-0.85 as determined by test refinements in an identical position to that of the native structure (Figure 5.4). The copper ion is ligated by the imidazole groups of three conserved histidine ligands at distances of 2.1, 2.0, and 2.0 Å (His456, His458, and His624, respectively) as well as by the amine group of pAF at a distance of 2.3-2.4 Å in a distorted square pyramidal geometry. The pAF amino acid side chain adopts an orientation similar to that of TPQ in its "on-copper" conformation in the native enzyme (see Figure 1.4B), and is nearly superimposable with the unprocessed precursor tyrosine residue that is modified to produce TPQ during biogenesis found in the structure of apoHPAO-1 (see Figure 2.3). The pAF side chain is also involved in a hydrogen bond with a well-ordered water molecule seen in many native CAO structures,

including HPAO-1 (W in Figure 5.4). All other active site residues are identical in position to those in the native HPAO-1 structure.

Table 5.2 X-ray crystallographic data collection, processing, and refinement statistics for Y405pAF HPAO-1.

Data collection and processing statistics	
	Cu(II)-Y405pAF HPAO-1
detector type	MARmosaic 300 CCD
beamline and source	23ID-D GM/CA-CAT, Advanced Photon Source
temperature (K)	100
space group	$C222_1$
unit cell dimensions	a = 139.4 Å, b = 153.7 Å, c = 223.3 Å
no. of molecules in the unit cell, Z	1.5
wavelength (Å)	1.0332
resolution (Å)[a]	50.00-1.57 (1.60-1.57)
no. of unique reflections	328,577
completeness (%)[a]	99.4 (87.7)
R_{merge}[a,b]	0.092 (0.566)
$I/\sigma I$[a]	37.6 (3.3)
redundancy[a]	7.9 (7.0)
Crystallographic refinement and model statistics	
resolution range (Å)[a]	29.12-1.57 (1.61-1.57)
no. of reflections in the working set[a]	311,940 (22,113)
no. of reflections in the test set[a]	16,564 (1,199)
R_{work} (%)[a,c]	0.13.1 (0.210)
R_{free} (%)[a,d]	0.160 (0.253)

[a]Numbers in parentheses refer to the highest-resolution shell. [b]R_{merge} = $\Box_{hkl}\Box_i\Box I_{hkl,I}$ - $\langle I_{hkl}\rangle\Box/\Box_{hkl}\Box_i I_{hkl,I}$, where I is the observed intensity and $\langle I\rangle$ is the average intensity for multiple measurements. [c]R_{work} = $\Box\Box F_o\Box$ - $\Box F_o\Box/\Box\Box F_o\Box$, where $\Box F_o\Box$ is the observed structure factor amplitude and $\Box F_c\Box$ is the calculated structure factor amplitude for 95% of the data used in refinement. [d]R_{free} based on 5% of the data excluded from refinement.

Figure 5.4 Active site of Y405pAF (crystal harvested at pH 7.0). Residues are shown in stick and colored by atom type (carbon, grey). A copper ion is shown as a gold sphere, and a water molecule is shown as a small red sphere. Metal-ligand interactions are shown as solid lines, and hydrogen bonds are shown as dashed lines. The $2F_o$-F_c electron density map is shown as blue mesh and contoured to 1.5σ.

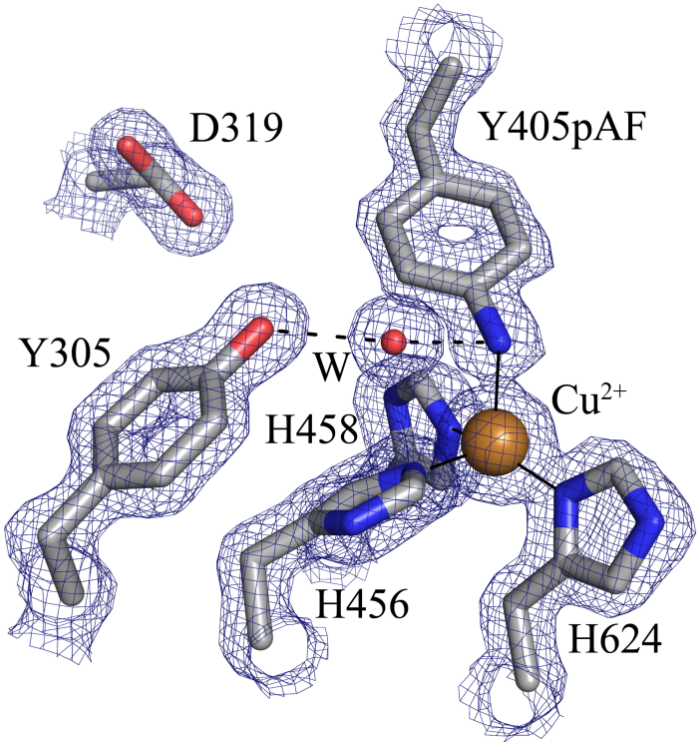

Single crystal UV/visible spectra collected from the Cu(II)-Y405pAF HPAO-1 crystal after data collection revealed a broad absorbance feature centered at 450 nm that is similar to the feature observed in solutions of Y405pAF HPAO-1 protein reconstituted with Cu(II) (Figure 5.5).

Figure 5.5 Single crystal UV/visible spectrum of Cu(II)-Y405pAF crystal after data collection revealing a broad absorbance feature centered at λ_{max} = 450 nm.

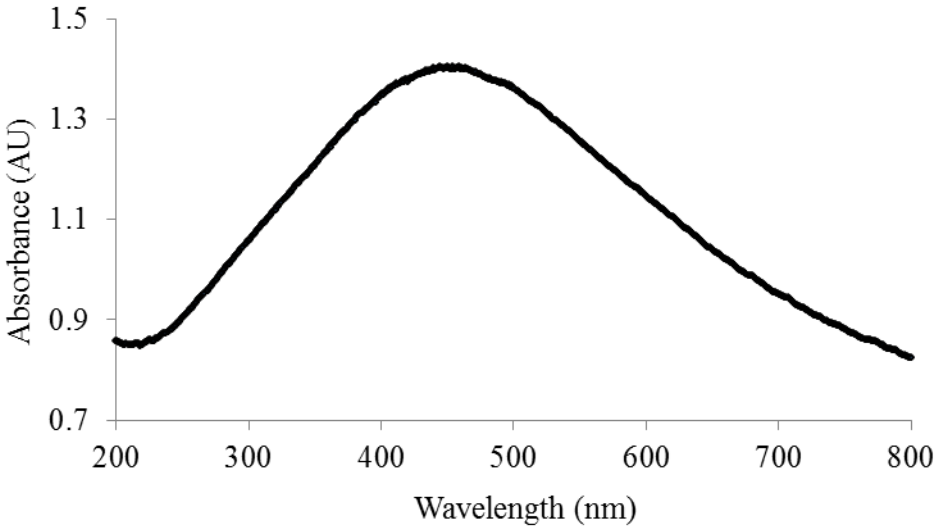

Because CAO contains a type 2 or "non-blue" copper center, which lacks the strong absorbance feature at ~600 nm characteristic of type 1 copper centers, this 450 nm absorbance feature is not due simply to copper binding. Taken together, the preliminary results from work using Y405pAF HPAO-1 both in solution and in crystallo suggest that the reconstitution of Y405pAF HPAO-1 protein with Cu(II) results in intramolecular electron transfer from the pAF side chain to the bound copper, forming a pAF radical species that gives rise to the absorbance feature observed at 450 nm.

Further work is needed to confirm this, particularly the use of solution and single

crystal X-ray absorption spectroscopy (XAS) to determine the oxidation state of the copper in Y405pAF HPAO-1 solution and crystalline samples before and after data collection. Additionally, confirmation of the EPR signal indicating the pAF radical formed after copper binding is necessary. The formation of a Cu(II)-tyrosine species in equilibrium with its Cu(I)-tyrosyl radical resonance form during TPQ biogenesis has been postulated (see Scheme 1.1), but a Cu(I)-tyrosyl radical species has not been directly observed either spectroscopically or through the use of radical-trapping agents (*184*).

Also intriguing is the fact that the incubation of Y305pAF HPAO-1 with Cu(II) gives rise to the same absorbance feature at 450 nm. This suggests that residue Tyr305 in the HPAO-1 active site, which is strictly conserved across CAOs, plays a role in activating the precursor tyrosine residue for the initial insertion of oxygen during biogenesis. Consequently, the X-ray crystal structure of Y305pAF HPAO-1 in complex with Cu(II) is being pursued. This residue is already known to be important in stabilizing biogenesis intermediates (with the mutation of Tyr305 to a phenylalanine resulting in the uncontrolled oxygenation of the precursor tyrosine ring (*75*)), as well as catalytic intermediates, so it will be exciting to learn more about any additional roles Tyr305 may play during biogenesis through future biochemical and structural characterization of Y305pAF HPAO-1.

REFERENCES CITED

1. Shih, J. C., Chen, K., and Ridd, M. J. (1999) Monoamine oxidase: from genes to behavior, *Annu. Rev. Neurosci. 22*, 197-217.
2. Seiler, N. (1990) Polyamine metabolism, *Digestion 46(2)*, 319-330.
3. Lucero, H. A., and Kagan, H. M. (2006) Lysyl oxidase: an oxidative enzyme and effector of cell function, *Cell. Mol. Life Sci. 63*, 2304-2316.
4. Okeley, N. M., and van der Donk, W. A. (2000) Novel cofactors via post-translational modifications of enzyme active sites, *Chem. Biol. 7*, 159-171.
5. Best, C. H. (1929) Disappearance of histamine from autolysing lung tissue, *J. Physiol. 67*, 256.
6. Wilce, M. C., Dooley, D. M., Freeman, H. C., Guss, J. M., Matsunami, H., McIntire, W. S., Ruggiero, C. E., Tanizawa, K., and Yamaguchi, H. (1997) Crystal structures of the copper-containing amine oxidase from *Arthrobacter globiformis* in the holo and apo forms: implications for the biogenesis of topaquinone, *Biochemistry 36*, 16116-16133.
7. Green, J., Haywood, G. W., and Large, P. J. (1983) Serological differences between the multiple amine oxidases of yeasts and comparison of the specificities of the purified enzymes from *Candida utilis* and *Pichia pastoris, Biochem. J. 211*, 481-493.
8. Wimalasekera, R., Villar, C., Begum, T., and Scherer, G. F. (2011) Copper amine oxidase 1 (CuAO1) of *Arabidopsis thaliana* contributes to abscisic acid- and polyamine-induced nitric oxide biosynthesis and abscisic acid signal transduction, *Mol. Plant 4*, 663-678.
9. Cona, A., Rea, G., Angelini, R., Federico, R., and Tavladoraki, P. (2006) Functions of amine oxidases in plant development and defence, *Trends in Plant Sci. 11*, 80-88.
10. Angelini, R., Cona, A., Federico, R., Fincato, P., Tavladoraki, P., and Tisi, A. (2010) Plant amine oxidases "on the move": an update, *Plant Physiol. Biochem. 48*, 560-564.
11. Campestre, M. P., Bordenave, C. D., Origone, A. C., Menendez, A. B., Ruiz, O. A., Rodriguez, A. A., and Maiale, S. J. (2011) Polyamine catabolism is involved in response to salt stress in soybean hypocotyls, *J. Plant. Physiol. 168*, 1234-1240.
12. Schwelberger, H. G. (2007) The origin of mammalian plasma amine oxidases, *J. Neural Transm. 114*, 757-762.
13. Novotny, W. F., Chassande, O., Baker, M., Lazdunski, M., and Barbry, P. (1994) Diamine oxidase is the amiloride-binding protein and is inhibited by amiloride analogues, *J. Biol. Chem. 269*, 9921-9925.
14. Yraola, F., Zorzano, A., Albericio, F., and Royo, M. (2009) Structure-activity relationships of SSAO/VAP-1 arylalkylamine-based substrates, *ChemMedChem 4*, 495-503.
15. Salmi, M., and Jalkanen, S. (2001) VAP-1: an adhesin and an enzyme, *Trends Immunol. 22*, 211-216.

16. Lyles, G. A. (1995) Substrate-specificity of mammalian tissue-bound semicarbazide-sensitive amine oxidase, *Prog. Brain Res. 106*, 293-303.
17. Gong, B., and Boor, P. J. (2006) The role of amine oxidases in xenobiotic metabolism, *Expert Opin. Drug Met. 2*, 559-571.
18. Maintz, L., Schwarzer, V., Bieber, T., van der Ven, K., and Novak, N. (2008) Effects of histamine and diamine oxidase activities on pregnancy: a critical review, *Hum. Reprod. Update 14*, 485-495.
19. McGrath, A. P., Hilmer, K. M., Collyer, C. A., Shepard, E. M., Elmore, B. O., Brown, D. E., Dooley, D. M., and Guss, J. M. (2009) Structure and inhibition of human diamine oxidase, *Biochemistry 48*, 9810-9822.
20. Toninello, A., Pietrangeli, P., De Marchi, U., Salvi, M., and Mondovi, B. (2006) Amine oxidases in apoptosis and cancer, *Biochim. Biophys. Acta, Rev. Cancer 1765*, 1-13.
21. Taksande, B. G., Kotagale, N. R., Patel, M. R., Shelkar, G. P., Ugale, R. R., and Chopde, C. T. (2010) Agmatine, an endogenous imidazoline receptor ligand modulates ethanol anxiolysis and withdrawal anxiety in rats, *Eur. J Pharmacol. 637*, 89-101.
22. Dunkel, P., Gelain, A., Barlocco, D., Haider, N., Gyires, K., Sperlagh, B., Magyar, K., Maccioni, E., Fadda, A., and Matyus, P. (2008) Semicarbazide-sensitive amine oxidase/vascular adhesion protein 1: recent developments concerning substrates and inhibitors of a promising therapeutic target, *Curr. Med. Chem. 15*, 1827-1839.
23. McDonald, A., Tipton, K., O'Sullivan, J., Olivieri, A., Davey, G., Coonan, A. M., and Fu, W. (2007) Modelling the roles of MAO and SSAO in glucose transport, *J. Neural Transm. 114*, 783-786.
24. Kivi, E., Elima, K., Aalto, K., Nymalm, Y., Auvinen, K., Koivunen, E., Otto, D. M., Crocker, P. R., Salminen, T. A., Salmi, M., and Jalkanen, S. (2009) Human Siglec-10 can bind to vascular adhesion protein-1 and serves as its substrate, *Blood 114*, 5385-5392.
25. Stolen, C. M., Marttila-Ichihara, F., Koskinen, K., Yegutkin, G. G., Turja, R., Bono, P., Skurnik, M., Hanninen, A., Jalkanen, S., and Salmi, M. (2005) Absence of the endothelial oxidase AOC3 leads to abnormal leukocyte traffic in vivo, *Immunity 22*, 105-115.
26. Mathys, K. C., Ponnampalam, S. N., Padival, S., and Nagaraj, R. H. (2002) Semicarbazide-sensitive amine oxidase in aortic smooth muscle cells mediates synthesis of a methylglyoxal-AGE: implications for vascular complications in diabetes, *Biochem. Biophys. Res. Commun. 297*, 863-869.
27. Jiang, Z. J., Richardson, J. S., and Yu, P. H. (2008) The contribution of cerebral vascular semicarbazide-sensitive amine oxidase to cerebral amyloid angiopathy in Alzheimer's disease, *Neuropath. Appl. Neuro. 34*, 194-204.
28. Janes, S. M., Mu, D., Wemmer, D., Smith, A. J., Kaur, S., Maltby, D., Burlingame, A. L., and Klinman, J. P. (1990) A new redox cofactor in eukaryotic enzymes: 6-hydroxydopa at the active site of bovine serum amine oxidase, *Science 248*, 981-987.

29. Klabunde, T., Eicken, C., Sacchettini, J. C., and Krebs, B. (1998) Crystal structure of a plant catechol oxidase containing a dicopper center, *Nat. Struct. Biol. 5*, 1084-1090.
30. Lerch, K. (1982) Primary structure of tyrosinase from *Neurospora crassa*: complete amino acid sequence and chemical structure of a tripeptide containing an unusual thioether, *J. Biol. Chem. 257*, 6414-6419.
31. Bravo, J., Fita, I., Ferrer, J. C., Ens, W., Hillar, A., Switala, J., and Loewen, P. C. (1997) Identification of a novel bond between a histidine and the essential tyrosine in catalase HPII of *Escherichia coli*, *Protein Sci. 6*, 1016-1023.
32. Yoshikawa, S., Shinzawa-Itoh, K., Nakashima, R., Yaono, R., Yamashita, E., Inoue, N., Yao, M., Fei, M. J., Libeu, C. P., Mizushima, T., Yamaguchi, H., Tomizaki, T., and Tsukihara, T. (1998) Redox-coupled crystal structural changes in bovine heart cytochrome c oxidase, *Science 280*, 1723-1729.
33. Ostermeier, C., Harrenga, A., Ermler, U., and Michel, H. (1997) Structure at 2.7 angstrom resolution of the *Paracoccus denitrificans* two-subunit cytochrome c oxidase complexed with an antibody F-V fragment, *Proc. Natl. Acad. Sci. U.S.A. 94*, 10547-10553.
34. Ito, N., Phillips, S. E. V., Stevens, C., Ogel, Z. B., Mcpherson, M. J., Keen, J. N., Yadav, K. D. S., and Knowles, P. F. (1991) Novel thioether bond revealed by a 1.7 angstrom crystal structure of galactose oxidase, *Nature 350*, 87-90.
35. Gielens, C., DeGeest, N., Xin, X. Q., Devreese, B., VanBeeumen, J., and Preaux, G. (1997) Evidence for a cysteine-histidine thioether bridge in functional units of molluscan haemocyanins and location of the disulfide bridges in functional units d and g of the beta(c)-haemocyanin of Helix pomatia, *Eur. J. Biochem. 248*, 879-888.
36. Taylor, T. C., and Andersson, I. (1997) The structure of the complex between rubisco and its natural substrate ribulose 1,5-bisphosphate, *J. Mol. Biol. 265*, 432-444.
37. Jabri, E., Carr, M. B., Hausinger, R. P., and Karplus, P. A. (1995) The crystal structure of urease from *Klebsiella aerogenes*, *Science 268*, 998-1004.
38. Benning, M. M., Kuo, J. M., Raushel, F. M., and Holden, H. M. (1995) 3-dimensional structure of the binuclear metal center of phosphotriesterase, *Biochemistry 34*, 7973-7978.
39. Yeh, J. I., Claiborne, A., and Hol, W. G. (1996) Structure of the native cysteine-sulfenic acid redox center of enterococcal NADH peroxidase refined at 2.8 A resolution, *Biochemistry 35*, 9951-9957.
40. Schmidt, B., Selmer, T., Ingendoh, A., and Vonfigura, K. (1995) A novel amino acid modification in sulfatases that is defective in multiple sulfatase deficiency, *Cell 82*, 271-278.
41. Nagashima, S., Nakasako, M., Dohmae, N., Tsujimura, M., Takio, K., Odaka, M., Yohda, M., Kamiya, N., and Endo, I. (1998) Novel non-heme iron center of nitrile hydratase with a claw setting of oxygen atoms, *Nat. Struct. Mol. Biol. 5*, 347-351.

42. Claiborne, A., Yeh, J. I., Mallett, T. C., Luba, J., Crane, E. J., 3rd, Charrier, V., and Parsonage, D. (1999) Protein-sulfenic acids: diverse roles for an unlikely player in enzyme catalysis and redox regulation, *Biochemistry 38*, 15407-15416.
43. Wang, S. X., Mure, M., Medzihradszky, K. F., Burlingame, A. L., Brown, D. E., Dooley, D. M., Smith, A. J., Kagan, H. M., and Klinman, J. P. (1996) A crosslinked cofactor in lysyl oxidase: redox function for amino acid side chains, *Science 273*, 1078-1084.
44. Mcintire, W. S., Wemmer, D. E., Chistoserdov, A., and Lidstrom, M. E. (1991) A new cofactor in a prokaryotic enzyme - tryptophan tryptophylquinone as the redox prosthetic group in methylamine dehydrogenase, *Science 252*, 817-824.
45. Vandenberghe, I., Kim, J. K., Devreese, B., Hacisalihoglu, A., Iwabuki, H., Okajima, T., Kuroda, S., Adachi, O., Jongejan, J. A., Duine, J. A., Tanizawa, K., and Van Beeumen, J. (2001) The covalent structure of the small subunit from *Pseudomonas putida* amine dehydrogenase reveals the presence of three novel types of internal cross-linkages, all involving cysteine in a thioether bond, *J. Biol. Chem. 276*, 42923-42931.
46. Yasunobu, K. T., Ishizaki, H., and Minamiura, N. (1976) The molecular mechanistic and immunological properties of amine oxidases, *Mol. Cell. Biochem. 13*, 3-29.
47. Ameyama, M., Hayashi, M., Matsushita, K., Shinagawa, E., and Adachi, O. (1984) Microbial production of pyrroloquinoline quinone, *Agric. Biol. Chem. Tokyo 48*, 561-565.
48. Lobensteinverbeek, C. L., Jongejan, J. A., Frank, J., and Duine, J. A. (1984) Bovine serum amine oxidase - a mammalian enzyme having covalently bound PQQ as prosthetic group, *FEBS Lett. 170*, 305-309.
49. Moog, R. S., Mcguirl, M. A., Cote, C. E., and Dooley, D. M. (1986) Evidence for methoxatin (pyrroloquinolinequinone) as the cofactor in bovine plasma amine oxidase from resonance raman spectroscopy, *Proc. Natl. Acad. Sci. U.S.A. 83*, 8435-8439.
50. Knowles, P. F., Pandeya, K. B., Rius, F. X., Spencer, C. M., Moog, R. S., Mcguirl, M. A., and Dooley, D. M. (1987) The organic cofactor in plasma amine oxidase - evidence for pyrroloquinoline quinone and against pyridoxal phosphate, *Biochem. J. 241*, 603-608.
51. Williamson, P. R., Moog, R. S., Dooley, D. M., and Kagan, H. M. (1986) Evidence for pyrroloquinolinequinone as the carbonyl cofactor in lysyl oxidase by absorption and resonance raman spectroscopy, *J. Biol. Chem. 261*, 6302-6305.
52. Airenne, T. T., Nymalm, Y., Kidron, H., Smith, D. J., Pihlavisto, M., Salmi, M., Jalkanen, S., Johnson, M. S., and Salminen, T. A. (2005) Crystal structure of the human vascular adhesion protein-1: unique structural features with functional implications, *Protein Sci. 14*, 1964-1974.
53. Jakobsson, E., Nilsson, J., Ogg, D., and Kleywegt, G. J. (2005) Structure of human semicarbazide-sensitive amine oxidase/vascular adhesion protein-1, *Acta Crystallogr., Sect. D: Biol. Crystallogr. 61*, 1550-1562.

54. Lunelli, M., Di Paolo, M. L., Biadene, M., Calderone, V., Battistutta, R., Scarpa, M., Rigo, A., and Zanotti, G. (2005) Crystal structure of amine oxidase from bovine serum, *J. Mol. Biol. 346*, 991-1004.
55. Li, R., Klinman, J. P., and Mathews, F. S. (1998) Copper amine oxidase from *Hansenula polymorpha*: the crystal structure determined at 2.4 A resolution reveals the active conformation, *Structure 6*, 293-307.
56. Chang, C. M., Klema, V. J., Johnson, B. J., Mure, M., Klinman, J. P., and Wilmot, C. M. (2010) Kinetic and structural analysis of substrate specificity in two copper amine oxidases from *Hansenula polymorpha*, *Biochemistry 49*, 2540-2550.
57. Duff, A. P., Cohen, A. E., Ellis, P. J., Kuchar, J. A., Langley, D. B., Shepard, E. M., Dooley, D. M., Freeman, H. C., and Guss, J. M. (2003) The crystal structure of *Pichia pastoris* lysyl oxidase, *Biochemistry 42*, 15148-15157.
58. Parsons, M. R., Convery, M. A., Wilmot, C. M., Yadav, K. D., Blakeley, V., Corner, A. S., Phillips, S. E., McPherson, M. J., and Knowles, P. F. (1995) Crystal structure of a quinoenzyme: copper amine oxidase of *Escherichia coli* at 2 A resolution, *Structure 3*, 1171-1184.
59. Kumar, V., Dooley, D. M., Freeman, H. C., Guss, J. M., Harvey, I., McGuirl, M. A., Wilce, M. C., and Zubak, V. M. (1996) Crystal structure of a eukaryotic (pea seedling) copper-containing amine oxidase at 2.2 A resolution, *Structure 4*, 943-955.
60. McGrath, A. P., Mithieux, S. M., Collyer, C. A., Bakhuis, J. G., van den Berg, M., Sein, A., Heinz, A., Schmelzer, C., Weiss, A. S., and Guss, J. M. (2011) Structure and activity of *Aspergillus nidulans* copper amine oxidase, *Biochemistry 50*, 5718-5730.
61. Brazeau, B. J., Johnson, B. J., and Wilmot, C. M. (2004) Copper-containing amine oxidases: biogenesis and catalysis, a structural perspective, *Arch. Biochem. Biophys. 428*, 22-31.
62. Smith, M. A., Pirrat, P., Pearson, A. R., Kurtis, C. R., Trinh, C. H., Gaule, T. G., Knowles, P. F., Phillips, S. E., and McPherson, M. J. (2010) Exploring the roles of the metal ions in *Escherichia coli* copper amine oxidase, *Biochemistry 49*, 1268-1280.
63. Sebela, M., Luhova, L., Frebort, I., Hirota, S., Faulhammer, H. G., Stuzka, V., and Pec, P. (1997) Confirmation of the presence of a Cu(II) topa quinone active site in the amine oxidase from fenugreek seedlings, *J. Exp. Bot. 48*, 1897-1907.
64. Cai, D., and Klinman, J. P. (1994) Evidence of a self-catalytic mechanism of 2,4,5-trihydroxyphenylalanine quinone biogenesis in yeast copper amine oxidase, *J. Biol. Chem. 269*, 32039-32042.
65. Matsuzaki, R., Fukui, T., Sato, H., Ozaki, Y., and Tanizawa, K. (1994) Generation of the topa quinone cofactor in bacterial monoamine oxidase by cupric ion-dependent autooxidation of a specific tyrosyl residue, *FEBS Lett. 351*, 360-364.
66. Ruggiero, C. E., and Dooley, D. M. (1999) Stoichiometry of the topa quinone biogenesis reaction in copper amine oxidases, *Biochemistry 38*, 9556-9556.

67. Mu, D., Janes, S. M., Smith, A. J., Brown, D. E., Dooley, D. M., and Klinman, J. P. (1992) Tyrosine codon corresponds to topa quinone at the active site of copper amine oxidases, *J. Biol. Chem. 267*, 7979-7982.
68. Kim, M., Okajima, T., Kishishita, S., Yoshimura, M., Kawamori, A., Tanizawa, K., and Yamaguchi, H. (2002) X-ray snapshots of quinone cofactor biogenesis in bacterial copper amine oxidase, *Nat. Struct. Mol. Biol. 9*, 591-596.
69. Schwartz, B., Dove, J. E., and Klinman, J. P. (2000) Kinetic analysis of oxygen utilization during cofactor biogenesis in a copper-containing amine oxidase from yeast, *Biochemistry 39*, 3699-3707.
70. Dove, J. E., Schwartz, B., Williams, N. K., and Klinman, J. P. (2000) Investigation of spectroscopic intermediates during copper-binding and TPQ formation in wild-type and active-site mutants of a copper-containing amine oxidase from yeast, *Biochemistry 39*, 3690-3698.
71. Su, Q., and Klinman, J. P. (1998) Probing the mechanism of proton coupled electron transfer to dioxygen: the oxidative half-reaction of bovine serum amine oxidase, *Biochemistry 37*, 12513-12525.
72. Dubois, J., and Klinman, J. P. (2005) The nature of O_2 reactivity leading to topa quinone in the copper amine oxidase from *Hansenula polymoropha* and its relationship to catalytic turnover, *Biochemistry 44*, 11381-11388.
73. Chen, Z., Schwartz, B., Williams, N. K., Li, R., Klinman, J. P., and Mathews, F. S. (2000) Crystal structure at 2.5 A resolution of zinc-substituted copper amine oxidase of *Hansenula polymorpha* expressed in *Escherichia coli*, *Biochemistry 39*, 9709-9717.
74. McGrath, A. P., Caradoc-Davies, T., Collyer, C. A., and Guss, J. M. (2010) Correlation of active site metal content in human diamine oxidase with trihydroxyphenylalanine quinone cofactor biogenesis, *Biochemistry 49*, 8316-8324.
75. Chen, Z. W., Datta, S., Dubois, J. L., Klinman, J. P., and Mathews, F. S. (2010) Mutation at a strictly conserved, active site tyrosine in the copper amine oxidase leads to uncontrolled oxygenase activity, *Biochemistry 49*, 7393-7402.
76. Schwartz, B., Green, E. L., Sanders-Loehr, J., and Klinman, J. P. (1998) Relationship between conserved consensus site residues and the productive conformation for the TPQ cofactor in a copper-containing amine oxidase from yeast, *Biochemistry 37*, 16591-16600.
77. DuBois, J. L., and Klinman, J. P. (2004) Methods for characterizing TPQ-containing proteins, *Method. Enzymol. 378*, 17-31.
78. Holm, R. H., Kennepohl, P., and Solomon, E. I. (1996) Structural and functional aspects of metal sites in biology, *Chem. Rev. 96*, 2239-2314.
79. Murray, J. M., Saysell, C. G., Wilmot, C. M., Tambyrajah, W. S., Jaeger, J., Knowles, P. F., Phillips, S. E., and McPherson, M. J. (1999) The active site base controls cofactor reactivity in *Escherichia coli* amine oxidase: x-ray crystallographic studies with mutational variants, *Biochemistry 38*, 8217-8227.
80. Wilmot, C. M., Murray, J. M., Alton, G., Parsons, M. R., Convery, V. B., Corner, A. S., Palcic, M. M., Knowles, P. F., McPherson, M. J., and Phillips, S. E. (1997)

Catalytic mechanism of the quinoenzyme amine oxidase from *Escherichia coli*: exploring the reductive half-reaction, *Biochemistry 36*, 1608-1620.
81. Pietrangeli, P., Nocera, S., Mondovi, B., and Morpurgo, L. (2003) Is the catalytic mechanism of bacteria, plant, and mammal copper-TPQ amine oxidases identical?, *Biochim. Biophys. Acta. 1647*, 152-156.
82. Dooley, D. M., McGuirl, M. A., Brown, D. E., Turowski, P. N., McIntire, W. S., and Knowles, P. F. (1991) A Cu(I)-semiquinone state in substrate-reduced amine oxidases, *Nature 349*, 262-264.
83. Welford, R. W., Lam, A., Mirica, L. M., and Klinman, J. P. (2007) Partial conversion of *Hansenula polymorpha* amine oxidase into a "plant" amine oxidase: implications for copper chemistry and mechanism, *Biochemistry 46*, 10817-10827.
84. Medda, R., Padiglia, A., Bellelli, A., Pedersen, J. Z., Agro, A. F., and Floris, G. (1999) Cu(I)-semiquinone radical species in plant copper-amine oxidases, *FEBS Lett. 453*, 1-5.
85. Shepard, E. M., and Dooley, D. M. (2006) Intramolecular electron transfer rate between active-site copper and TPQ in *Arthrobacter globiformis* amine oxidase, *JBIC, J. Biol. Inorg. Chem. 11*, 1039-1048.
86. Mukherjee, A., Smirnov, V. V., Lanci, M. P., Brown, D. E., Shepard, E. M., Dooley, D. M., and Roth, J. P. (2008) Inner-sphere mechanism for molecular oxygen reduction catalyzed by copper amine oxidases, *J. Am. Chem. Soc. 130*, 9459-9473.
87. Turowski, P. N., McGuirl, M. A., and Dooley, D. M. (1993) Intramolecular electron transfer rate between active-site copper and topa quinone in pea seedling amine oxidase, *J. Biol. Chem. 268*, 17680-17682.
88. Barker, R., Boden, N., Cayley, G., Charlton, S. C., Henson, R., Holmes, M. C., Kelly, I. D., and Knowles, P. F. (1979) Properties of cupric ions in benzylamine oxidase from pig plasma as studied by magnetic-resonance and kinetic methods, *Biochem. J. 177*, 289-302.
89. Juda, G. A., Shepard, E. M., Elmore, B. O., and Dooley, D. M. (2006) A comparative study of the binding and inhibition of four copper-containing amine oxidases by azide: implications for the role of copper during the oxidative half-reaction, *Biochemistry 45*, 8788-8800.
90. Mills, S. A., and Klinman, J. P. (2000) Evidence against reduction of Cu2+ to Cu+ during dioxygen activation in a copper amine oxidase from yeast, *J. Am. Chem. Soc. 122*, 9897-9904.
91. Mills, S. A., Goto, Y., Su, Q., Plastino, J., and Klinman, J. P. (2002) Mechanistic comparison of the cobalt-substituted and wild-type copper amine oxidase from *Hansenula polymorpha*, *Biochemistry 41*, 10577-10584.
92. Padiglia, A., Medda, R., Pedersen, J. Z., Finazzi Agro, A., Lorrai, A., Murgia, B., and Floris, G. (1999) Effect of metal substitution in copper amine oxidase from lentil seedlings, *JBIC, J. Biol. Inorg. Chem. 4*, 608-613.

93. Drummond, J. T., and Matthews, R. G. (1994) Nitrous oxide degradation by cobalamin-dependent methionine synthase: characterization of the reactants and products in the inactivation reaction, *Biochemistry 33*, 3732-3741.
94. Schwartz, B., Olgin, A. K., and Klinman, J. P. (2001) The role of copper in topa quinone biogenesis and catalysis, as probed by azide inhibition of a copper amine oxidase from yeast, *Biochemistry 40*, 2954-2963.
95. Dawkes, H. C., and Phillips, S. E. (2001) Copper amine oxidase: cunning cofactor and controversial copper, *Curr. Opin. Struct. Biol. 11*, 666-673.
96. Mills, S. A., Brown, D. E., Dang, K., Sommer, D., Bitsimis, A., Nguyen, J., and Dooley, D. M. (2012) Cobalt substitution supports an inner-sphere electron transfer mechanism for oxygen reduction in pea seedling amine oxidase, *JBIC, J. Biol. Inorg. Chem. 17*, 507-515.
97. Mure, M., and Klinman, J. P. (1993) Synthesis and spectroscopic characterization of model compounds for the active site cofactor in copper amine oxidases, *J. Am. Chem. Soc. 115*, 7117-7127.
98. Hartmann, C., Brzovic, P., and Klinman, J. P. (1993) Spectroscopic detection of chemical intermediates in the reaction of para-substituted benzylamines with bovine serum amine oxidase, *Biochemistry 32*, 2234-2241.
99. Cai, D., Dove, J., Nakamura, N., Sanders-Loehr, J., and Klinman, J. P. (1997) Mechanism-based inactivation of a yeast methylamine oxidase mutant: implications for the functional role of the consensus sequence surrounding topaquinone, *Biochemistry 36*, 11472-11478.
100. Hevel, J. M., Mills, S. A., and Klinman, J. P. (1999) Mutation of a strictly conserved, active-site residue alters substrate specificity and cofactor biogenesis in a copper amine oxidase, *Biochemistry 38*, 3683-3693.
101. Hirota, S., Iwamoto, T., Kishishita, S., Okajima, T., Yamauchi, O., and Tanizawa, K. (2001) Spectroscopic observation of intermediates formed during the oxidative half-reaction of copper/topa quinone-containing phenylethylamine oxidase, *Biochemistry 40*, 15789-15796.
102. Mure, M., and Klinman, J. P. (1995) Model studies of topa quinone: synthesis and characterization of topa quinone derivatives, *Method. Enzymol. 258*, 39-52.
103. Johnson, B. J., Cohen, J., Welford, R. W., Pearson, A. R., Schulten, K., Klinman, J. P., and Wilmot, C. M. (2007) Exploring molecular oxygen pathways in *Hansenula polymorpha* copper-containing amine oxidase, *J. Biol. Chem. 282*, 17767-17776.
104. Nakamura, N., Matsuzaki, R., Choi, Y. H., Tanizawa, K., and Sanders-Loehr, J. (1996) Biosynthesis of topa quinone cofactor in bacterial amine oxidases: solvent origin of C-2 oxygen determined by raman spectroscopy, *J. Biol. Chem. 271*, 4718-4724.
105. Chiu, Y. C., Okajima, T., Murakawa, T., Uchida, M., Taki, M., Hirota, S., Kim, M., Yamaguchi, H., Kawano, Y., Kamiya, N., Kuroda, S., Hayashi, H., Yamamoto, Y., and Tanizawa, K. (2006) Kinetic and structural studies on the catalytic role of the aspartic acid residue conserved in copper amine oxidase, *Biochemistry 45*, 4105-4120.

106. Wilmot, C. M. (1999) Visualization of dioxygen bound to copper during enzyme catalysis, *Science 286*, 1724-1728.
107. Frebort, I., Toyama, H., Matsushita, K., and Adachi, O. (1995) Half-site reactivity with p-nitrophenylhydrazine and subunit separation of the dimeric copper-containing amine oxidase from *Aspergillus niger*, *Biochem. Mol. Biol. Int. 36*, 1207-1216.
108. Morpurgo, L., Agostinelli, E., Mondovi, B., Avigliano, L., Silvestri, R., Stefancich, G., and Artico, M. (1992) Bovine serum amine oxidase: half-site reactivity with phenylhydrazine, semicarbazide, and aromatic hydrazides, *Biochemistry 31*, 2615-2621.
109. Agostinelli, E., Morpurgo, L., Wang, C., Giartosio, A., and Mondovi, B. (1994) Properties of cobalt-substituted bovine serum amine oxidase, *Eur. J. Biochem. 222*, 727-732.
110. Morpurgo, L., Agostinelli, E., Muccigrosso, J., Martini, F., Mondovi, B., and Avigliano, L. (1989) Benzylhydrazine as a pseudo-substrate of bovine serum amine oxidase, *Biochem. J. 260*, 19-25.
111. De Biase, D., Agostinelli, E., De Matteis, G., Mondovi, B., and Morpurgo, L. (1996) Half-of-the-sites reactivity of bovine serum amine oxidase: reactivity and chemical identity of the second site, *Eur. J. Biochem. 237*, 93-99.
112. Takahashi, K., and Klinman, J. P. (2006) Relationship of stopped flow to steady state parameters in the dimeric copper amine oxidase from *Hansenula polymorpha* and the role of zinc in inhibiting activity at alternate copper-containing subunits, *Biochemistry 45*, 4683-4694.
113. Coleman, A. A., Hindsgaul, O., and Palcic, M. M. (1989) Stereochemistry of copper amine oxidase reactions, *J. Biol. Chem. 264*, 19500-19505.
114. Scaman, C. H., and Palcic, M. M. (1992) Stereochemical course of tyramine oxidation by semicarbazide-sensitive amine oxidase, *Biochemistry 31*, 6829-6841.
115. Uchida, M., Ohtani, A., Kohyama, N., Okajima, T., Tanizawa, K., and Yamamoto, Y. (2003) Stereochemistry of 2-phenylethylamine oxidation catalyzed by bacterial copper amine oxidase, *Biosci., Biotechnol., Biochem. 67*, 2664-2667.
116. Taki, M., Murakawa, T., Nakamoto, T., Uchida, M., Hayashi, H., Tanizawa, K., Yamamoto, Y., and Okajima, T. (2008) Further insight into the mechanism of stereoselective proton abstraction by bacterial copper amine oxidase, *Biochemistry 47*, 7726-7733.
117. Duff, A. P., Trambaiolo, D. M., Cohen, A. E., Ellis, P. J., Juda, G. A., Shepard, E. M., Langley, D. B., Dooley, D. M., Freeman, H. C., and Guss, J. M. (2004) Using xenon as a probe for dioxygen-binding sites in copper amine oxidases, *J. Mol. Biol. 344*, 599-607.
118. Pirrat, P., Smith, M. A., Pearson, A. R., McPherson, M. J., and Phillips, S. E. (2008) Structure of a xenon derivative of *Escherichia coli* copper amine oxidase: confirmation of the proposed oxygen-entry pathway, *Acta Crystallogr., Sect. F: Struct. Biol. Cryst. Commun. 64*, 1105-1109.

119. Salmi, M., Yegutkin, G. G., Lehvonen, R., Koskinen, K., Salminen, T., and Jalkanen, S. (2001) A cell surface amine oxidase directly controls lymphocyte migration, *Immunity 14*, 265-276.
120. Shen, S. H., Wertz, D. L., and Klinman, J. P. (2012) Implication for functions of the ectopic adipocyte copper amine oxidase (AOC3) from purified enzyme and cell-based kinetic studies, *PLoS One 7*, 29270.
121. Obata, T. (2006) Diabetes and semicarbazide-sensitive amine oxidase (SSAO) activity: a review, *Life Sci. 79*, 417-422.
122. Cai, D., and Klinman, J. P. (1994) Copper amine oxidase: heterologous expression, purification, and characterization of an active enzyme in *Saccharomyces cerevisiae*, *Biochemistry 33*, 7647-7653.
123. Samuels, N. M., and Klinman, J. P. (2005) 2,4,5-trihydroxyphenylalanine quinone biogenesis in the copper amine oxidase from *Hansenula polymorpha* with the alternate metal nickel, *Biochemistry 44*, 14308-14317.
124. Samuels, N. M., and Klinman, J. P. (2006) Investigation of Cu(I)-dependent 2,4,5-trihydroxyphenylalanine quinone biogenesis in *Hansenula polymorpha* amine oxidase, *J. Biol. Chem. 281*, 21114-21118.
125. Okajima, T., Kishishita, S., Chiu, Y. C., Murakawa, T., Kim, M., Yamaguchi, H., Hirota, S., Kuroda, S., and Tanizawa, K. (2005) Reinvestigation of metal ion specificity for quinone cofactor biogenesis in bacterial copper amine oxidase, *Biochemistry 44*, 12041-12048.
126. Cai, D., Williams, N. K., and Klinman, J. P. (1997) Effect of metal on 2,4,5-trihydroxyphenylalanine (topa) quinone biogenesis in the *Hansenula polymorpha* copper amine oxidase, *J. Biol. Chem. 272*, 19277-19281.
127. Gomes, L., Pereira, E., and de Castro, B. (2000) Nickel(II) complexes with N2OS and N2S2 co-ordination spheres: reduction and spectroscopic study of the corresponding Ni(I) complexes, *J. Chem. Soc. Dalton*, 1373-1379.
128. Puig, S., and Thiele, D. J. (2002) Molecular mechanisms of copper uptake and distribution, *Curr. Opin. Chem. Biol. 6*, 171-180.
129. Faber, K. N., Haima, P., Gietl, C., Harder, W., Ab, G., and Veenhuis, M. (1994) The methylotrophic yeast *Hansenula polymorpha* contains an inducible import pathway for peroxisomal matrix proteins with an N-terminal targeting signal (PTS2 proteins), *Proc. Natl. Acad. Sci. U.S.A. 91*, 12985-12989.
130. Hassett, R., and Kosman, D. J. (1995) Evidence for Cu(II) reduction as a component of copper uptake by *Saccharomyces cerevisiae*, *J. Biol. Chem. 270*, 128-134.
131. Tanizawa, K., Kishishita, S., Okajima, T., Kim, M., Yamaguchi, H., Hirota, S., Suzuki, S., Kuroda, S., and Mure, M. (2003) Role of copper ion in bacterial copper amine oxidase: spectroscopic and crystallographic studies of metal-substituted enzymes, *J. Am. Chem. Soc. 125*, 1041-1055.
132. D'Arcy, A., Mac Sweeney, A., and Haber, A. (2003) Using natural seeding material to generate nucleation in protein crystallization experiments, *Acta Crystallogr., Sect. D: Biol. Crystallogr. 59*, 1343-1346.

133. Otwinowski, Z., and Minor, W. (1997) Processing of X-ray diffraction data collected in oscillation mode, *Method. Enzymol. 276*, 307-326.
134. Li, R., Chen, L., Cai, D., Klinman, J. P., and Mathews, F. S. (1997) Crystallographic study of yeast copper amine oxidase, *Acta Crystallogr., Sect. D: Biol. Crystallogr. 53*, 364-370.
135. (1994) The CCP4 suite: programs for protein crystallography, *Acta Crystallogr., Sect. D: Biol. Crystallogr. 50*, 760-763.
136. Emsley, P., and Cowtan, K. (2004) Coot: model-building tools for molecular graphics, *Acta Crystallogr., Sect. D: Biol. Crystallogr. 60*, 2126-2132.
137. Murshudov, G. N., Vagin, A. A., and Dodson, E. J. (1997) Refinement of macromolecular structures by the maximum-likelihood method, *Acta Crystallogr., Sect. D: Biol. Crystallogr. 53*, 240-255.
138. Laskowski, R. A., MacArthur, M. W., Moss, D. S., and Thornton, J. M. (1993) *PROCHECK*: a program to check the stereochemical quality of protein structures *J. Appl. Crystallogr. 26*, 283-291.
139. Feng, Z., Westbrook, J., and Berman, H. (1998) NUCheck, NDB-407 Rutgers University, New Brunswick, NJ.
140. Vaguine, A. A., Richelle, J., and Wodak, S. J. (1999) SFCHECK: a unified set of procedures for evaluating the quality of macromolecular structure-factor data and their agreement with the atomic model, *Acta Crystallogr., Sect. D: Biol. Crystallogr. 55*, 191-205.
141. Lovell, S. C., Davis, I. W., Arendall, W. B., 3rd, de Bakker, P. I., Word, J. M., Prisant, M. G., Richardson, J. S., and Richardson, D. C. (2003) Structure validation by Cα geometry: phi, psi and Cβ deviation, *Proteins 50*, 437-450.
142. McNicholas, S., Potterton, E., Wilson, K. S., and Noble, M. E. (2011) Presenting your structures: the CCP4mg molecular-graphics software, *Acta Crystallogr., Sect. D: Biol. Crystallogr. 67*, 386-394.
143. Duff, A. P., Shepard, E. M., Langley, D. B., Dooley, D. M., Freeman, H. C., and Guss, J. M. (2006) A C-terminal disulfide bond in the copper-containing amine oxidase from pea seedlings violates the twofold symmetry of the molecular dimer, *Acta Crystallogr., Sect. F: Struct. Biol. Cryst. Commun. 62*, 1168-1173.
144. Aksam, E. B., de Vries, B., van der Klei, I. J., and Kiel, J. A. (2009) Preserving organelle vitality: peroxisomal quality control mechanisms in yeast, *FEMS Yeast Res. 9*, 808-820.
145. Dudev, T., and Lim, C. (2000) Tetrahedral vs octahedral zinc complexes with ligands of biological interest: a DFT/CDM study, *J. Am. Chem. Soc. 122*, 11146-11153.
146. Mure, M., Mills, S. A., and Klinman, J. P. (2002) Catalytic mechanism of the topa quinone containing copper amine oxidases, *Biochemistry 41*, 9269-9278.
147. Roh, J. H., Suzuki, H., Azakami, H., Yamashita, M., Murooka, Y., and Kumagai, H. (1994) Purification, characterization, and crystallization of monoamine oxidase from *Escherichia coli K12*, *Biosci., Biotechnol., Biochem. 58*, 1652-1656.

148. Cronin, C. N., and Kirsch, J. F. (1988) Role of arginine292 in the substrate specificity of aspartate aminotransferase as examined by site-directed mutagenesis, *Biochemistry 27*, 4572-4579.
149. Youdim, M. B., Edmondson, D., and Tipton, K. F. (2006) The therapeutic potential of monoamine oxidase inhibitors, *Nat. Rev. Neurosci. 7*, 295-309.
150. Kawaguchi, S., Nobe, Y., Yasuoka, J., Wakamiya, T., Kusumoto, S., and Kuramitsu, S. (1997) Enzyme flexibility: a new concept in recognition of hydrophobic substrates, *J. Biochem. 122*, 55-63.
151. Tsugeno, Y., and Ito, A. (1997) A key amino acid responsible for substrate selectivity of monoamine oxidase A and B, *J. Biol. Chem. 272*, 14033-14036.
152. De Hoop, M. J., Valkema, R., Kienhuis, C. B., Hoyer, M. A., and Ab, G. (1992) The peroxisomal import signal of amine oxidase from the yeast *Hansenula polymorpha* is not universal, *Yeast 8*, 243-252.
153. Lander, E. S., Linton, L. M., Birren, B., Nusbaum, C., Zody, M. C., Baldwin, J., Devon, K., Dewar, K., Doyle, M., FitzHugh, W., Funke, R., Gage, D., Harris, K., Heaford, A., Howland, J., Kann, L., Lehoczky, J., LeVine, R., McEwan, P., McKernan, K., Meldrim, J., Mesirov, J. P., Miranda, C., Morris, W., Naylor, J., Raymond, C., Rosetti, M., Santos, R., Sheridan, A., Sougnez, C., Stange-Thomann, N., Stojanovic, N., Subramanian, A., Wyman, D., Rogers, J., Sulston, J., Ainscough, R., Beck, S., Bentley, D., Burton, J., Clee, C., Carter, N., Coulson, A., Deadman, R., Deloukas, P., Dunham, A., Dunham, I., Durbin, R., French, L., Grafham, D., Gregory, S., Hubbard, T., Humphray, S., Hunt, A., Jones, M., Lloyd, C., McMurray, A., Matthews, L., Mercer, S., Milne, S., Mullikin, J. C., Mungall, A., Plumb, R., Ross, M., Shownkeen, R., Sims, S., Waterston, R. H., Wilson, R. K., Hillier, L. W., McPherson, J. D., Marra, M. A., Mardis, E. R., Fulton, L. A., Chinwalla, A. T., Pepin, K. H., Gish, W. R., Chissoe, S. L., Wendl, M. C., Delehaunty, K. D., Miner, T. L., Delehaunty, A., Kramer, J. B., Cook, L. L., Fulton, R. S., Johnson, D. L., Minx, P. J., Clifton, S. W., Hawkins, T., Branscomb, E., Predki, P., Richardson, P., Wenning, S., Slezak, T., Doggett, N., Cheng, J. F., Olsen, A., Lucas, S., Elkin, C., Uberbacher, E., Frazier, M., Gibbs, R. A., Muzny, D. M., Scherer, S. E., Bouck, J. B., Sodergren, E. J., Worley, K. C., Rives, C. M., Gorrell, J. H., Metzker, M. L., Naylor, S. L., Kucherlapati, R. S., Nelson, D. L., Weinstock, G. M., Sakaki, Y., Fujiyama, A., Hattori, M., Yada, T., Toyoda, A., Itoh, T., Kawagoe, C., Watanabe, H., Totoki, Y., Taylor, T., Weissenbach, J., Heilig, R., Saurin, W., Artiguenave, F., Brottier, P., Bruls, T., Pelletier, E., Robert, C., Wincker, P., Smith, D. R., Doucette-Stamm, L., Rubenfield, M., Weinstock, K., Lee, H. M., Dubois, J., Rosenthal, A., Platzer, M., Nyakatura, G., Taudien, S., Rump, A., Yang, H., Yu, J., Wang, J., Huang, G., Gu, J., Hood, L., Rowen, L., Madan, A., Qin, S., Davis, R. W., Federspiel, N. A., Abola, A. P., Proctor, M. J., Myers, R. M., Schmutz, J., Dickson, M., Grimwood, J., Cox, D. R., Olson, M. V., Kaul, R., Shimizu, N., Kawasaki, K., Minoshima, S., Evans, G. A., Athanasiou, M., Schultz, R., Roe, B. A., Chen, F., Pan, H., Ramser, J., Lehrach, H., Reinhardt, R., McCombie, W. R., de la Bastide, M., Dedhia, N., Blocker, H., Hornischer, K., Nordsiek, G., Agarwala, R., Aravind, L., Bailey, J.

A., Bateman, A., Batzoglou, S., Birney, E., Bork, P., Brown, D. G., Burge, C. B., Cerutti, L., Chen, H. C., Church, D., Clamp, M., Copley, R. R., Doerks, T., Eddy, S. R., Eichler, E. E., Furey, T. S., Galagan, J., Gilbert, J. G., Harmon, C., Hayashizaki, Y., Haussler, D., Hermjakob, H., Hokamp, K., Jang, W., Johnson, L. S., Jones, T. A., Kasif, S., Kaspryzk, A., Kennedy, S., Kent, W. J., Kitts, P., Koonin, E. V., Korf, I., Kulp, D., Lancet, D., Lowe, T. M., McLysaght, A., Mikkelsen, T., Moran, J. V., Mulder, N., Pollara, V. J., Ponting, C. P., Schuler, G., Schultz, J., Slater, G., Smit, A. F., Stupka, E., Szustakowski, J., Thierry-Mieg, D., Thierry-Mieg, J., Wagner, L., Wallis, J., Wheeler, R., Williams, A., Wolf, Y. I., Wolfe, K. H., Yang, S. P., Yeh, R. F., Collins, F., Guyer, M. S., Peterson, J., Felsenfeld, A., Wetterstrand, K. A., Patrinos, A., Morgan, M. J., de Jong, P., Catanese, J. J., Osoegawa, K., Shizuya, H., Choi, S., and Chen, Y. J. (2001) Initial sequencing and analysis of the human genome, *Nature 409*, 860-921.

154. Elmore, B. O., Bollinger, J. A., and Dooley, D. M. (2002) Human kidney diamine oxidase: heterologous expression, purification, and characterization, *JBIC, J. Biol. Inorg. Chem. 7*, 565-579.
155. Marti, L., Abella, A., De La Cruz, X., Garcia-Vicente, S., Unzeta, M., Carpene, C., Palacin, M., Testar, X., Orozco, M., and Zorzano, A. (2004) Exploring the binding mode of semicarbazide-sensitive amine oxidase/VAP-1: identification of novel substrates with insulin-like activity, *J. Med. Chem. 47*, 4865-4874.
156. Langer, G., Cohen, S. X., Lamzin, V. S., and Perrakis, A. (2008) Automated macromolecular model building for X-ray crystallography using ARP/wARP version 7, *Nature Protoc. 3*, 1171-1179.
157. van Roermund, C. W., de Jong, M., L, I. J., van Marle, J., Dansen, T. B., Wanders, R. J., and Waterham, H. R. (2004) The peroxisomal lumen in *Saccharomyces cerevisiae* is alkaline, *J. Cell Sci. 117*, 4231-4237.
158. Wilmot, C. M., Saysell, C. G., Blessington, A., Conn, D. A., Kurtis, C. R., McPherson, M. J., Knowles, P. F., and Phillips, S. E. (2004) Medical implications from the crystal structure of a copper-containing amine oxidase complexed with the antidepressant drug tranylcypromine, *FEBS Lett. 576*, 301-305.
159. Hartmann, C., and Klinman, J. P. (1991) Structure-function studies of substrate oxidation by bovine serum amine oxidase: relationship to cofactor structure and mechanism, *Biochemistry 30*, 4605-4611.
160. Cooper, R. A., Knowles, P. F., Brown, D. E., McGuirl, M. A., and Dooley, D. M. (1992) Evidence for copper and 3,4,6-trihydroxyphenylalanine quinone cofactors in an amine oxidase from the gram-negative bacterium *Escherichia coli K-12*, *Biochem. J. 288(2)*, 337-340.
161. Hacisalihoglu, A., Jongejan, J. A., and Duine, J. A. (1997) Distribution of amine oxidases and amine dehydrogenases in bacteria grown on primary amines and characterization of the amine oxidase from *Klebsiella oxytoca*, *Microbiology 143(2)*, 505-512.
162. Parrott, S., Jones, S., and Cooper, R. A. (1987) 2-phenylethylamine catabolism by *Escherichia coli K12*, *J. Gen. Microbiol. 133*, 347-351.

163. Jalkanen, S., and Salmi, M. (2001) Cell surface monoamine oxidases: enzymes in search of a function, *EMBO J. 20*, 3893-3901.
164. McIntire, W. S. (1998) Newly discovered redox cofactors: possible nutritional, medical, and pharmacological relevance to higher animals, *Annu. Rev. Nutr. 18*, 145-177.
165. Tisi, A., Angelini, R., and Cona, A. (2008) Wound healing in plants: cooperation of copper amine oxidase and flavin-containing polyamine oxidase, *Plant Signaling Behav. 3*, 204-206.
166. Enrique-Tarancon, G., Marti, L., Morin, N., Lizcano, J. M., Unzeta, M., Sevilla, L., Camps, M., Palacin, M., Testar, X., Carpene, C., and Zorzano, A. (1998) Role of semicarbazide-sensitive amine oxidase on glucose transport and GLUT4 recruitment to the cell surface in adipose cells, *J. Biol. Chem. 273*, 8025-8032.
167. McCoy, A., Grosse-Kunstleve, R. W., Adams, P. D., Winn, M., Storoni, L. C., and Read, R. J. (2007) Phaser crystallographic software, *J. Appl. Crystallogr. 40*, 658-674.
168. Tsuzuki, S., Honda, K., Uchimaru, T., Mikami, M., and Tanabe, K. (2002) Origin of attraction and directionality of the pi/pi interaction: model chemistry calculations of benzene dimer interaction, *J. Am. Chem. Soc. 124*, 104-112.
169. Tsuzuki, S., Honda, K., and Azumi, R. (2002) Model chemistry calculations of thiophene dimer interactions: origin of pi-stacking, *J. Am. Chem. Soc. 124*, 12200-12209.
170. Klinman, J. P., Hevel, J. M., and Mills, S. A. (1999) Mutation of a strictly conserved, active-site residue alters substrate specificity and cofactor biogenesis in a copper amine oxidase, *Biochemistry 38*, 3683-3693.
171. Kurtis, C. R., Knowles, P. F., Parsons, M. R., Gaule, T. G., Phillips, S. E., and McPherson, M. J. (2011) Tyrosine 381 in *E. coli* copper amine oxidase influences substrate specificity, *J. Neural. Transm. 118*, 1043-1053.
172. Murakawa, T., Hayashi, H., Taki, M., Yamamoto, Y., Kawano, Y., Tanizawa, K., and Okajima, T. (2012) Structural insights into the substrate specificity of bacterial copper amine oxidase obtained by using irreversible inhibitors, *J. Biochem. 151*, 167-178.
173. Elovaara, H., Kidron, H., Parkash, V., Nymalm, Y., Bligt, E., Ollikka, P., Smith, D. J., Pihlavisto, M., Salmi, M., Jalkanen, S., and Salminen, T. A. (2011) Identification of two imidazole binding sites and key residues for substrate specificity in human primary amine oxidase AOC3, *Biochemistry 50*, 5507-5520.
174. Chang, C. M. (2009) *Investigation of substrate specificity in copper amine oxidases from Hansenula polymorpha*. (Doctoral dissertation). Received from ProQuest Dissertations and Theses. (Accession No. 3382860)
175. Chang, M. C., Yee, C. S., Nocera, D. G., and Stubbe, J. (2004) Site-specific replacement of a conserved tyrosine in ribonucleotide reductase with an aniline amino acid: a mechanistic probe for a redox-active tyrosine, *J. Am. Chem. Soc. 126*, 16702-16703.

176. Jonsson, M., Lind, J., Eriksen, T. E., and Merenyi, G. (1994) Redox and acidity properties of 4-substituted aniline radical cations in water, *J. Am. Chem. Soc. 116*, 1423-1427.
177. Harriman, A. (1987) Further comments on the redox potentials of tryptophan and tyrosine, *J. Phys. Chem. 91*, 6102-6104.
178. Lide, D. R., and Frederikse, H. P. R. (1994) *Handbook of Chemistry and Physics*, 75 ed., CRC Press, Boca Raton, FL.
179. Liu, C. C., and Schultz, P. G. (2010) Adding new chemistries to the genetic code, *Annu. Rev. Biochem. 79*, 413-444.
180. Young, T. S., Ahmad, I., Brock, A., and Schultz, P. G. (2009) Expanding the genetic repertoire of the methylotrophic yeast *Pichia pastoris*, *Biochemistry 48*, 2643-2653.
181. Wu, N., Deiters, A., Cropp, T. A., King, D., and Schultz, P. G. (2004) A genetically encoded photocaged amino acid, *J. Am. Chem. Soc. 126*, 14306-14307.
182. Lemke, E. A., Summerer, D., Geierstanger, B. H., Brittain, S. M., and Schultz, P. G. (2007) Control of protein phosphorylation with a genetically encoded photocaged amino acid, *Nat. Chem. Biol. 3*, 769-772.
183. Summerer, D., Chen, S., Wu, N., Deiters, A., Chin, J. W., and Schultz, P. G. (2006) A genetically encoded fluorescent amino acid, *Proc. Natl. Acad. Sci. U.S.A. 103*, 9785-9789.
184. Dubois, J. L., and Klinman, J. P. (2005) Mechanism of post-translational quinone formation in copper amine oxidases and its relationship to the catalytic turnover, *Arch. Biochem. Biophys. 433*, 255-265.
185. Neumann, R., Hevey, R., and Abeles, R. H. (1975) The action of plasma amine oxidase on β-haloamines: evidence for proton abstraction in the oxidative reaction, *J. Biol. Chem. 250*, 6362-6367.

APPENDIX A: CHAPTER 2 SUPPLEMENTARY METHODS

Cloning

Because of the unavailability of the *H. polymorpha* genome at the start of the investigation, the *hpao-2* gene (1967 bp) was cloned out of the *H. polymorpha* genome by "genome walking," using iterations of primers to progressively amplify the entire gene. Initially, mass spectrometry of trypsin-digested protein isolated from cell extracts of *H. polymorpha* grown on benzylamine-enriched growth media that demonstrated CAO activity yielded peptide sequences distinct from that of the original HPAO (HPAO-1). Degenerated primers were designed on the basis of the new peptide sequences, and subsequent PCR resulted in a 600 bp gene fragment of *hpao-2*. The 5'- end and 3'- end sequences of the fragment were then used for upstream and downstream genome walking to yield 1967 bp of the full-length *hpao-2* sequence. The identity of the full-length gene was verified by comparison to the now available *H. polymorpha* genome (Rhein Biotech, personal communication). The *hpao-2* gene was inserted into the *S. cerevisiae* expression vector, pYES2 (Invitrogen), under inducible control by the *GAL1* promoter, via cloned KpnI and XbaI restriction enzyme cut sites present in the multiple cloning site.

Expression

Invitrogen's INVSC-1 *S. cerevisiae* cells were transformed with selection for uracil-independent growth, conferred by the *ura3* gene on pYES2. Importantly, *S. cerevisiae* contains no CAO genes and thus no background CAO expression. Starter cultures were grown in URA^- minimal medium containing 6.7% yeast nitrogen base

without amino acids and 0.77 g/L complete supplemental mixture without uracil (MP Biomedicals) with 2% raffinose as a carbon source at 30°C and 225 rpm in a New Brunswick Scientific Innova 4300 temperature-controlled platform shaker. At an OD_{600} of ~5, cells were diluted to an OD_{600} of 0.4 into URA^- minimal medium with 30 μM $CuSO_4$, 1% raffinose, and 2% galactose for induction of expression. Induced cultures were grown in 1.5 L volumes in 4 L flasks. After being induced for 24 h, cells were pelleted by centrifugation in a Sorvall RC 5C Plus centrifuge at 5,000 rpm in an SLA-300 fixed angle rotor for 5 min at 4°C. Typically, 9 L of cell culture yields 60-70 g of cell pellet.

Purification

Protein purification followed the previously developed purification strategy for HPAO-1 with some modifications (*122*). Cells were lysed with glass beads (425-600 μm, Sigma G8772) in the presence of four protease inhibitors: 0.5 mM phenylmethanesulfonyl fluoride, 5 mM 1,10-phenanthroline, 1 μM pepstatin A, and 5 μM E-64 (Sigma). Approximately 150 mL of glass beads was combined with a ~250 mL suspension of cell pellet and cold 10 mM potassium phosphate (pH 7.2) in a bead beater. Cells were lysed by five cycles of grinding for 5 min and resting for 2 min, with changes in the ice and water surrounding the bead-beating chamber between cycles. The cell extract was then separated from cellular debris by centrifugation in Sorvall RC 5C Plus centrifuge in ~40 mL aliquots at 12,000 rpm in an SS-34 fixed angle rotor at 4°C for 1 h.

The lysate was loaded onto a ~200 mL (5 cm diameter, ~20 cm height) Q-Sepharose column pre-equilibrated with 5 mM potassium phosphate (pH 7.2). This column was washed with 1 L of 5 mM potassium phosphate (pH 7.2). Protein was eluted as follows: 300 mL total volume of a linear gradient from 5 to 100 mM potassium phosphate (pH 7.2) followed by 200 mL of 100 mM potassium phosphate (pH 7.2), then a 300 mL total volume of a linear gradient from 100 to 400 mM potassium phosphate (pH 7.2), and finally 300 mL of 400 mM potassium phosphate (pH 7.2). Fractions (10 mL) were collected at a rate of 1 min/fraction (elution by gravity). The column was washed with 1 L of 400 mM potassium phosphate and 1 M NaCl between preparations and then re-equilibrated with ~1 L of 5 mM potassium phosphate (pH 7.2).

Fractions 28-58 were pooled at 4°C and dialyzed (Pierce SnakeSkin Pleated Dialysis Tubing 10,000 MWCO, catalog no. 68100) into 4 L of 50 mM potassium phosphate (pH 7.2) overnight at 4°C. Dialyzed pooled fractions were then centrifuged at 12,000 rpm (1 h at 4°C) to separate out precipitated protein. Cleared pooled fractions were concentrated to approximately 6 mL using Amicon concentrators with a polyethersulfone 50,000 NMWL ultrafiltration membrane.

Aliquots (2 mL) of the concentrated pool were centrifuged at 13,000 rpm for 5 min at 4°C in a benchtop microcentrifuge to clear any precipitation prior to being loaded onto an S-300 column. This was run overnight and eluted with 50 mM potassium phosphate (pH 7.2). Fractions were collected every 10 min at a flow rate of 0.2 mL/min (for ~2 mL/fraction).

Pooled fractions 46-58 were concentrated using an Amicon concentrator with a polyethersulfone 50,000 NMWL ultrafiltration membrane. After a final volume of ~2-3 mL had been reached, 50-100 μL aliquots of purified protein were made, snap-frozen in liquid nitrogen, and kept at -20°C for short-term storage or -80°C for long-term storage. Concentrated purified HPAO-2 samples were peach in color.

Kinetic Measurements

Methylamine, [1,1,1-$^2H_3$]methylamine, and benzylamine hydrochlorides were purchased form Sigma and used without further purification. [1,1-$^2H_2$]Benzylamine hydrochloride was prepared as previously described (*185*). The purity of synthesized [1,1-$^2H_2$]benzylamine hydrochloride and commercial [1,1,1-$^2H_3$]methylamine was verified by NMR with no evidence of contamination by protium substrate found. In all cases with protio and deuterio substrates, NMR spectra also indicated no significant level of chemical contaminant.

Observation of the formation of benzaldehyde from benzylamine (*159*) served as a preliminary enzyme activity assay during the purification of HPAO-2 and in subsequent kinetic studies of benzylamine. Benzaldehyde absorbs at 250 nm (ε = 12,800 $M^{-1}cm^{-1}$), and its production is easily followed on a Hewlett-Packard 8452A diode array spectrophotometer. Enzyme activity with a varying level of methylamine was monitored by oxygen consumption with a Clark oxygen electrode. Unless otherwise noted, all kinetic studies were conducted at 25°C in 100 mM potassium phosphate (pH 7.2), controlled for an ionic strength of 300 mM by the addition of potassium chloride (*122*).

In HPAO-2 assays, the range of concentration for amine substrates was 0.5-20 mM for methylamine and 1-200 μM for benzylamine. In HPAO-1, 0.05-1.5 mM methylamine and 0.2-5 mM benzylamine were used for steady state kinetic rate parameter determination. Buffers used for the pH studies were: 100 mM potassium phosphate, pH 6.2-8.3; 25 mM sodium pyrophosphate, pH 8.6; and 0.1 M potassium carbonate, pH 9.2-9.5 (Sigma). Ionic strength was maintained at 300 mM with potassium chloride for potassium-based buffers, and sodium chloride for sodium-based buffer. These were carried out at 1-150 μM benzylamine at 25°C. Enzyme activity at varying levels of oxygen, at saturating amine concentrations, for determination of $k_{cat}/K_m(O_2)$ values was monitored by oxygen consumption with a Clark oxygen electrode. The kinetic parameters, k_{cat} and k_{cat}/K_m, were derived from data fit to the Michaelis-Menton equation by nonlinear regression using Kaleidagraph (Abelbeck Software).